UCL Université catholique de Louvain

École polytechnique de Louvain (EPL)

epl

Fabrication of a high aspect ratio biosensor for bacteria detection

Dissertation presented by
Ariane LITEANU

for obtaining the Master's degree in
Biomedical Engineering

Supervisor(s)
Pr. Laurent FRANCIS

Reader(s)
Pr. Sophie DEMOUSTIER, Dr. Lamia EL FISSI , Dr. Jonathan RASSON

Academic year 2015-2016



Abstract

Even if most of the micro-organisms we carry are harmless and even beneficial, some are dangerous and may be at the origin of different infectious diseases. For the health sector as well as for food industries, there is an urgent need for reliable, rapid and affordable solutions to detect, in the most accurate way possible, the concentration of those pathogens.
Nowadays, traditional methods which exist can achieve a reasonable limit of detection but are not user friendly. Biosensors are an alternative that could, in the coming years, combine a compact design with a high sensitivity and selectivity.
Among the numerous transducer means available, this master thesis will focus on an impedance-based interdigitated electrodes (IDE) sensor previously developed by Dr. Numa Couniot at the UCL.
Our aim is to study the ability of thicker electrodes to capture and detect bacteria and to compare these results with standard electrodes. Indeed, increasing the electrodes thickness leads to a greater capacitance value but also to a larger cavity of concentrated electric field in which bacteria should settle. However, changing one parameter requires to re-think the whole process of manufacture. Indeed, aluminium, which was selected for an eventual integration with CMOS technology, can no longer be used as main component of electrodes. Furthermore, special resists must be used to reach thicknesses greater than 3 μm. This master thesis presents a new process based on electroplated nickel forming the sensor's electrodes.
Once fabricated, sensors are tested under dry environment to compare their raw electric properties with theoretical values. For the impedance modulus, we obtained an average discrepancy less than 1 %.
Afterwards, we tested sensors under liquid environments with an inflow of *Staphylococcus Epidermidis* in PBS through a microfluidic system. This strain was selected for its proximity to the *Staphylococcus Aureus* without its dangerousness. To increase the adhesion of bacteria to the sensors' wall, we use polydopamine also known as a biological glue.
The results show that the normalised admittance increased all along the incubation period during which bacteria can be deposited on electrode walls.
We also calculated the sensitivity of each sensors as $S = ||\frac{|Y_B|-|Y_D|}{Y_D}||$, with Y_B and Y_D respectively the signal admittance with and without bacteria. For the purpose of the comparison we defined a metric S_M which was the average of sensitivities calculated at 10^5 and 10^6 Hz.

Acknowledgements

As I prepare to complete this master thesis, I think it is time to give some grateful thanks.
None of this experience would have been possible without my advisor, Professor Laurent Francis. I would like to thank him for his support and guidance throughout this academic year. I wish to acknowledge Professor Sophie Demoustier as the second reader of this thesis.
I also would like to thank my mentor, Lamia El fissi, for her time, useful advices and more generally for the help she has given me for the development of the fabrication process. Always present both from a technical and moral viewpoint, she allowed me to discover the world of research and always found time to answer my questions, as numerous as they may be.
The office atmosphere wouldn't have been the same without Jonathan, who is the daily news specialist, Meddy, the french pool champion, Olivier and Xiaoya. I enjoyed spending time with them.
Many thanks to the people of the SMALL group and the Winfab team for their help whenever I needed, the discussions in the cafeteria, the advices and their sympathy. Their support during more difficult times was very valuable to me.
I also found a great help from the MIAE labaratory directed by Jacques Maillon, and from Catherine Nannan who even improvised herself mover.

I have a special thought for those who were on the front line to help me, my mom and David. They had the patience to listen to my questions and provided me with unfailing support and continuous encouragement throughout this year. I also think about those who were a little further but still helped me in a way or an other.
To all of them, thank you.

Contents

1 Introduction **1**

2 State of the Art **4**
2.1 Bacterial detection 4
2.1.1 Performances: key concepts 5
2.1.2 Traditional methods 7
2.2 Biosensors 10
2.2.1 Optical biosensors 11
2.2.2 Acoustic biosensors 14
2.2.3 Electrochemical biosensors 15
2.2.4 Selectivity means 19
2.3 Impedance spectroscopy 21
2.3.1 Impedance calculation 22
2.3.2 Electrodes 23
2.3.3 Circuit Models 23
2.3.4 Microfluidic 26
2.4 Fabrication techniques 27
2.4.1 High aspect ratio structures 27
2.4.2 Passivation layer 29

3 Methodology **31**
3.1 Design 33
3.1.1 Proportions optimisation 33
3.1.2 Sensors' types 34
3.1.3 Electrode materials 34
3.2 Fabrication 35
3.2.1 Nickel electro-deposition 35
3.2.2 Process 37
3.2.3 Microfluidic cap 40
3.3 Electrical tests 41
3.4 Measurements with Bacteria 43
3.4.1 Material 43
3.4.2 Bacteria handling 44
3.4.3 Surface plate counting 44
3.4.4 Polydopamine 44
3.4.5 Measurements 44

4 Experimental results and discussion **47**
4.1 Fabrication . . . 47
4.1.1 Photolithography . . . 47
4.1.2 Electroplating . . . 50
4.1.3 Under-deposition of nickel . . . 53
4.1.4 ALD . . . 54
4.2 Electrical tests . . . 54
4.2.1 Dry environment . . . 55
4.2.2 Liquid environment . . . 57
4.3 Bacterial response . . . 57
4.3.1 Polydopamine layer . . . 59
4.3.2 Bacterial incubation . . . 61
4.3.3 Sensitivity . . . 62
4.3.4 Influence of the thickness . . . 66
4.4 Reconsiderations: variance factors encountered . . . 67

5 Conclusion **69**

A Process development **79**
A.1 Biological preparations . . . 83

Chapter 1

Introduction

To better understand the context of this master thesis, let project ourself in a future, which may be closer than we imagine...
Mary has just arrived for a complete physical exam with her family doctor. She complains about several common symptoms that might just as well be caused by a bacterial infection. If it is, perhaps antibiotics should be prescribed.

Luckily enough, Mary will not have to wait long to know. Yet, in the waiting room, a **small medical device**, which fits in one hand, has been given to her. It is a **bacteria sensor**. Similarly to a blood-sugar level sensor, the device will **collect a few drops of blood** in order to analyse it.

After **15 minutes**, it is her turn. The sensor makes a small noise, its analyse is already done. The doctor starts by looking at the results. Those ones hold very accurate information about **concentrations** of a selection of well known bacteria that are potentially pathogenic.
For Mary, nothing to worry about, these levels are all under their safety limit and all signals remained in the green. Yet, some bacteria possess infectious doses as low as ten cells per millilitre!
After some other additional examinations, Mary goes home with her prescription. The doctor has taken the sensor back because it is **reusable after an adequate washing**. It is a model working on impedimetric measures. He knows that one of his colleague possess one based on acoustic waves, but anyway, all of those biosensors produce faster results than older methods such as agar-based cultures. Moreover, no specialised staff is required and that is quite handy for a small physician office.

Even if Mary' story is only a fiction, hospital-acquired infections are not. Even if medicine did amazing progress over the past years, so called *nosocomial* infections are not necessary disappearing. According to the OMS, even in high-income countries, over one hundred patients, at least seven will contract a nosocomial infection.
Indeed, the environment as well as medical devices are difficult to control and a simple contact between an health worker and a patient can be enough for the spreading.
For bacteria, immunosuppressive therapy related to implants are real boon and consequences are not negligible. From simple abscess, otitis, urinary tract infection to pneumonia or meningitis, bacterial infections are varied and can lead to death.
There is, of course, not only one responsible bacterium. However, *Staphyloccocus Aureus* is frequently mentioned for its significant pathogenic power and its Methicillin-Resistant strains (MRSA) that causes so much trouble to hospital staffs. Consequently, there is an urgent need for efficient detectors to struggle nosocomial infections.

In the adult human body, the infectious dose of *Staphilococcus* is about **100 000 micro-**

organisms[1] [1]. This represents an extremely low concentration in the whole body that is very difficult to detect in early stages of the infection.
The detection of bacteria is not new. Traditional methods as agar-based cultures and counting, PCR and ELISA have proven their efficiency but still lack ease of use and rapidity. Specialised biosensors precisely step into this breach.
By the means of optical, mechanical or even electrochemical transducers, they succeed in detecting ever smaller concentrations or activities of chemical species, but also living cells, in various types of sample. With regards to bacteria, the ultimate aim is to reach a sensitivity at least as well as traditional methods but with a much lower cost in time and money.
Nowadays, this is not exactly the case and only few scientific authors claim a limit of detection as small as 10 CFU/mL [2].

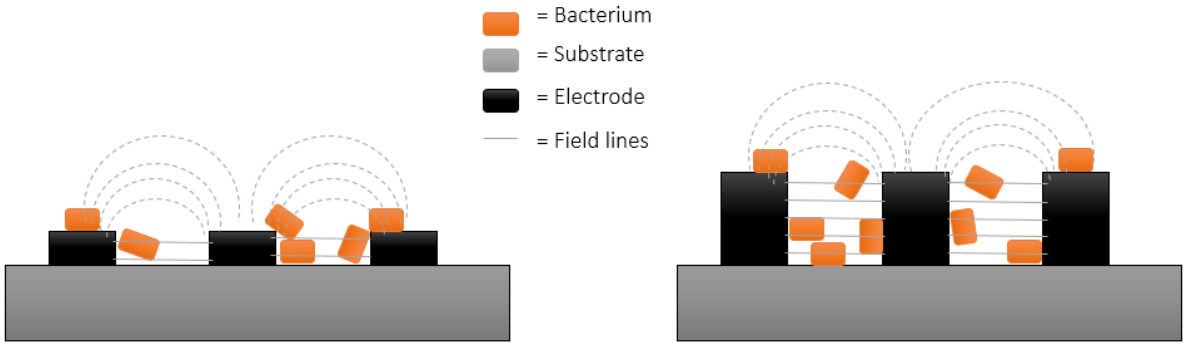


Figure 1.1: Building thicker electrodes might increase the probability of trapping bacteria between them as well as the capacitance. At the same time, bacteria are less likely to settle on top of these electrodes where they have a minimum impact on the global impedance.

In this master thesis, we focused on an electrochemical biosensor and, more specifically, an impedance-based IDE [3] sensor previously developed by Numa Couniot during his PhD thesis [2]. In those rectangular comb-like electrodes, the thickness might have a positive impact on the sensitivity of the sensor. Indeed, by increasing the electrodes thickness the global measured capacitance will be more important which will increase the sensitivity. Theoretically, a larger cavity also means more chance for bacteria to settle into a concentrated electric field zone and therefore to be detected. Increasing electrodes thickness is our first objective in order to analyse whether or not this parameter does significantly improve the sensor performances.
However, changing one parameter often requires to re-think the whole process. For an eventual integration with CMOS technology, the previous sensor involved aluminium electrodes. This can no longer be as aluminium is limited to thin film depositions. High aspect ratio structures also involve special resists in order to reach thicknesses larger than 3 μm.
We improved the process step by step to reach targeted dimensions with the best definition possible. The result is a new process based on electroplated nickel forming the sensor's electrodes. These electrodes are then covered with alumina to protect them from corrosion.

Once manufactured, sensors were tested under dry environment to compare their raw electric properties with theoretical values.

Afterwards, we tested sensors under liquid environment with inflow of *Staphylococcus Epidermis* in PBS through a microfluidic system. This strain was selected for its proximity to the

[1] Number of micro-organisms in the inoculum to successfully infect a host.
[2] **C**olony **F**orming **U**nit
[3] **I**nter**D**igitated **E**lectrodes.

Staphylococcus Aureus without its dangerousness. To increase the adhesion of bacteria to sensors, we used polydopamine, known as a biological glue.
Afterwards, admittances were injected in the following equation $S = ||\frac{|Y_B|-|Y_D|}{Y_D}||$, with Y_B and Y_D respectively the signal admittance of solution with and without bacteria, in order to compute the sensitivity.

The final process is described in Chapter 3. An analyse of manufactured sensors is detailed in the Chapter 4 as well as an analyse of those experiments. Results will be exposed and commented with the support of a simulation. Finely, the last chapter will present the conclusion and the perspectives drawn from these results.

Chapter 2

State of the Art

2.1 Bacterial detection

What is a bacterium?

Vander's Human Physiology [3] gives the following definition:

"Bacteria are unicellular organisms with an external surfacing (cell wall) in addition to a plasmic membrane. In opposition to eukaryotes, bacteria have no organelles surrounded by membranes."

Bacteria are microscopic living organisms which can be found everywhere on Earth.
Even if most bacteria are not harmful and can even be beneficial to its host, some can still cause infectious diseases [4]. They can, among other things, cause tissue damages while replicating or even produce toxins that can disrupt physiological functions through the blood stream.

Why do we need to detect bacteria?

Given their ability to multiply quickly and easily in various environments, the consequences of a bacterial infection must not be taken lightly. In 1999, of all annual deaths, 40 % were due to infectious diseases [4]. Bacteria which can cause such diseases are qualified as pathogenic. In 2013, the *Center for Disease Control and Prevention* reported at least 23 000 deaths each year in the United States of America due to bacteria that are resistant to antibiotics.
This resistance is often due to the inappropriate use of antibiotics. Therefore, being able to detect the concentration and identifying which type of bacteria we are dealing with is essential.

In the field of bacterial detection, various methods already exist. They include a wide range of techniques, all trying to optimise important parameters such as the **Limit of Detection** (LoD) and **speed**.

A rapid and accurate detection is especially important when the patient condition is life threatening. In this domain, biosensors could soon become a convenient tool for doctors. Some authors go further and claim that we *"could find the molecules of disease right away, identifying them in a doctor's office while the patient waits 20 minutes"* [5]. However, at this stage, most of these newest techniques are not fully adapted to everyday use. In addition to the high cost, the bacteria biosensor must be able to exhibit a high degree of selectivity: in blood it may be as much as 1000 target-bacteria for billions irrelevant particles.

Medicine is not the only domain where it is important to control the presence of bacteria. The legislation governing the food industry is particularly strict in this respect [6].
For example, in the dairy industry, and more specifically, yoghurt making, probiotics (e.g.: *streptococcus thermophilus*) are used in the manufacturing process. These bacteria are healthy but their concentration still needs to be controlled in order to obtain an optimal product.
Conversely, some pathogenic bacteria are not tolerable. *Salmonella enterica*, responsible for gastroenteritis, must not be found at all in 25 g of the final product [7] [8]. However, nowadays, the detection limit obtained with PCR methods are only slightly better than 10 cells in 10 g of product [9].
In order to follow regulations, industries must have reliable techniques to facilitate the quick and precise detection of micro-organisms. For food, as well as for water and environmental quality control, there is a real need to obtain analytical results in the shortest time possible [6].

Few years ago, biosensors were qualified as "promising new approaches". Nowadays, they are better understood and are starting to compete with what we could call "traditional techniques". They have the potential to shorten the time span between sample uptake and results but still need to be improved in respect of better selectivity and sensitivity [6].
There is still much work to do before biosensors become a real alternative. Nonetheless, in 2007, biosensor technology was ranked fourth in the field of pathogen detection (Ref: [6]).

2.1.1 Performances: key concepts

Before describing these techniques, it is important to understand what criteria we are looking for. Indeed, whether it is a conventional method or a biosensor, all detection devices must meet a number of requirements. Below is a list of the major parameters identified by Ivnitski *et al.* [4]:

- Low detection limit
- Species selectivity
- Strain selectivity
- Assay time
- Precision
- Assay protocol
- Measurement
- Format
- Operator
- Viable cell count
- Size

To meet these requirements, we need efficient tools to compare performances. Details and quantities used to characterize the performance of biosensor include [2]:

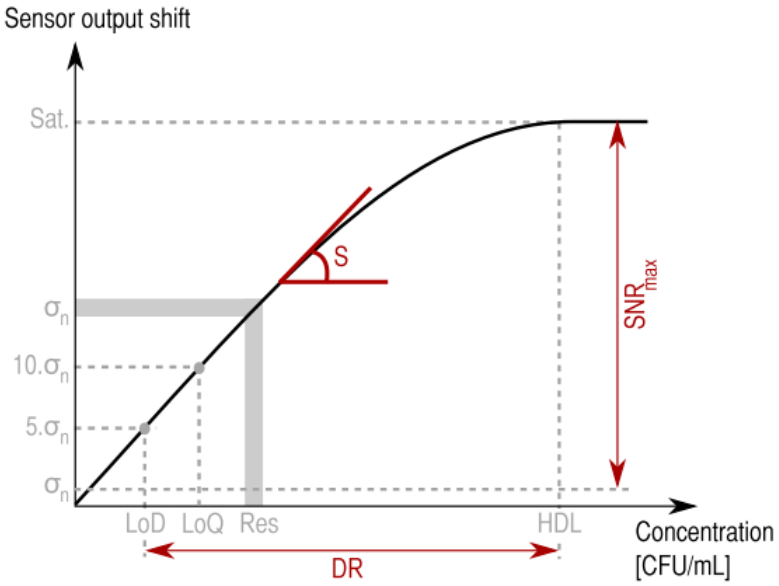


Figure 2.1: Schematic representation of the sensor output shift versus the bacterial concentration where *LoD* stands for Limit of Detection, *Res* for resolution, *HDL* for Highest Detectable Level and *S*, sensitivity (illustration from [2]).

- **Limit of detection** (**LoD**) is defined as the smallest amount of target that can be reliably detected [10] and is usually expressed in CFU/mL [2]. It is frequently confused with **sensitivity**, which is the slope of the response curve and describes the rate of change in response to a change in analyte concentration. Both can be found on the graph in Figure 2.1
  The LoD can be obtained by measuring the sensor response to ever smaller concentration of the target. It will be the smallest concentration at which the response is clearly distinguishable from a solution with no target bacteria.
  A comparison with a blank response is important, otherwise the results can be overestimated. Likewise, the user must be careful because this limit of detection is often calculated from clean samples where only the target biological species can be found. This is of course very different from real-world samples.
  Reproducibility also has an impact on the limit of detection. Requirements vary according to the application. For a high affinity probe-target, conventional techniques like ELISA (Enzyme Linked Immunosorbent Assay, see section 2.1.2 for further detail) routinely obtain pg/mL detection limits.

- **Dynamic Range** (**DR**) is the ratio of the largest measurable target concentration (**HDL** = Highest detectable level) to the limit of detection [10]. Testing less and less diluted solution can be a way to detect the upper concentration. When reaching the **HDL** surface saturate, the signal loses its linearity.
  The DR is important in applications requiring the quantification of the bacterial concentration and not only the detection of its presence.

- **Resolution** (**Res**) is also called the precision. It is the smallest detectable change [10], or error expressed in CFU/mL [2] in the target concentration. It is associated with the sensor noise σ_n resulting from electrical and biological noise sources.

- **Maximal Signal To Noise Ratio** is a measure to compare the level of a desired signal to the level of background noise.

- **Detection Time** is the time taken to obtain unambiguous stable signal that can be interpreted. It encompasses all steps from the sample conditioning.
- **Multiplexing** is the detection of several targets in the same biological sample. It is a way to save time and reduce both cost and sample volume.
- **Selectivity** : In real-world applications actual samples typically contain an uncontrolled and significant amount of **non-target molecules**. For example blood serum typically contains 70 mg/mL of all type of proteins but the biosensor must detect only the target. Daniels *et al.* [10] give us the following example of prostate specific antigen (PSA), a biomarker for prostate cancer, that needs to be detected at a concentration of 2 ng/mL in blood.
  "Generally speaking, label-free biosensors cannot distinguish between specific and nonspecific interactions except by probe selectivity, regardless of the readout method" [10]. *Non specific binding* is a major issue because it prevents target binding and causes false positives. To alleviate this problem, the use of a *blocking agent* or *antifouling agents* is one solution. But, sometimes a simple wash before readout can improve selectivity as it washes away the non-specifically adsorbed molecules [10].

2.1.2 Traditional methods

What is referred to as a "traditional method" in this paper is a detection technique that is commonly used for at least 10 years and does not involve transducer elements. They are better known and mastered than biosensors, but still in development.
They include **culture and colony counting**, Polymerase Chain Reaction (**PCR**) which involves DNA analysis, **immunology-based** methods (antigen–antibody interactions) and matrix-assisted laser desorption ionization time-of-flight mass spectroscopy (**MALDI-TOF MS**) which we will explain in more detail further in this work.

Conventional bacterial detection methods may take up to 7 or 8 days to yield a response, which is time-consuming and is labour-intensive [11]. But they are still frequently used because of their high selectivity and sensitivity [6].
The most commonly studied model bacterium is *Escherichia coli* but we can also find a large number of articles which test and compare different techniques using *Salmonellae* [6] [4] and *Staphylococcus aureus* or often its less dangerous version (but nonetheless potentially pathogenic) *Staphylococcus epidermidis* [12].

Culture and colony counting:

This test is based on the growth abilities of bacteria. The infected environment is spread on a growth medium, usually agar-based (a type of gel made from algae [13]), suitable for the development of specific micro-organisms. One single cell will therefore grow into a colony under controlled laboratory conditions (temperature, oxygen, nutriments) and give a similar result as in Figure 2.2.

These colonies become visible and can be counted. The use of a selective [15] or differential media will enable the researcher to select which bacteria will be able to develop itself. The sample's microbial population can therefore be calculated as the number of colony forming units (**CFU**). However this measure is skewed. Detected colonies, in fact, only origine from cells that can grow under test conditions. Moreover, a colony does not always originate from a single cell but instead represents the cells that happened to separate on the plate. The more numerous they are, the less distinguishable and this is why this method presents an upper limit. Its relatively narrow countable range (about 25-250 CFU bacteria on a standard petri dish) represents one of



Figure 2.2: A bacteria culture on agar plate (illustration from [14]).

its major limitations [16].

This is the oldest bacterial detection method and also the **most time-consuming** [17]. Indeed, the amplification step alone can take from a few hours to days [11] depending on the type of bacteria.
Usually a single test does not provide a definitive answer but will require a complex series of tests. It requires at least the following basic steps: pre-enrichment, selective enrichment, biochemical screening (for more accurate identification of the pathogen), and serological confirmation. It may take 5 to 7 days to get a confirmed result according to Swaminathan and Feng (1994) [15]. Lazcka *et al.*[6] even mention 14 to 16 days.

Polymerase Chain Reaction:

The Polymerase Chain Reaction (**PCR**) is another frequently used technique to detect and identify bacteria. It probably represents the fastest traditional methods [18] but, unlike the on-medium culture, DNA strands are detected, not entire bacteria colonies.

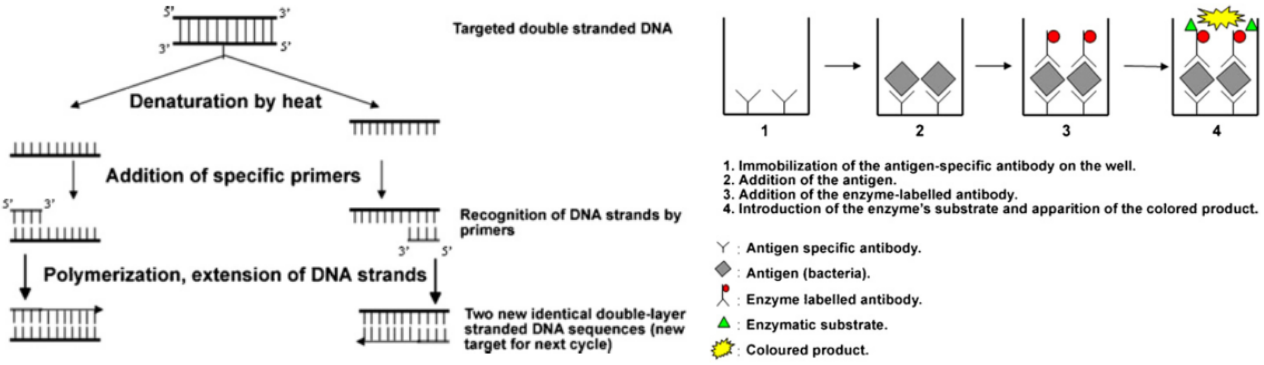
To be properly amplified, bacteria are broken (cell lysis) and their DNA released. Then it still has to undergo several steps: **strand separation** by heating the purified DNA (denaturation) [19], followed by an **extension phase** using specific primers (hybridization with the DNA) and a thermostable polymerization enzyme. Then, each new double-stranded DNA acts as a target for a new cycle. This is how **exponential amplification** is obtained [6](Figure 2.3a).
This DNA multiplication is very efficient. At the end of 25 PCR cycles, 35 millions target DNA molecules are obtained [20]. They can be trapped using their complementary strands, which are immobilised on a support, because the single-strands on its own is unstable. If sample's DNA have been previously paired with a dye, the corresponding areas will be recognisable.
Of course, PCR amplified sequences can also be subsequently detected by gel electrophoresis or even using biosensors.

However, this technique cannot differentiate living cells from dead ones as DNA is present in both. The **Real-Time-PCR** method was developed in order to solve this problem. It synthesizes single-stranded DNA from RNA strands and several genes only present during bacterial growth can then be detected [6], but it may take more than 24 hours [21].
Other limitations are, among others, inhibition phenomenon of the PCR and cross contamination between samples [18].

PCR is commonly used and many different versions of it can be found, for example:

- **Multiplex PCR**: allows the simultaneous detection of several organisms by introducing different primers to amplify DNA regions coding for specific genes of each bacterial strain targeted. The dyes linked to the PCR primers are of various colors.
- **Real-Time** or quantitative chain reaction (**qPCR**): The amplified DNA is detected as the reaction progresses given that the fluorescence intensity is proportional to the amount of the targeted gene [19].

PCR is not the only ultra-sensitive detection methods based on nucleic acid amplification that was introduced. LCR (ligase chain reaction) and SDA (strand displacement amplification) [22], among others, are employed.
All of these techniques are capable of detecting low numbers of bacterial cells within several hours. However, this is expensive and requires prior isolation of bacterial DNA. Bacterial cell lysis is a laborious and time-consuming process, especially for *S. aureus* (Gram-positive bacteria) requiring lysostaphin to break down the thick cell wall [22].



(a) (b)

Figure 2.3: a) Schematic representation of one PCR cycle (illustration from [6]) and b), schematic representation of the sandwich-ELISA protocol (illustration from [6]).

Immunology-based methods:

The most commonly used technique is the Enzyme-Linked Immunosorbent Assay (**ELISA**). It is based on the interaction between antibodies and bacterial surface, which is a major mechanism in the immune system that enables a rapid and accurate targeting of a pathogen. The addition of substrate giving *coloured, fluorescent, or luminescent reaction products* makes it possible to determine the concentrations of the reactants at very low levels [23] down to an LoD of 10^5 CFU/mL in [2].

Different configurations exist. Among them, the *sandwich ELISA*, illustrated in Figure 2.3b, is the most common.
First, each well is precoated with **capture antibodies**. They are named this way because because of their ability to selectively bind the target bacteria. It is precisely a solution suspected to contain this bacteria (the **analyte**) that is next introduced. Then, after washing, specific antibodies that can bind to the bacteria antigens are added. They form a sandwich-like structure. This second probe ("**detection antigen**") is labelled or can be detected by introducing another labelled probe binding to all the secondary probes. Depending on the labelling, the fluorescence

	Culture	**ELISA**	**PCR**	**MALDI-TOF**
Complexity	Very low	High	Very high	Very high
Cost	Very low	High	Very high	High
LoD	1 CFU/mL	10^{1-6} CFU/mL	10^{1-2} CFU/mL	10^{5-6} CFU/mL
Analysis Time	>2 days	10 - 24 h	1-2 h	10 min
Selectivity	Very high	High	Very high	High
Reference	[6]	[15]	[6]	[26]

Table 2.1: Conventional methods for the detection of bacterial cells (from [2]).

or colorimetric level can then be measured to quantify the presence of target bacteria [10]. Unfortunately, there are many factors that influence the sensitivity achieved by a sandwish assay and the affinity of the antibody is one of them.
For pre-treatment or pre-concentration steps, immunomagnetic separation can be done by introducing antibody coated magnetic beads in a bacterial suspension and combining it with almost any detection methods [6].

Matrix-Assisted Laser Desorption Ionization Time-Of-Flight Mass Spectroscopy:

Unlike previous techniques, which required lengthy incubation procedures, **MALDI-TOF MS** can identify bacterial species in a few minutes, directly from a freshly grown colony [21]. Therefore, identification of bacteria can be directly done from clinical samples, such as blood culture [24].

The classic Mass Spectroscopy is the production of spectra from the detection of mass-to-charge ratio *(m/z)* of a bioanalyte. However, this method is restricted to low molecular masses as small protein (from 1,000 Da to 9,000 Da).
MALDI-TOF, which is a *soft ionisation* technique, proved to be an effective bacterial identification [24], it allows mainly the detection of macromolecules (above 10,000 Da) in complex mixtures without prior purification [25].
The *most probable species identity* is deduced from a comparison of the mass fingerprint of the microbial sample with a database. Results are not always obvious as this is based on the analysis of *phenotypic characters*, which can vary with culture media and incubation times. [24]. The distinction between Gram-positive bacteria is not possible either.

If using MALDI-TOF MS is faster (10 [26] to 20 minutes [25]), it is also relatively expensive. However, some research suggest that it could be used to analyse the antibiotic susceptibility of bacteria [25]. For *Staphylococcus*, spectral profiles differ greatly whether it is a methicillin-susceptible or methicillin-resistant (MRSA) *S.aureus*.

The comparative Table 2.1 shows that the limit of detection of 10^{5-6} CFU/mL [26] is not the best compared to ELISA, PCR or especially culture. These characteristics are closer to devices of the next section: biosensors.

2.2 Biosensors

Even though aforementioned traditional techniques are very sensitive and often used, there is a real need today for smaller, faster and more precise devices to enable an effective and convenient

bacterial detection and identification. Biosensors present such potential but still requires further enhancement to reach at least the same detection levels as established methods which lie within **10 and 100 CFU/mL** at a reasonable cost.
Another preoccupation is the ease of use, thus having a device which does not require highly qualified technical staff. Other biosensors requirements are mentioned in the section 2.1.1.

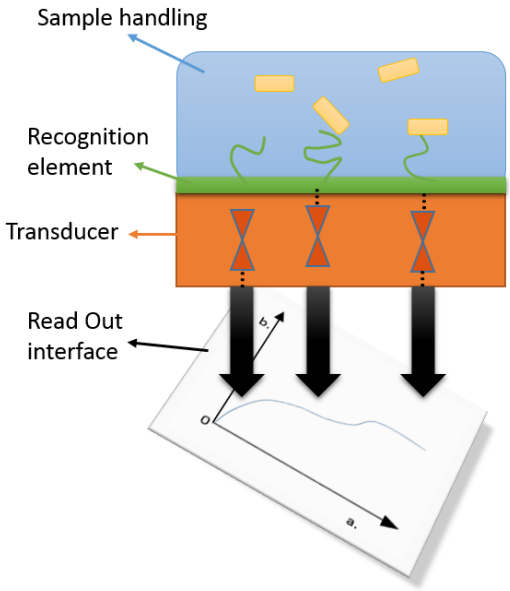


Figure 2.4: Schematic representation of the four main parts of a biosensor.

What exactly is a Biosensor?
"A biosensor is a system or device which incorporates a biologically active material in intimate contact with an appropriate transduction element for the purpose of detecting the concentration or activity of chemical species in any type of sample" [27].

Biosensors are very different from each other but each of them can be divided into 4 important parts illustrated in Figure 2.4: **sample handling**, a **recognition element**, a **transducer**, and a **readout interface**. To be able to achieve detection levels with ever smaller concentrations, some devices include one and sometimes multiple amplification systems [28].

The following section classify biosensors depending on their transduction methods or, in other words, how the presence of bacteria is converted into a physical signal, proportional to their concentration. Three major classes will be described : **optical**, **acoustic** and **electrochemical** transducers. Nevertheless, literature also reports **thermal** and **magnetic** transducers which are not detailed in this work.

2.2.1 Optical biosensors

This kind of biosensors detects bacteria through minute variations in **optical phenomena** (absorbance, fluorescence, luminescence, reflectance). This could be due to a label or a change in the refractive index or thickness [4], attesting interactions between target analytes and the bioreceptor [27]. The resulting selectivity and sensitivity make this technique very popular for bioanalysis [6].
Mechanical techniques as Quartz Crystal Microbalance (QCM) and Surface-Plasmon Resonance

(SPR), described in the following section, are notable examples of devices that can operate as label-free, real-time biosensors [10]. But labels are all the same used as amplification methods to increase these sensors abilities to detect relatively small changes in surface properties.

Tapered Optical-Fibre Biosensors

TOFBS are based on one reliable and sensitive optical method that is evanescent sensing [29].

Initially intended for light propagation with minimal loss (by total internal reflection (TIR)), optical fibres can also be used for sensing. Reducing, if not removing, the fibre's cladding will enable the light travelling inside the core to interact with the fibre's surrounding. If this cladding is replaced by the analyte, interaction with the evanescent field of the transmitted light, as well as attenuations, will provide information on its nature.

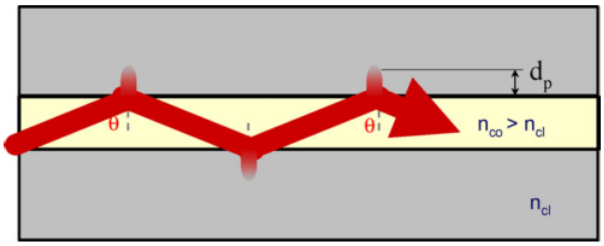


Figure 2.5: *"The cross-section profile of an optical fibre cut along the long axis. The thick arrow represents one mode of light entering in multi-mode with an angle of incidence θ. Even though most of the light is propagated, there is a small portion known as the evanescent field that decays to 1/e of its value at the core-cladding interface at a distance of d_p. Typical SM fibers that operate at 1310 - 1550 nm have a core of of 8 μm and an overall diameter of 125 μm"* (illustration from [29]).

However, the penetration depth (d_p in Figure 2.5) is typically too small ($\sim$ 0.145 μm) for sensing bacteria (around 1 μm) and is quite limited for protein (around 10 nm). Therefore, investigators have attempted to manipulate the evanescent field to increase sensitivity and indirectly, the penetration depth.

Advantages of fibre-optic biosensors include chemical-inertness, compatibility to a wide range of surface modifications which allow for a better selectivity, low-cost, and the ready availability of inexpensive lasers and photo-detectors.

Surface-Plasmon Resonance

Surface Plasmon Resonance (**SPR**) is another use of the evanescent wave.
The main feature is the presence of a thin metal surface (often gold or silver [29]) covering the dielectric material. This dielectric can be a fibre but also a plate or even a prism so that the path of light is controlled. The optical energy, instead of interacting directly with analyte or exciting fluorescent molecule, is transferred to the metal layer as packets of electron called *plasmon* [29].

After this surface has been irradiated with p-polarised light, reflectivity is measured as a function of the angle of incidence θ. The collective oscillatory excitement of electrons propagating between the metal film and dielectric interface (the plasmon wave), lead to an almost complete

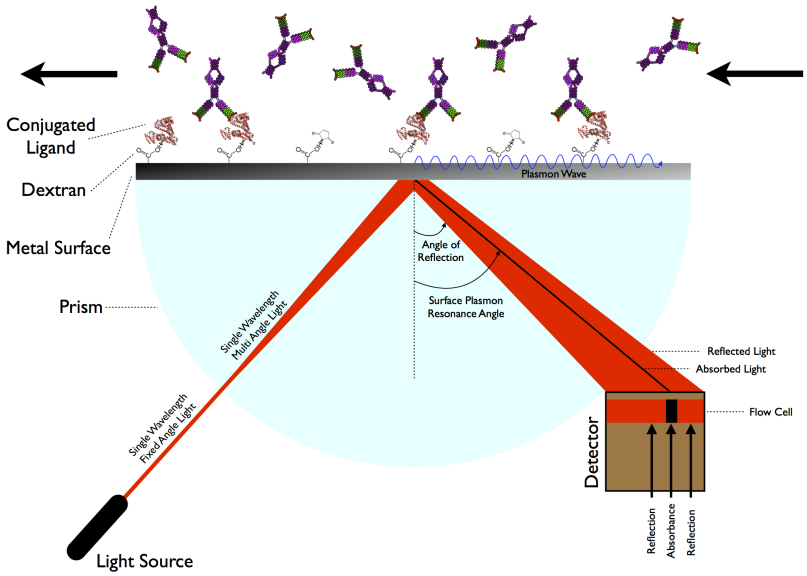


Figure 2.6: Illustration of Surface Plasmon Resonance working principle (illustration from [30]).

absorption of light at a specific θ [27]. Therefore, the intensity of reflected light is greatly reduced and the resulting plot is a curve showing a minimum at this angle.
The condition for resonance, and so the SPR minimum, depends on the properties of the metal-solution interface. These properties might be influenced by the refractive index of the analyte. Perturbations as low as an antigen linking to an antibody are enough to change the signal. Therefore by measuring the resonance angle, information about the bacteria concentration can be obtained.

Some drawbacks to this method are its complexity and large size instruments. *"The development of fibre optic-based SPR should alleviate some of these problems"*[29]. It is a powerful technique but still expensive [6].

Fluorescence detection

To enhance sensitivity, several techniques take advantage of a certain form of luminescence called the fluorescence.
The aim is to produce an extra signal that could be detected. This is called an indirect detection in opposition to direct sensing that detect a specific target before and after a reaction.
In indirect sensing, a label able to bind to the bacteria is used. This label, previously exited by absorption of light of sufficient energy, is able to emit a photon (in less than 1 ns [6]). This phenomena is called fluorescence and happens with little thermal loss.

Another type of sensing is known as the Fluorescence Resonance Energy Transfer **FRET**. It requires two probes to generate a unique fluorescence signal: one donor (a fluorophore) and one acceptor (chromophore). By playing on the the nature of these probes or the distance between them, we can generate a controlled fluorescent signal.
This distance can be tuned by bringing two different molecules together or by a conformational change if both donnor and acceptor are on the same molecule [27].

The most common way to bind labels (fluorophores, quantum dots or gold nanoparticules (NP)) to their target is through antibodies. However, most fluorescent molecules, such as *Fluorescein isothiocyanate (FITC)*, have a limited lifetime which complicates the process.

Using fluorescence require a light detection device but is most efficient when combined with established techniques such as PCR and ELISA [6, 11]. In 2015, Wang *et al.* developed a novel approach using multicolours quantum dots (QDs) with various emission wavelengths conjugated with specific antibodies to subsequently capture separately three types of bacteria. Authors consider that this multiplex fluoroimmunoassay could have enormous potential for *"rapid, simultaneous multiple pathogenic bacteria detection in various food samples"*. They obtain a LoD close to 10^2 CFU/mL [11] which is one of the lowest quantity up to now.

Colorimetry, Fourier Transform Infrared spectroscopy (FTIR) and Bioluminescence are other physical principles that can be operated in optical biosensors but won't be detailed in this work.

2.2.2 Acoustic biosensors

These are mass sensitive biosensors. The principle that is tapped to obtain a "weighing of bacteria" is the piezoelectricity (revealed in 1880 by the brothers Pierre and Jacques Curie) [31] [32]. More specifically, it is the **converse piezoelectric effect** which produces acoustic waves in the device if a suitable electric field has been applied on some specific materials [33]. These waves propagate through the substrate and are then transformed back into an electric field for measurement. When the piezoelectric element experiences a load [34], it presents a frequency shift. This is why it can be used to make highly sensitive balances.

Depending on the wave propagation path, either through or on the surface of the piezoelectric substrate, acoustic devices can be sorted into different categories: **bulk** and **surface** wave respectively.

With different crystallographic orientation of the quartz substrate (or the piezo-ceramic material) during excitation, many forms of wave can be generated. They can be **longitudinal**, **transversal** or even a mix of both (**Rayleigh wave**).
Longitudinal waves cannot be employed in liquid due to the fact that their excitation is perpendicular to the liquid environment and would therefore be too attenuated. This is problematic for the purpose of bacteria detection because their natural environment is a liquid media and they can't be dehydrated without risking a denaturation. The Transverse Shear Mode (**TSM**) does not have this problem. Its particle displacements are normal to the direction of wave propagation, then allowing the use of the sensor in liquid media.

The quartz substrate can have varying dimensions and typically operate at frequencies between 1 MHz and 10 MHz, with a frequency-determination limit of 0.1 Hz and a LoD of mass bound to the electrode surface of 10^{-10} to 10^{-11} g [27]. When it comes to Surface Accoustic Waves (**SAW**), these frequencies are more important (30 to 500 MHz [33]) as the propagation of the wave does not require to go through the whole substrate but only the surface.
Bleustein-Gulyaev (BG) mode, shear-horizontal surface acoustic waves (SH-SAW), Love mode or Lamb mode are examples of surface generated acoustic waves that experienced a growing interest in the sensor field in the past few years. We wont go into details in this work but you can find a lot of information about such devices in the literature [34].
The main problem with the extreme sensitivity of the piezoelectric element is that it is also sensitive to all kinds of perturbation on the electric field path [2].

Acoustic biosensors can adopt many shapes. In the following paragraphs, we will describe two of them.

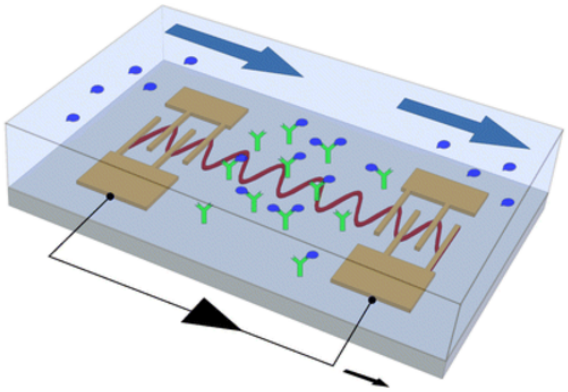


Figure 2.7: *"SAW based biosensor immersed in a sample flow. Analyte molecules binding to the immobilized antibodies on the sensor surface will influence the velocity of the SAW and hence the output signal generated by the driving electronics"* (illustration from [35]).

The first is **Quartz Crystal Microbalances** (**QCM**).
It operates with bulk acoustic waves as it is made of a thin AT-cut quartz crystal sandwiched between two metal electrodes [36]. The electric field is established across the crystal.
These mass-sensitive devices were extensively investigated as a transducer in hybridization based nucleic acid biosensors for the detection of gene mutation [32]. DNA is trapped by hybridation or anti-ssDNA antibodies. In some cases (detection coupled with PCR) gold nanoparticles signal amplification [32] can be used but this still requires a preliminary cell lysis. To bind whole bacterial cells, the sensing surface can be covered with the appropriate antibodies. The chemical functionalization can be done via a chemical functionalization on self assembled monolayers. Carefully controlling the surface density of immobilized probes increases the limit of detection and quantification significantly [27].
QCM devices can also be used in the study of microbial biofilm and surface adhesion when working with whole bacteria.

An other form of mechanical acoustic application is as **micro-cantilevers**. It uses the same principle as described before: antibodies are immobilized on the sensor surface and as soon as the antigenic target (pathogen) binds, the increase of mass causes either a shift in resonance frequency or a simple deflection of the cantilever. This shift or deflection are both signal proportional to the target concentration.
What makes them "cantilever" is their shape: composite of a piezoelectric layer (that can bend, twist or oscillate) bonded to a nonpiezoelectric base. Hence their name piezoelectric-excited millimeter-sized cantilever (**PEMC**) sensors. In fact it is the same technology as in a scanning probe microscope [37]. Consequently, batch fabrication and low cost can be achieved.
Just as AFM, micro-cantilevers can be affected by changes in temperature, humidity [38] and pH but have the key advantage of being able to detect species in liquid medium, and that, without any labels. Detection levels as small as 10 cells per ml in a 10 ml sample were reported [39].
However, the position of the target cell along the cantilever affects the frequency shift and therefore the result [40].

2.2.3 Electrochemical biosensors

Electromechanical transducers are mainly based on the observation of parameters such as current or potential changes. It excludes previously described biosensors (optical and acoustic).

These devices provide signals in the form of an electrochemical response as results of target-analytes reactions, such as a bacteria-antigen binding [10].
Electrochemical biosensors have the ability to operate in turbid media, unlike analytical transducing systems. Moreover, they have a greater potential of miniaturisation and cheaper equipment which does not always required skilled personnel [41].

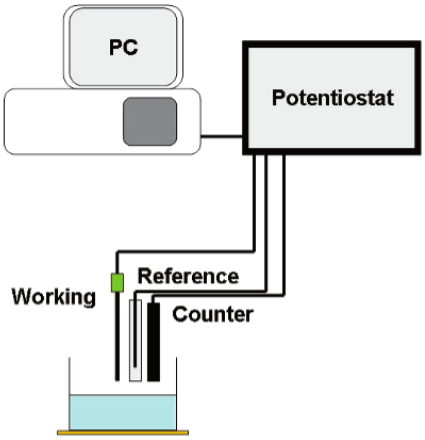


Figure 2.8: An example of a voltametric system. Potentiostat (= data aquisition system) (illustration from [42]).

These devices can be classified into three main categories depending on the type of signal that is measured: current, potential or impedance.

Amperometric methods work on the ground of an existing linear relationship between analyte concentration and **current** when a fixed potential is applied on the sensor. The voltage, depending on the redox reaction involved, will oxidize or reduce the analyte which ends up producing a current at the electrodes.
This may call for redox mediators when direct electron exchange is not permitted. Redox mediators are *"small size compounds able to reversibly exchange electrons between both the sensor and the enzyme of choice"* [6] In biosensors, they are used in combination with a redox enzyme system that catalytically converts electrochemically non-active analytes into products that can be oxidized or reduced at a working electrode [42]. For example, with glucose oxidase enzymes trapped on electrodes, this type of transducers have successfully been used as glucose detector [6, 43]. In this case, $K_3Fe(CN)_6$ (the mediator) is electrochemically detected after accepting electron from Glucose Dehydrogenase. However, $K_3Fe(CN)_6$ can also be reduced by microbial metabolism and this allows the quantitative determination of bacteria in 20 min [41]. It has been tested on *E.Coli* with a detection range from $4.7{\cdot}10^6$ to $2.4{\cdot}10^9$ CFU/mL in cultivation medium [44].

Potentiometric methods measure an open circuit DC voltage whereas the amperometric system worked on a shorted current.
In this case, when a DC current is applied, electrochemical reactions happen and influence the potential. Measuring it will therefore provide information on the ionic activity.
These methods are the least used. But they could theoretically detect extremely small changes in concentration.

Electrochemical impedance spectroscopy (EIS) works without using enzyme labels or redox mediators [18]. This simplifies greatly the sensors' preparation. It is a promising device due to low cost and ease of miniaturisation [10].

EIS consists in the application of a small amplitude A.C. signal superimposed over a base constant potential or current. The resulting impedance of the system then provides information related to interfacial and bulk phenomena [18].
Studying the impedance, requires a mathematical treatment more complex because of its imaginary part. This is why, its magnitude and phase are more often analysed than the complete signal.
This work being based on impedance-biosensors, this topic will be further developed in the following sections.

Until now, the main drawback of this technique was that it had relatively poor detection sensitivity compared to traditional methods. However, some authors succeeded in improving the results by means of some parameters optimisation. Some have managed to improve performances by changing the recognition element (aptamers in [45]), the sample delivering method (microfluidic in [46]), or even to overcome limitations due to extremely low cell numbers by increasing the concentration of the target bacteria via electrical techniques [47].

Lazcka *et al.* [6] in 2007 wrote *"it is not entirely unreasonable to believe that using the appropriate electrode configuration and sample pre-treatment steps, detection limits below* 10^3 *CFU/mL could be achieved"*.
But at the same time, Daniels *et al.* [10] seemed more pessimistic and *"doubt that label-free affinity impedance biosensors will ever achieve the same sensitivity as label-based techniques such as conventional ELISAs due to the limitations of both label-free detection (eliminating the possibility of chemical amplification) and sensitivity of impedance readout."*

Yasukawa *et al.*[28] presented a slightly different use of current analysis as the actual signal is obtained by anodic stripping voltametry which is an electrochemical method for trace analyses of metal. This amount of metal will be directly related to the presence of their target analyte. Metal stripping voltametry is considered as *"the most sensitive of all commonly used electroanalytical techniques"* [48], it is very effective to detect extremely low levels of metal and thus, minute changes. Even if Yasukawa's technique is more oriented towards protein detection than whole bacteria, it has already reached promising detection limits (0.01 ng/mL).

	Method	Medium	Bacteria	Selectivity	LoD	Time	Source
Optical	SPR	PBS	*S.aureus*	Ab	10^5 CFU/mL	NA	[49]
	SPR	PBS	*MRSA*	Bacteriophages	10^3 CFU/mL	20 min	[50]
	SPR	NA	*S.aureus*	Ab	$\sim$ 20 CFU/mL	NA	[51]
	Colorimetry	CS	*MRSA*	PCR + NP	500 ng amplic.	NA	[52]
	Fluorescence	SELEX	*S.aureus*	Ap. + MP+NP	1 CFU/mL	1.5 h	[22]
	Dual-color Fluo.	PBS	*S.aureus*	Ap. + MNP	8 CFU/mL	NA	[53]
Acoustic	SAW	PBS	*wc E.coli*	Ab-SAM	10^6 CFU/mL	1 h	[54]
	SPQC	Milk	*S.aureus*	Aptamers	41 CFU/mL	1 h	[55]
Electrochemical	Potentiometry	PBS	*S.aureus*	Aptamers	$8 * 10^2$ CFU/mL	20 min	[45]
	Voltametry	milk	*S.aureus*	RbIgG	$3.7 * 10^2$ CFU/mL	90 min	[56]
	Amperometry	milk	*S.aureus*	Ab-ELISA	1 CFU/g	18 h	[57]
	Voltametry	GM.	*S.aureus*	Antibiotics	$6.5 * 10^2$ CFU/mL	3 h	[58]
	EIS.	PBS	*S.aureus*	Ab-SAM	10^2 CFU/mL	2 h	[59]
	EIS.	PBS	*S.aureus*	Ab-SAM	10 CFU/mL	NA	[60]
	EIS.	PBS	*MRSA*	PCR	10 nm	$\sim$ 2 h	[61]
	EIS.	PBS	*S.aureus*	Ab	10^2 CFU/mL	NA	[62]
	ISFET	NaCl	*Salmonella*	Ab	100 CFU/mL	1 h	[63]

Table 2.2: Comparison between several kinds of biosensors for bacterial detection (adapted from [2]). The time parameter takes into account the sample preparation.

2.2.4 Selectivity means

Biosensors are very useful micro-systems which can have a wide range of use. However, when it comes to organic and living element, we have to pay an extra attention to possible interactions. In the case of a bacterium (as *S. aureus*), electrode surface (before and after modification) should not affect the sample composition or integrity in any way. Gold, which is a well known bio-compatible metal, is often used when dealing with bacteria.
The ideal biosensor must not only respond to low concentrations of analytes, but also have the ability to **discriminate among species** [29]. Sometimes, this is done by using a medium in which targets can selectively grow [15].
Most biosensors rather include **bio-recognition elements**. They are biological species which are added to the system due to their ability to **selectively bind the target**. These can be antibodies which can detect the whole cell, DNA strands but also aptamer and peptides. Lytic enzymes and bacteriophages, which will fragment the cell and release inside compounds which will become detectable, can also be used.

Integrating these bio-receptors to the micro-system can be done by different techniques.
For bacterial sensing, antibodies and enzymes are commonly grafted on the surface using either **physisorption** or **self-assembled monolayers** (SAMs) [2, 6].
The former is easier as molecules are simply deposed on the surface. But it may results in a poor coverage, reproducibility and robustness to wash. When the adsorption is stronger (high affinity functional groups), protein may partly denature and thus lose structure and/or function [18]. This activity loss is usually balanced by the high number of molecules immobilised.
Using **SAMs** helps to control organic surfaces composition, structure and properties by using long molecules, often alkanethiols when the substrate is covered with gold, forming ordered molecular assemblies by adsorbing on solid surfaces. The thiol-extremity allows to develop a stable bond with gold substrates (red dots in Figure 2.9). The other extremity presents a functional group which can be modified to bind selected bio-molecules.

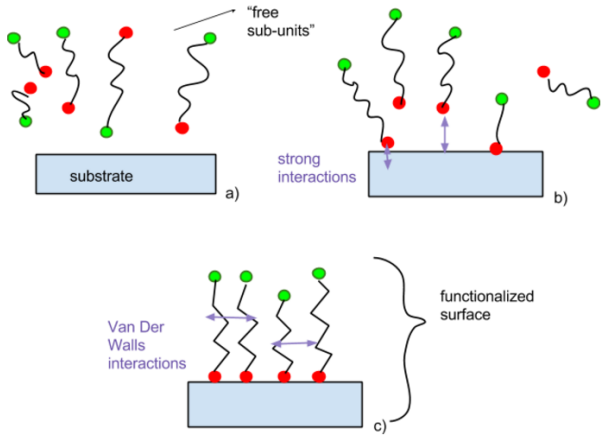


Figure 2.9: Self Assembled Monolayers formation: a) active surfactant, b) chemisorbption of head-groups onto a substrate, c) interactions among backbone hydrocarbon chains ensure an efficient packing of the monolayer and contribute to stabilize the structures with increasing chain length.

Some SAMs are reversible and, using the right removal techniques allows for the re-utilization of the substrate. Lazcka *et al.* [6] also offered another system more expensive but very effective: the **avidin-biotin system**. In this system, biomolecules are anchored to avidin coated surfaces

but the non-covalent nature of the bonding allows for multiple washing and therefore a possible re-use of the same sensing device.

Ideally, detection devices should have a high sensitivity to detect bacteria directly in real samples without pre-enrichment [41]. Real-time readout may improve the achievable detection limit by monitoring the transient sensor response. This way, the binding signal could be separated from the slower non-specific adsorption signal and drift in the readout electronics [10].

Instead of trapping the bacteria itself, another innovative approach consists in immobilising samples of the bacteria directly on the electrode surface so that it would detect anti-pathogen antibodies present in potentially infected patients [18] (a strategy similar to ELISA). However, if the concentration is too small, signal changes might be too small as well and undetectable by impedance biosensors. Moreover, antibodies concentration does not provide an image of the instant concentration of pathogen. There may be a delay for their production.

Lytic enzymes as selectivity means

Another way of selectively detecting a bacteria is to trap every organic species and lyse only the target to get a differential signal. This approach involves lytic enzymes to target the desired bacteria.

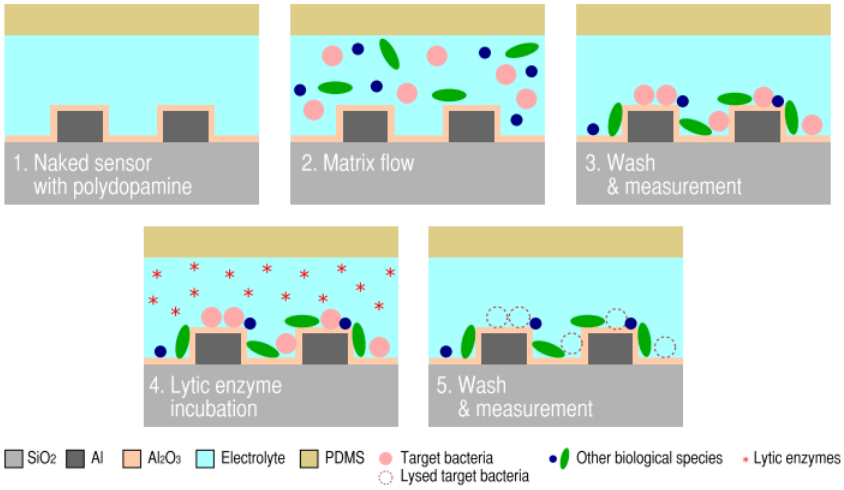


Figure 2.10: Principle of the selectivity method using lytic enzymes (illustration from [2]).

Couniot *et al.* [2] gave us the following 5-steps method illustrated in Figure 2.10:

1. The sensor is coated with polydopamine which will bind most of the biological species.
2. The matrix sample containing target bacteria is flown over a clean sensor during 20 min.
3. The sensor is washed with low-conductive PBS 1:1000 to fully remove non-adhering species and enable sensitive measurement of the admittance over frequency ($\| Y/\omega \|$) at 1 MHz.
4. Introduction of lytic enzymes (flown during 30 min) that will selectively lyse target bacteria if present on the sensor surface.
5. After a second wash with PBS, admittance is measured again

If bacteria we are looking for are present on the sensor surface, they should be lysed and induce a shift in the $\| Y/\omega \|$ measure. This shift is therefore a sign of our target bacteria's presence.

Lysostaphin, an endopeptidase specific for *Staphilococci* cell wall peptidoglycans [2, 64, 65], was used to selectively break them down. Couniot *et al.* also used *E.faecium* as control bacteria.

Labels or not?

Yang *et al.* remind us that bio-recognition elements are not necessarily immobilized directly on the sensor' surface [15]. Labels which are directly grafted on the surface of bacteria play an important role as recognition elements in the biosensor system.
We can define labels as *"fluorophores, magnetic beads, nanoparticles coated with desired antibodies, active enzymes with an easily detectable product, or anything else allowing facile target conjugation and convenient detection"*[10] They will either be the detected signal, either amplify the existing one. Labels contribute to enhance the *selectivity* by binding only to target cells and *sensitivity* by causing drastic changes in impedance and allow a smaller quantity of cells to be detected.
The problem is that some label binding can alter the biomolecule properties. One solution is to use indirect labelling (sandwich essays) as in ELISA.
However, due to its cost, it is mainly restricted to the research field. Labels require **extra time**, **expense**, and **sample handling**. Not to mention that label-free operations enable detection of target-probe binding in real time [10].

This is therefore a choice left to the designer.

2.3 Impedance spectroscopy

In this work, we focus on an impedance-based biosensor with interdigitated electrodes. This section describes more precisely what is **impedance spectroscopy** and its underlying equations.

Whether it is suspended in the electrolyte (*volume-based impedimetry*) or captured on the sensor's surface (*surface-based impedimetry*), the impedance-based electrochemical biosensor will react to the presence of the target cells between its electrodes.
Many reviews report two kinds of detection: *direct* and *indirect* detection. While the first detects perturbations caused by the bacteria's presence or their metabolism's products, the indirect technique does not measure the change in impedance itself. Instead, electrodes detect a variation in the conductance caused by reactions with gases produced by bacterial metabolism. It can also make use of the highly ionic cytoplasm of the cells, which is therefore highly conductive (1 S/m) [15]. By the release of the cytoplasm of *E.Coli*, the solution conductance increases and the detection of 10^2 CFU/mL was reported [66].

In the direct technique, the resulting current is measured and compared to the incoming voltage signal which is applied at a fixed frequency. From this impedance study, information can be extracted and be used to determine the target cell concentration. The change in electrical impedance might come from the bacteria itself or from a chemical product produced by bacteria during their growth [15]. *"Because of their highly insulated cell mem-brane, cells attached on an electrode surface effectively reduce the electrode area that the current reaches and hence increase the interface impedance"* [15].
A significant asset of **growth-based** (direct or indirect) impedance methods is that they allow the user to distinguish between viable and dead cell. However, the cell growth takes time and

makes this method way more **time-consuming**.

Impedance spectroscopy holds promises due to its simple instrumentation, potentially low cost, the ease of device assembly [46], its potential for miniaturisation, ability to multiplexed lab-on-chip applications and above all, its label-free characteristic [10].
It is particularly adapted for applications for which low cost, small instrument size, and speed of analysis are crucial, but cutting-edge accuracy and very low detection limits are not essential. This could be a test during a clinic visit or, ideally, part of the medical routine check-up. Nevertheless, there are still some issues about selectivity. Indeed, in real-world, samples also contains a large amount of non-target molecules.
It is important to specify that, to the best of current knowledge, only surface-based methods can be used for selective detection of bacterial cell [2].

Studying the impedance (current-voltage ratio) requires a complex mathematical treatment because of its imaginary part.
To extract information from the impedance signal, the easiest method consists in building a **system's equivalent circuit** in terms of electrical components, namely resistors and capacitors so that it matches independent processes which contributes to the system behaviour. Experimental data can then be fitted on it. Indeed, this is less tedious than solving a system of equations which would describe all electrochemical phenomena. However information is obtained in capacitance and resistance terms and their translation into actual physical system parameters is not always immediate [18].

2.3.1 Impedance calculation

As mentioned above, the impedance measurement's principle is the comparison a voltage input with the current response in order to detect the bacterial perturbation.
First, we apply a small AC voltage of amplitude V_0 with a variable frequency f ranging from 10 kHz to 100 MHz, on one electrode and we measure the generated AC current (amplitude I_0 and phase θ) at the other one [2].
"Voltage excitation is usually employed in EIS because the most troublesome parasitic impedances are in parallel with the measured electrode-solution impedance. In most cases, the measurement process is repeated at different frequencies, yielding $Z(\omega)$" [10].

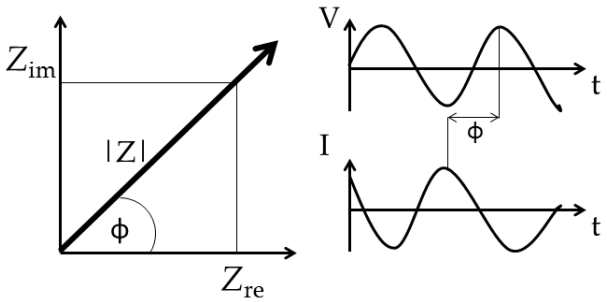


Figure 2.11: *"Complex impedance plane diagram and relation of voltage, current, and phase"*(illustration from [67]).

Signals can be defined as:

$$\begin{cases} V_{test} &= V_{DC} + V_{AC}cos(\omega t) \\ I_{test} &= I_{DC} + I_{AC}cos(\omega t + \theta(\omega)) \end{cases} \tag{2.1}$$

With $\theta(\omega)$, the frequency related phase-shift.
The system can be considered as linear if: $V_0 < U_t = k_b T/q \simeq 26$ mV [68] (U_t = thermal voltage)
The cosinus signal can also be seen as the real part of a complex signal: $cos(\omega t + \theta) = \Re\{e^{j(\omega t+\theta)}\}$

The impedance is defined by the following ratio:

$$Z(\omega) \triangleq \frac{V_0.e^{(j\omega t)}}{I_0.e^{j(\omega t+\theta(\omega))}} = \frac{V_0}{I_0}.e^{-j\theta(\omega)} = \|Z\|.e^{-j\theta(\omega)} \tag{2.2}$$

with $\omega \triangleq 2\pi f$, the angular frequency.

Most of the time, studying impedance can be done by analysing its modulus $\|Z\|$ and its phase $\theta(\omega)$ whose complex representation is illustrated in Figure 2.11.

2.3.2 Electrodes

A standard Impedance Spectroscopy set-up requires the followings:

At least 2, usually 3 electrodes: two-electrode measurements are usually discouraged, except perhaps when working with interdigitated electrodes [18].
- A *Working electrode* (**WE**) where current is measured and that can be biofunctionalized.
- A *Reference electrode* (**RE**) that maintains a fixed, reproducible electrical potential between the metal contact and the solution.
- A *Counter electrode* (**CE**) which supplies current to the solution to maintain the desired electrode solution voltage.

When sensors have a pathogen detection goal, a relatively large surface area and a large surface to volume ratio is required to reach very low levels of detection [15]. *"This is particularly true in the case of small size interdigitated electrodes, IDE, where the electrode width and gap, typically of comparable sizes, are also of a similar order of magnitude to the target pathogen."* [18] Indeed, in an IDE system, also known as InterDigitated Array (IDA), bacteria cells in the growth medium have more opportunities to adhere to the interdigitated electrodes' walls [15]. Depending on geometry, the inter-electrode capacitance can degrade sensitivity to changes at the electrode-solution interface. Indeed, it was reported that 95% of the current between the two finger electrodes in an IDA flows above the electrode surface within a distance that equals the sum of electrode width and space. Each sensor should therefore be designed according to the biological entity it aims to detect. For bacterial detection, micrometer IDA electrodes are most suitable. *"Generally, microelectrodes have great advantages over conventional electrodes for analytical measurements, such as low resistance, high signal-to-noise ratio, rapid attainment of steady state, and the use of small solution volumes"* [69] from 1-2 ml to 15 ml.

2.3.3 Circuit Models

As seen previously, the easiest method to extract information from the impedance signal consists in building a **system's equivalent circuit** in terms of electrical components combined in series or in parallel. This equivalent circuit will itself have an impedance that can be calculated and its modulus and phase could be represented in a Bode plot. Circuits' component can be resistors, capacitors or inductances. Details on their impedance modulus and phase can be found in Table 2.3.

The capacitance expression can be simplified as follows:

$$C = \frac{\varepsilon_r \varepsilon_0 A}{d}$$

with $\varepsilon_0 = 8.854$ x 10^{-12} F/m which is the vacuum permittivity, ε_r the relative dielectric constant. A is the surface of plates composing the capacitance or here, electrode area and d is the distance between these plates which can be the "insulator thickness" or, when looking at electrodes, the "gap" between them.

In order to create an equivalent circuit as representative as possible, there are some aspects of impedance-based detection in liquid media that should be studied. Here is a list [10] of different circuit's elements that will play an important role in the signal interpretation followed by their origin.

- R_{sol} and C_{sol} the solution resistance and capacitance linked to its ions content.
- C_{surf}, the capacitance between the metal electrode and ions that include the capacitance due to the surface modification (as insulating layer) and double layer capacitance. It can often be modelled by a *constant phase element* (CPE) instead of a capacitance.
- R_{leak}, resistive path present in parallel of C_{surf} in nonfaradaic sensors. It is replaced by Z_w and R_{ct} in series in faradaic sensors.
- $Z_w \simeq \frac{A\sqrt{2}}{\sqrt{\omega}}$ is the *Warburg impedance* corresponding to a delay arising from the diffusion of the electroactive species. Phase shift: $-45°$.
- R_{ct} is the *Charge transfer resistance* which is due to two effects. Energy potential associated with the oxidation or reduction event at the electrode and the energy barrier of the redox species reaching the electrode due to electrostatic repulsion or steric hindrance.

  These components can be determined separately using specific frequencies and experimental conditions [2, 15].

Signal representation: In the case of interdigitated electrodes, the results should mainly follow a capacitive behaviour. This means that the impedance signal, as written in Table 2.3, can be defined as $Z \approx \frac{1}{j\omega C}$.
To study the evolution of the signal measured across a frequency range from 100 to 10^6 Hz, we focus on its modulus and phase. The Bode diagram is a log-log plot of the magnitude and phase of an impedance, transfer function, or other frequency-dependent complex-valued quantity which can help the interpretation of resulting responses with respect to the frequency [70]. Magnitude and phase are respectively expressed in decibels and degrees. They are plotted using logarithmic x-axes and the magnitude a logarithm y-axis as well.
Decibels expression of a dimensionless quantity G is obtained as follows: $\|G\|_{dB} = 20log_{10}(\|G\|)$. It is recommended to avoid taking the logarithm of a quantity having a dimension. Ideally, the impedance magnitude should be first normalised by dividing by a base impedance R_{base}. A common choice is $R_{base} = 1\Omega$.

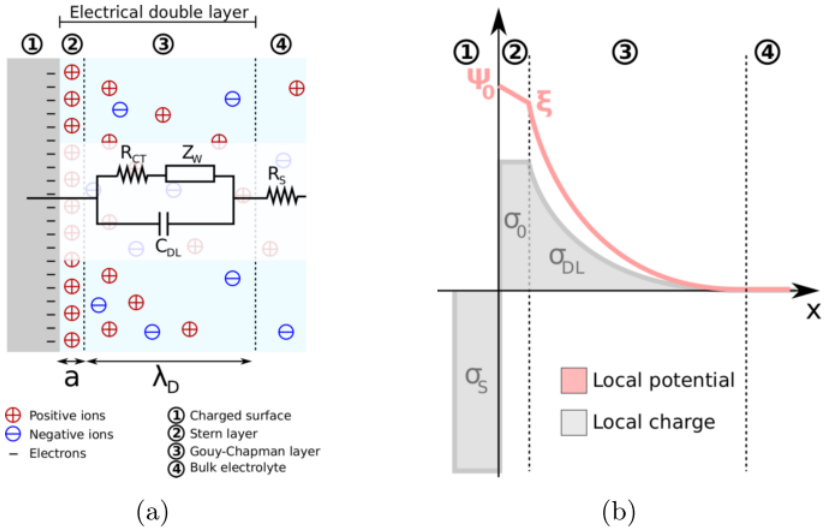
The developed expression for the logarithm of the impedance modulus is $log(Z) = -(log(\omega) + log(C))$. Therefore we expect a straight line with a negative slope. In a bode plot, this slope would be -20 dB/decade. In any case, the expected phase is a constant close to $-90°$.

Debye's length: A material immersed in electrolytes leads to charge redistribution. The *Debye's length*, proportional to the square root of ion concentration [10], describes an area over which any electric field arising at the electrode will decay due to a local buildup of excess ions of opposite charge.

	Impedance (Z)	**Modulus**	**phase**
Resistance	R	R	$0°$
Capacitance	$\frac{1}{j\omega C}$	$\frac{1}{\omega C}$	$-\frac{\pi}{2} = -90°$
Inductance	$j\omega L$	ωL	$\frac{\pi}{2} = 90°$

Table 2.3: Equivalent circuit's components impedance.

This effect creates a capacitance called the double layer capacitance C_{DL}. It appears in Figure 2.12.
The double layer capacitance is voltage-dependent because, increasing the electrode voltage, attracts the diffuse ion layer which modify the capacitance [10]. This term will be in series with C_{ins}, the capacitance formed by the insulator which might cover the electrode. Together, they are sometimes referenced as C_{surf}.



(a) (b)

Figure 2.12: *"Schematic representation and equivalent electrical model of the solid-electrolyte interface.(a) R_{CT} is the charge transfer resistance, Z_W the Warburg impedance, C_{DL} the double layer capacitance and R_S the electrolyte resistance. (b) Dependence of the local charge and potential with the distance. Ψ_0 is the surface potential, ξ is the zeta potential, σ_s the charge of the solid material, σ_0 the charge in the Stern layer and σ_{DL} the charge within the electrical double layer."* (illustration from [2])

The Solution: In addition to the nature of the electrodes, the bulk solution also influences the resultant signal due to the presence of ions. This solution is represented by the parallel association of C_{sol} and R_{sol}, and should not be affected by cell binding unless some of the cytoplasm, which has a high conductivity, is released into it.

Bacteria: The cell membrane, consisting of a lipid bilayer, can be seen as a parallel combination of resistances which symbolise its ionic channels. It has highly insulating properties. The membrane resistivity is in the range of 1 M to 100 GΩ/μm^2, or a conductivity around 10^{-7} S/m, whereas the inside of the cell can reach 1 S/m which is quite high [15]. It contains

membrane-covered particulates, organelles, and many dissolved charged molecules which make the cytoplasm so conductive.
For a thickness of approximately 8 nm, the membrane capacitance is around 0.01 $pF/\mu m^2$
"The study showed that the presence of intact cell membranes on the electrodes determined the current flow and thus the sensor signal." [15] But a growing cell also influence the signal as the occupied electrode' surface increases as well as the interface impedance.
These different contribution must be carefully separated during the analysis.

Faradaic vs non faradaic interfaces: When electrochemical reactions between biological species and the electrolyte medium happen, an electron transfer takes place through *faradaic* electrodes. This often implies redox reactions.
For example, in [71], $Fe(CN)_6^{3-/4-}$ is used as a redox probe. Electron transfer between this redox probe and the electrode is progressively blocked by the binding of *E.coli* (the target cell) on the antibody-modified surface and bio-catalysed precipitations which create a signal amplification.

If no DC current flows through the solid-electrolyte interface R_{ct} and Z_w can be discarded, the interface simply consists in C_{DL} in series with R_{sol}. This is the case in bacteria detection which involves no redox reaction and electron exchange. Such electrodes are *non-faradaic*.
This is similar to the model suggested by L. Yang and R. Bashir [15] whereby the impedance can be expressed as: $\mid Z \mid = \sqrt{R_{sol}^2 + (\frac{1}{\pi f C_{DLD}})^2}$

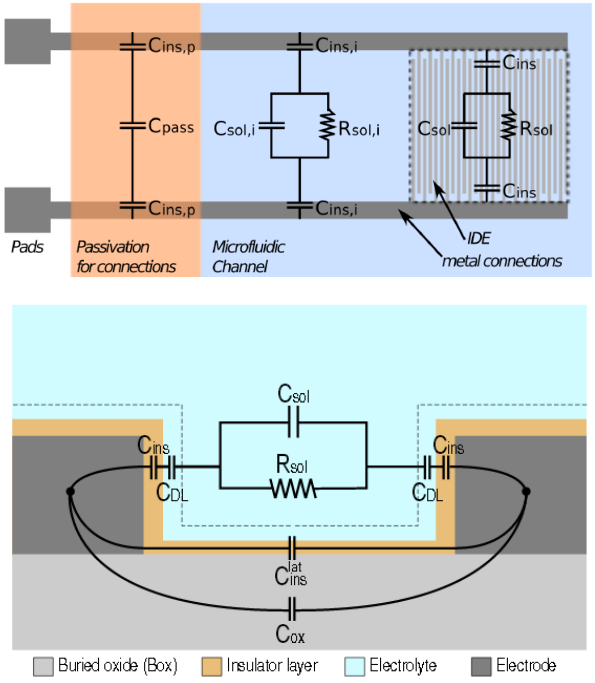


Figure 2.13: Schematic top and side view (not at scale) of a rectangular IDE (illustration from [2]). For reason of convenience, only two electrodes are represented but sufficient to depict components that compose the equivalent circuit.

2.3.4 Microfluidic

Conventional impedance-based method are not very effective for very small bacterial cell concentration. It might take a while for the impedance to change by a measurable amount [72].

One solution is to detect the same number of cells but in a smaller volume, the effective cell concentration and the impedance variation being increased.
When we use **microfluidic**, we can get volumes as small as nanoliters (even attoliters in some cases [73]) using channels with dimensions of one to hundreds of micrometers. Therefore, the sample amount required is reduced. Not to mention that it makes it possible to develop compact and portable systems [73].

When using microfluidic devices for cell biological application, poly-dimethyl siloxane (**PDMS**) is widely used. This elastomer is transparent, bio-compatible, permeable to gas and can be transformed into microfluidic devices through simple molding procedures [74].

This field is of great importance for the development of technological applications like lab-on chips. Getting smaller also means shortened diffusion time and a better predictability of the flows. Indeed, at this scale, forces like **gravity** have negligible impact, and the flow is **laminar** in most cases. The liquid propagation might be driven by "electro-osmotic flow", "shear-flow" or, pressure. The time required for the diffusion of a molecule is also reduced which enables fast response micro-system.
However, this technique has some drawbacks which includes: a relatively slow diffusive mixing, complication of protocols and the affinity of PDMS for small hydrophobic molecules and thus a possible adsorption that could bias the experimental conditions [59].

2.4 Fabrication techniques

In this master thesis, we focus on the electrodes' geometry. More accurately, we are interested in varying electrodes' height/thickness in such a way that bacteria would be more likely located between two of them. Indeed, this space is where the electric field will be the most concentrated and thus field variations can be more accurately detected.

Materials used in electrochemical biosensors are classified as follows [75]:

- Materials for the **electrode** and supporting substrate
- Materials for the immobilisation of **biological recognition elements**
- Materials for the fabrication of the **outer membrane**
- **Biological elements**, such as enzymes, antibodies, antigens, mediators and cofactors

As in a lot of microfabrication processes, we will use a silicon wafer and glass (borosilicate, pyrex type) as support. Silicon is often employed for its favourable mechanical and electrical properties.

In the previous design developed by Couniot *et al.* [2], electrodes reached a maximum thickness of 1 μm. This can still be qualified of thin film and, therefore, aluminium deposition by evaporation was relevant. It would not be the case in this work for reasons which will be described in section 2.4.1.

With regard to biological element, we choose to keep the polydopamine coating used by N. Couniot [2].
As for the packaging, which has a secondary role, we will not discuss it here. Indeed, sensors are still at an experimental stage and will only be tested in a microfluidic circuit.

2.4.1 High aspect ratio structures

In microfabrication, High Aspect Ratio (**HAR**) structures are more complex to realize but several techniques are still possible.

Lithography, electroforming, molding (LIGA) and other photolithography-related processes address the aspect ratio problem by employing deep resist layers.

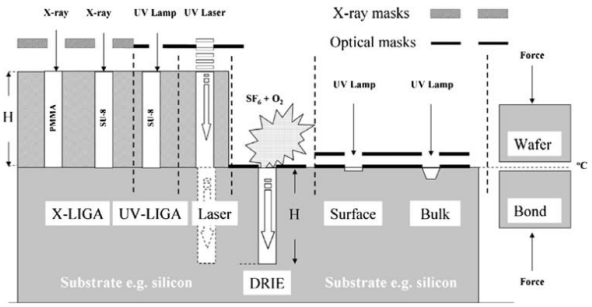


Figure 2.14: High aspect ratio microfabrication techniques (illustration from [76]).

To be suitable for thick deposition, the resist must satisfy stringent requirements. A high viscosity is required to reduce the lateral flow and obtain the stable thick resist films needed in HAR patterning [77]. This is the case of polyimide, with achievable thicknesses ranging from 1 to 10 μm. With this resist, process can be performed upon substrates containing standard CMOS circuitry [78]. Nonetheless, some problem of copper migration can occur in this polymer.
Initially, the **LIGA** resist was mainly PMMA (poly-methyl-methacrylate), which required 5–10 h exposure with x-rays from a synchrotron. At an energy of 3 to 10 keV, X-rays penetrate deep resist layers without significant absorption or scattering [76], which allows for reaching resolutions of 1-5 μm.
With the advent of the SU-8 resist, exposure time was reduced from hours to minutes. As soon as it was realized that SU-8 resist was sensitive to UV radiation as well, the cost competitive technique UV LIGA was created. While X-rays requires expensive gold-on-beryllium masks, photolithography with SU-8 can be done with a conventional mask aligner and conventional, commercially available, chrome-on-quartz masks.

A better alternative is the high contrast and epoxy-based photoresist **KMPR**. It is designed to coat 4 – 120 μm-thick layers in a single step thanks to its high viscosity *(see microChem data sheet* [79]).
Even if SU-8 resist is currently the most widely used thick resist for electroforming masking, KMPR has a considerable advantage: it can easily be removed after the process using commercially available chemical removers [80].

Besides, other techniques are available for the creation of high aspect ratio structures but they do not meet our needs.
Thin film **multilayers** (sometimes involving sacrificial layers) are possible and, unlike thick resist, structures produced following this method can have vertical features. However, when using different materials, this technique creates numerous interfaces which are a significant source of weaknesses. Furthermore, such structures are limited in height. A cheap way to overcome this problem and form structures such as buried micro-channels is **wafer bonding**.
Hot embossing also shows good results, allowing a low cost and flexible fabrication but it is limited to polymeric microsystems [81].
Another option consist in removing material from a thick layer to create 3D microstructures: **Deep Reactive Ion etching (DRIE)** can produce such structures in the wafer itself without requiring an intermediary thick resist [76]. First, a conventional lithography step will define features in a masking layer on the surface of the wafer. Non-protected areas will be etched.
To etch deeply enough, this form of plasma etching alternates vertical etching and sidewall passivation steps. However, this etching technique is limited to silicon-based substrates.
Excimer laser machining, electrical discharge machining, and even ion beam milling are

material removal methods that are becoming effective construction tools on micrometer scales, but they lack of geometric versatility of formation and are limited by the properties of the material to be transformed [82].

Problems related to in thick resist films [79]:

When using thick resist to define high ratio structures, there are several points that must be considered.

▷**Spinning curve:** To predict the thickness of the resist film, spin curve can be used. They contain information about time and speed required to reach the targeted thickness. More viscous resist will tend to stay thicker for a same speed but also form edge bead.

▷**UV exposure:** A thick resist is is defined by film thickness much higher than the penetration depth of the exposure light [83]. This means more than 5 μm thick for a standard positive resist and exposure wavelength (g-, h-, i- lines). The phenomenon which makes a complete exposure possible is the **bleaching of the resist**. In fact, DNQ-based resists (including AZ series) become UV-transparent during exposure and allows a progressive light penetration.
The consequence is that a thick resist will need a longer exposition and thus a higher dose. Special attention should be paid to the determination of the optimum exposure dose. Indeed, if it is too high, undesired exposure by scattering, diffraction and reflection of the resist which should not be exposed might happen.

▷**Surface adhesion** is very important to avoid a peeling of the resist, which could be problematic for next steps. There are some process improvements that can increase this adhesion. Metals such as aluminium or titanium generally induce a very good resist adhesion. An optimal soft bake contributes to this as well as the use of adhesion promoters such as hexamethyldisilazane (HMDS) or TI PRIME (titanium primer), which make hydrophilic surfaces hydrophobic, thus improving the resist adhesion.

▷**Mechanical cracks:** During exposure of DNQ-based resists (such as the AZ4562), the photo active compound *diazonaphtoquinone* (DNQ) is converted into indene carboxylic acid with a nitrogen molecule (N_2) as a side product. The N_2, once trapped into the resist film, causes strong mechanical stress expanding and cracking the resist. They also increase dark erosion, the loss of unexposed resist film thickness.
A too long soft bake might also embrittle the resist film by reducing too much its solvent concentration.

2.4.2 Passivation layer

In this work, our biosensors present multiple electrodes which will be in contact with the analytes' solution. To protect these electrodes from corrosion and promote cell adhesion, the hydrophilic nature of alumina (Al_2O_3) [84] and its chemical inertia are highly desirable.
Alumina is the most common species among the aluminium oxides and is often referenced as **aluminium oxide** [85]. It is commonly found under a crystalline polymorphic phase and its most common crystalline form, known as corundum, is the second hardest material after diamond. Any exposed aluminium surface will turn into Al_2O_3, a passivation layer, which protects the metal from further oxidation.
This major engineering material offers a combination of good mechanical and electrical properties. It includes a good strength and stiffness, a popular corrosion resistance and thermal stability

and, for electrical features, excellent dielectric properties [85]. Its non-toxicity makes it an ideal choice for biological applications.

Hereafter we describe two deposition techniques for alumina: **Anodization** of an aluminium layer and the Atomic Layer Deposition (**ALD**).

▷**Anodization :** It takes advantage of the natural passivation phenomena that occurs on aluminium surface if exposed to the right condition.
The first step will consist in depositing a layer of aluminium on the surface. It will automatically oxidize upon contact with the air, producing a thin layer of native oxide. The anodization properly speaking is the electrochemical process employed to increase the thickness of this native oxide by oxidation of the underlying metal.
To meet the thickness requirement of our biosensor, we avoided aluminium electrodes. For this reason, anodization is not suitable.

▷**ALD :** It stands for **Atomic Layer Deposition**. This method relies on alternate pulsing of the precursor gases onto the substrate surface [86], on a sequential exposure, and on self-limiting surface reactions of chemical species to deposit thin films [84].
For example, the deposition of alumina (Al_2O_3) on silicon is achieved by using exposures of trimethylaluminium (TMA, $Al(CH_3)_3$) and water [87]. Between precursor pulses (TMA), the reactor is purged with an inert gas, hence the name of sequential exposures.
Under proper conditions, the growth of the alumina layer is stable and constant between each deposition cycles but it remains nonetheless very slow [86]. The resulting coating is conformal and has a highly controllable thickness.
ALD can be performed following two different methods: the conventional thermally-driven ALD or the plasma-assisted ALD. The latter, by replacing H_2O by O_2 plasma, leads to a wider choice in material properties, substrate temperature, and even processing conditions [88].

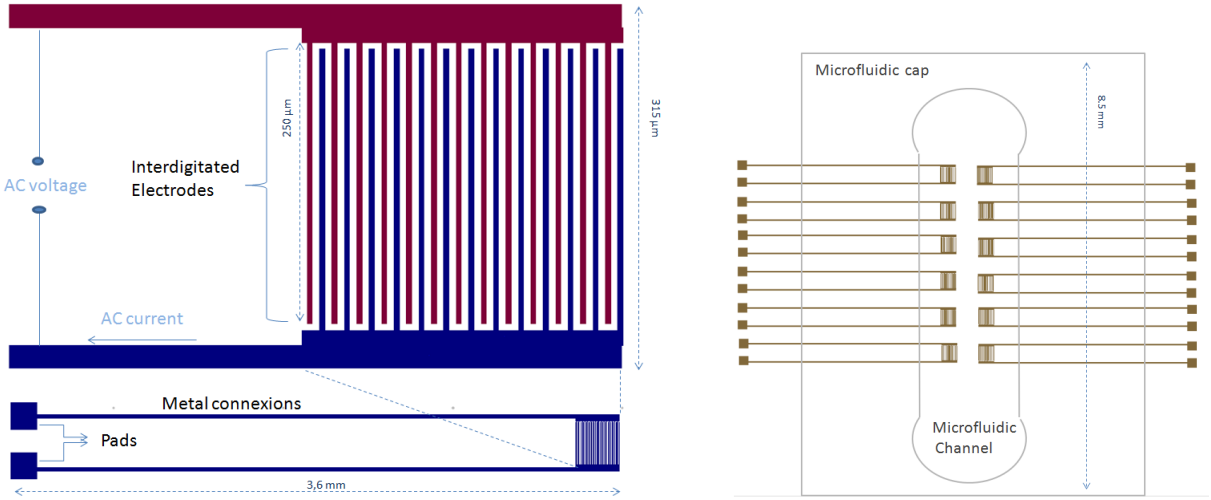
Alumina ALD on nickel is uncommon. Jeffrey R. Wank *et al.* [87] reported a coating of nickel particle with Al_2O_3 with a ALD-Fluidized Bed Reactor however the coating thickness never exceeded 11 nm.

Chapter 3

Methodology

In this master thesis, we focus on one sensor type: an impedance spectroscopy detection via interdigitated electrodes.
The reference design is inspired from those developed by *Numa Couniot* in his PhD thesis [2]. They are small rectangular (illustrated in Figure 3.1a) or circular shaped sensors with interdigitated 1 μm thick aluminium electrodes.
In his thesis, Couniot mentioned the possible gain of sensitivity by slightly increasing the electrode thickness. Based on numerical simulations, he identified an optimum at $h = 0.7$ μm, however, this only holds when considering that the number of trapped bacteria between electrodes is independent of their thickness. It was therefore interesting to investigated the real impact of this parameter. This is the aim of this work.

This chapter describes the methodology used for the fabrication and bacteriological tests of these modified sensors.



(a) (b)

Figure 3.1: a) Schematic representation of a rectangular IDE sensor's top view. b) Schematic representation of sensors organised on a chip and the microfluidic cap position (top view).

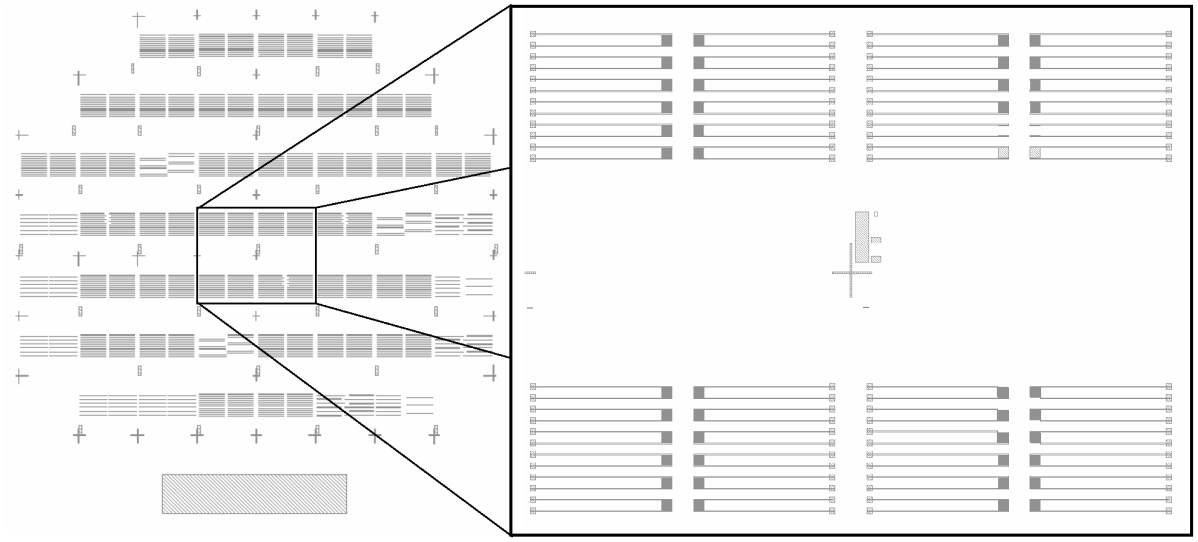


Figure 3.2: The mask created with CADENCE for the photolithography step. Different kind of cells have been reproduced all over the mask. Each of them contains 12 sensors.

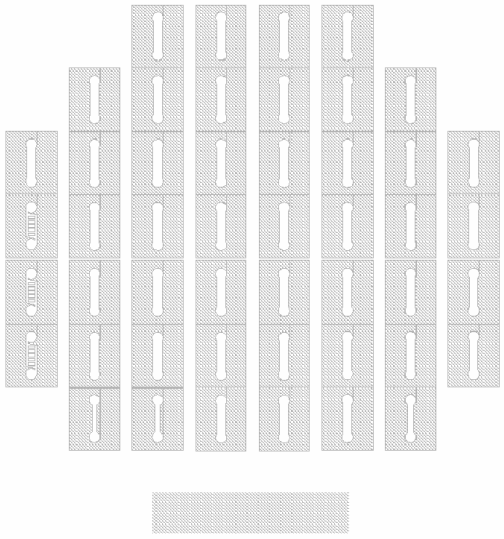


Figure 3.3: The mask created with CADENCE software for the definition of PDMS caps. Only the models of the middle are used for PDMS caps.

3.1 Design

3.1.1 Proportions optimisation

The proportions of the sensors have an important impact on the final results. We analysed how the thickness (h), the electrode width (w) and the gaps (d) between the electrodes (illustrated in Figure 3.4a), would influence the bacterial detection.
The more h and d increase, the more important the effective surface. This is the area on which bacteria can adsorb and then be detected. Depending on where they adsorb (see Figure 3.4b), bacteria will not have the same impact on the detected signal and the sensitivity ΔS.
The electric field is the strongest right between the electrodes and thus, species present in this spot will have an impact of $P = 1$ whereas these on top of electrodes are in the leakage field and have a smaller weight ($P'(< 1)$).

$$S \propto w * P' + (2h + d)P \tag{3.1}$$

$$C = \frac{\varepsilon_r \varepsilon_0 * h * L}{d} \tag{3.2}$$

In order to get the best ΔS as possible as well as a high capacitance, a higher h is always beneficial. However, w should be kept as small as possible whereas d is the most debatable. It increases the effective surface but is present in the capacitance's denominator which decreases its value.



(a) (b)

Figure 3.4: a) Schematic IDE cross section. b) Different possible placements of a bacterium between two finger electrodes and their respective weight on the electric effect P or P'.

As we decided to test higher electrodes, h is more important and thus compensates the larger gap. If we decided to keep the same ratio h/d than the original one [1], which is 1/4, for an average of 5 μm high electrodes, we could theoretically have gaps of 20 μm which is bigger than our largest gap (8 μm).

For the tests with bacteria, we only used sensors of design 'C'[2] ($w = 2\mu$m and $d = 6$ μm). According to this analysis, this geometry is more than acceptable to get optimum results.

[1] Form Numa Couniot's PhD thesis.
[2] This notation is explained the next section 3.1.2 and in Table 4.3.

Gap d (μm)	**2**	**4**	**6**	**8**
Width w (μm)				
1	/	I	/	/
2	K	A	C	L
4	J	B	D	E
6	/	H	G	F

Table 3.1: Summary of every electrode proportions tested. Each type name from 'A' to 'L' has a different combination of width and space between electrodes.

3.1.2 Sensors' types

Increasing the electrodes thickness might create difficulties. Indeed, narrow structures might collapse or, at least, lose in stability. To prevent such things from happening, we chose to test various fingers electrodes width and gaps (Figure 3.4a) between them. The gap should not be too large as it increases the volume in which bacteria might get diluted and, consequently, reduces the signal.

The photolithography step, explained in following sections, requires a chromium mask to pattern the resist. We created this mask using the software CADENCE. It is illustrated in Figure 3.2. On this mask, we chose to only create rectangular sensors as the circular shape brings an extra difficulty in the interpretation. Moreover, its benefits over a rectangular shape are not clearly established.
Table 4.3 gathers every width - gap combinations tested. Each width - gap combination is named with a letter from A to L.

For the microfluidic, we selected a model of cap present in N. Couniot's thesis [2], a single channel large enough to contain two rows of six sensors (Figure 3.3). These twelve sensors are gathered in what we will call "cells" or, once diced, "Chips". These "Chips" are represented in Figure 3.1b.
There is, at the end, seven different types of cells which were duplicated all over the first chromium mask used for the photolithography step.

3.1.3 Electrode materials

Motivated by its compatibility with microelectronic processes (CMOS), the original process included aluminium electrodes. In this work, it was no longer an option because the aluminium layer was build up by evaporation and this process only works with thin films (around 1 μm). Because the aim of this master thesis is to study thicker electrodes (more than 1 μm thick), this is no longer applicable.
We have therefore changed, not only the process but also the metal used for the electrodes fabrication.
In most applications, gold is a favoured choice for the fabrication of the electrodes. Indeed, as platinum, this noble metal is inert and known for its bio-compatibility. It is known as well for being used as thin adhesion layer in thiol-based SAMs. However, when thicker structures are required, gold becomes a very expensive option.
Chromium and indium-tin oxide (ITO) are other widely used materials.

The selected technique is electroplating. We had the choice between **gold, cooper and nickel** as widely plated metals [89]. Gold was excluded for price reasons. Nickel, which also have a really good electric conductivity, is, as chromium, known for its properties of anti-oxidant and

wear resistance. This is a clear advantage over copper which has not only antimicrobial actions but oxidise itself really fast over two hours.

For all these reasons, we selected electroplated nickel to form the sensor's electrodes.

3.2 Fabrication

The fabrication of thick electrodes requires thick resist films to act as a template during the electroplating. KMPR and SU-8 have been considered for use but these resists are quite specific and really viscous. This could cause troubles for fines structures, sometimes 1 μm large lines, we would like to create. As our maximum desired resist thickness is about 10 μm, **AZ4562** positive resist (which has an attainable thickness up to 30 μm) is a better option. It has an optimized adhesion for common plating process and is compatible with all common developers and strippers. As it is a positive resist, all exposed areas of the resist will go away. This parameter must be taken into account in the mask conception.

3.2.1 Nickel electro-deposition

The solution we selected to obtain high aspect ratio electrodes is electro-deposition. Its operating principle is the following: from a liquid phase, a metallic salt is reduced and will coat the cathodic surface.

Because of its high deposition rate, nickel is suitable for depositing hundreds of μm to several millimetres coating. It is also a well studied electrolyte which is mastered and does not produce hazardous gases when electrolysed. Nickel sulfamate is known for easy handling and is relatively cheap.
Nickel coating is created from a simple salt solution, which produces a lot of cation because it is almost fully dissociated and has a high cathodic optimum yield. The reduction which happens when nickel is deposited on the substrate is the following:

$$\mathrm{Ni}^{2+} + 2\mathrm{e}^{-} \longrightarrow \mathrm{Ni} \tag{3.3}$$

The total mass dropped off (m) is a function of the average current intensity **I** and of the time $\boldsymbol{t}$ during which I is applied [90]:

$$m = \frac{I.t}{F}.\frac{M}{n} \tag{3.4}$$

with **M** the molar mass, expressed in g/mole, $\boldsymbol{F}$ the Faraday constant (F = 96,485 C.mol^{-1} [91]), and $\boldsymbol{n}$ the number of electron involved in the reduction.
For nickel, whose M = 58.59 g/mole and n = 2, $\frac{M}{nF}$ can be considered as a constant of $1,095$ g/C.

Even if this formula is already a good approximation, it does not take into account the electrode efficiency. If accurate values are required, $\frac{M}{nF}$, the proportionality constant, must be multiplied by α, the actual electrode efficiency ratio.
For the anode, α is set to 1 because it is almost always 100 % under practical electroplating conditions for nickel dissolution [92]. It is interesting to note that, under unusual conditions (pH of the solution too high, chloride ion concentration too low), the nickel anode might become passive and α, for anode dissolution, will drop close to zero [92].

Regarding the cathode, α is never 100 % due to the existence of some parasitic reactions. Indeed, some of the coulomb supplied will be used for proton reduction. The discharge of hydrogen ions from water, which forms bubbles of hydrogen gas at the cathode surface, will

reduce its efficiency. Its value drops to approximately 96% in an additive-free nickel electroplating solution.
The importance of these secondary reactions can be estimated by studying the ratio between real metal mass deposited and its theoretical value.

$$\alpha \approx \frac{m_{experimental}}{m_{theoretic}} \tag{3.5}$$

α ranges from 0.90 to 0.97 for different nickel plating solutions. We can use an average cathode efficiency of 95.5% to make estimates when precise values are not essential [92].

The parameter we would like to control is the average thickness ($\boldsymbol{e}$). The following equation gives $\boldsymbol{e}$ starting from the total mass dropped off [93].

$$m = v \times \rho \text{ and } e = \frac{v}{S} \text{ or } e = \frac{m \times 100}{\rho \times S} \tag{3.6}$$

with ρ [kg/dm^3] or [g/cm^3] , and v being respectively the density and the volume of deposited metal while **S** is the surface covered.
In the case of nickel, the density at room temperature is $\rho = 8.907$ [g/cm^3] .

The average speed of deposition **V** [μm/h] is given by Equation 3.7.

$$V = \frac{e}{t} = \frac{M}{nF\rho}.\frac{I}{S} \tag{3.7}$$

And the current density we need for a given thickness can be expressed by Equation 3.8.

$$J_{local} = \frac{nF\rho}{M}.\frac{e_{local}}{r.t} \text{ in } A/dm^2 \tag{3.8}$$

with e in μm and the time t in hours.
A phenomenon to pay attention to is "current concentration inhomogeneities". This is especially important on edges of resist delimited patterns. The insulating-conducting material junctions are the most likely to cause electrical discontinuity but it also might take place on bumps of a rough surface. These inequalities tend to increase as current concentration will lead to a larger metal deposition [90].
Reducing the current density minimises edge-effects and resulting in a more homogeneous metal thickness.
Other techniques like using isolating shapes to modify the current flow are also possible.

Adhesion interface

The electroplating requires a conducting surface to deposit the plated metal onto. Both substrate we use have insulating surface, therefore, we need to add a metallic layer that will act as a conduction layer.

Strong adhesion exists in nickel film on copper surface. However, the opposite is not true: void will be created between Cu film and Ni substrate even if both present a crystallographic coherency and metal-metal bonds can form at the interface [94].
Consequently, a metallisation step of copper must be planned on a titanium layer, which will ensure copper adhesion on silicon.

Deposition of Al_2O_3

To obtain conformal and well controlled passivation layers, we chose the **Atomic Layer Deposition** method. Alumina (Al_2O_3), which has often been used as non-toxic coating, seemed appropriate for our application. Its main utility is to protect nickel electrodes from corrosion when they are used in bacterial solutions.

We based ourselves on previous works, including Numa Couniot's thesis, to choose the atomic layer deposition. Nevertheless, performing ALD at room temperature is an extremely long process and even thicknesses as small as 30 nm might take days to be achieved. Furthermore, thermally deposited ALD layers exhibited better electrical characteristics (based on capacitance measurements) [95] for alumina deposition with TMA, there is no advantages to choose either thermal or plasma. Therefore we chose the standard procedure: a temperature of 150 °C and a *thermal ALD* with an expected Growth Rate Per Cycle of 0.9 Å/cycle instead of plasma ALD.

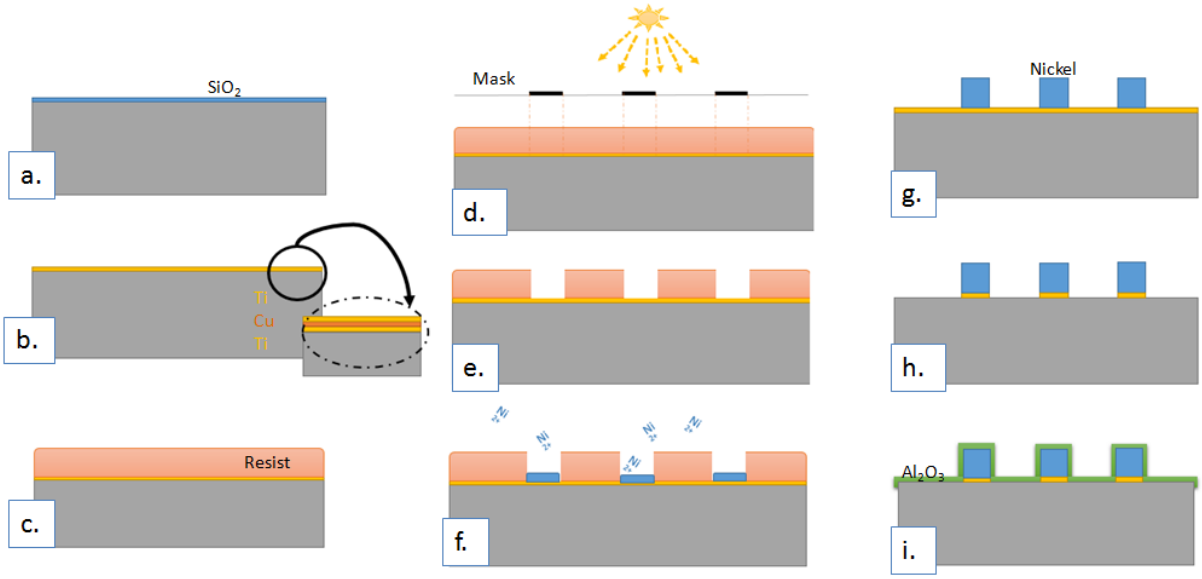


Figure 3.5: Fabrication process of high aspect ratio nickel electrodes.

3.2.2 Process

Biosensors are manufactured on wafers with a 76.2 mm (3 inches) diameter.
We started with ten silicon wafers (330 μm-thick) and then moved to transparent fused Quartz substrates ($500 \pm 20\mu$m-thick)[3] for a possible inverted microscope analysis.

▷ **1. Cleaning**:
All wafers were first cleaned following a standard method.
First, a piranha bath (H_20_2 : H_2SO_4, 2:5) during 10 min. One bath is enough because wafers were all new ones.
Then, all of them were rinsed in 5 bath of DI water. Silicon substrates (but not quartz) underwent an extra step, an immersion in a 2% solution of hydrofluoric acid (HF) to remove the thin oxidation that the piranha created.

▷ **2. Oxidation (only silicon wafers)**: *(Figure 3.5 a.)*

[3]Reference T23004 by SIEGERT WAFER.

Layer	Deposition rate	Pressure	Current	Power
Titanium 1	1 Å/s	1.5 $\cdot 10^{-7}$ mbar	80 mA	16.2 %
Copper	1 Å/s	2 $\cdot 10^{-7}$ mbar	29.3 mA	5.9 %
Titanium 2	1 Å/s	1.1 $\cdot 10^{-7}$ mbar	86 mA	17.4 %

Table 3.2: Metallisation parameters for the VACOTEC.

To avoid possible leakage due to the semiconductor nature of the silicon, a thin layer of oxide is created for electric insulation. The **wet oxidation of the silicon surface** is performed at $\sim$ 900 °C to obtain a 300 nm thick oxide layer.

▷ **3. Adhesion layer** : *(Figure 3.5 b.)*

Before proceeding to the electroplating, a conductive layer is needed. Moreover, this layer will also improve the nickel adhesion.
We chose to deposit a **titanium - copper - titanium** sandwich structure with standard ratio: **5 nm Ti - 100 nm Cu - 10 nm Ti**.
The adhesion as such is provided by the first titanium layer and by the copper: copper adhere with the nickel electrodes and titanium allows the copper adhesion on silicon. The second titanium layer has a protective role for copper against oxidation and should be removed right before the electroplating.
The metallisation of both titanium and copper are done by evaporation in a rotate mode in the Dual E-gun evaporation system Vacotec with parameters in Table 3.2.

▷ **4. Photolithography**: *(Figure 3.5 c. d. and e.)*

To define the desired electrodes pattern, a photolithography step is needed. The adapted chromium mask has previously been designed on CADENCE software (Figure 3.2).

Two resists were selected: **AZ ©6632** and **AZ ©4562** from MicroChemicals.
AZ6632 is an advanced photoresist which presents a high thermal stability while AZ4562 is a positive resist adapted to 3 μm and more deposition. They both have a high development rate.

Initial parameters were the following:

∗ **AZ4562:**

- Spin coating: 21 °C – 2000 rpm for an expected thickness of 8.77μm
- Soft bake: 100 °C on a hotplate during 60 seconds
- Exposition: Hard contact with K& W *MA 1006* [4], 46.5 seconds (UV power$\sim$ 450 mJ/cm^2)
- Development: AZ 826 MIF, about 2 minute 30 with agitation and rinsing with water
- Post bake: 115 °C, 50 seconds (hotplate)

∗ **AZ6632:**

[4]Photolithography machine.

- Spin coating: @ 21 °C – 2000 rpm for an expected thickness of 3.7μ m
- Soft bake: @ 110 °C on a hotplate during 50 seconds
- Exposition: Hard contact with K& W *MA 1006*, 12.5 seconds (UV power $\sim$ 100 mJ/cm^2)
- Development: AZ726 MIF, about 2 minute 30 with agitation and rinsing in water.
- Post bake: @ 125 °C 50 seconds (hotplate)

▷ **5. Electroplating of Nickel**: *(Figure 3.5 f.)*

Before starting the electroplating, the titanium protective layer must be removed. To do so, we use *Titanium Etchant TFT* [5] with an etching rate of 25 Å/sec at 20 °C. Therefore, for a 10 nm layer, 5 seconds of immersion is needed.

Nickel which composes the electrodes is deposited by electroplating from a *nickel sulfamate solution* [6] with a nickel typical content of 10.2 *oz/gal* ($\sim$7.66 g/L).
We targeted 4 different electrode thicknesses: 1 μm, 2 μm, 5 μm and 10 μm. The time and the current applied to obtain such thicknesses e, are predicted by Equation 3.7.
In order to set the proper current, we calculated the total surface that would be plated by means of the software CLEWIN (S = 1.318829 cm^2).

To ensure a good adhesion and decrease internal stresses, we first applied a current of 2.63 mA during 2 minutes to create a very thin seed layer. Afterwards, we applied a current density of 7 mA/cm^2 which correspond to a current of 9.2318 mA.

▷ **6. Layers removal**: *(Figure 3.5 g. and h.)*

To remove the resist, AZ 100 remover, DMSO or other common organic solvents can be used. A simple acetone bath is enough but not recommended because of its high vapour pressure. Nevertheless, as we used it, a subsequent rinse with isopropyl alcohol immediately after the acetone step was performed in order to remove the resist contaminated acetone residual-free [96].
Before going further, the remaining "protective titanium layer" must be removed using the *Ti TFT solution*.
Afterward, to suppress copper between electrodes we use: **« Copper etch 49-1 »** which has a 22 Å/s rate at a temperature of 30 °C. This gives us an approximative time of 46 s of application. This product is said to be "nickel compatible" [97].

Then the "titanium adhesion layer" is removed as well with the same product as mentioned earlier. 25 Å /s @ 20° C means about 2 seconds of application are necessary to etch the 5 nm layer.

▷ **7. Alumina ALD**: *(Figure 3.5 i.)*

The wafer is covered with a desired Al_2O_3 thickness of 30 nm using a thermal ALD[7] with trimethylaluminium (TMA) and H_2O as precursors.
The temperature was 150 °C and the cycle was repeated 330 times.

▷ **8. Connections**:

To be able to reach nickel under the insulation layer of alumina, pads' surface is scratched with the probes right before the measurements.

[5] Integrated circuits and SiO_2 compatible and low nickel etching.
[6] Sulfamate Nickel Plating SN-10 by TRANSENE.
[7] On the ALD system Cambridge Fiji from WinFab.

3.2.3 Microfluidic cap

Once the sensors are fabricated, we manufactured the microfluidic part. The main component is a thick PDMS cap that will guide fluid onto a set of sensors.
However, in order to be able to carry out a proper measurement, connections must be kept out of the channel and protrude from the PDMS as illustrated in Figure 3.1b. This means the PMDS must cover structures which can be up to 10 μm thick. To prevent any leakage, KMPR walls were previously created to support the microfluidic cap using the following steps:

1. Cleaning wafers using the standard cleaning.
2. HMDS treatment.
3. Coating of *KMPR 1050* at 1500 rotation per minute (rpm) and 1000 rpm/s during 60 sec.
4. Soft bake: 20 min at 100 °C. After, the wafer must cool down overnight.
5. Exposure during 120 s at 260 W ($\backsim$ 1200 mJ/cm^2) through the mask in Figure 3.3.
6. Post exposure bake: 4 min at 100 °C.
7. Development in AZ 726 MIF Developer during 6 min.

Due to the high aspect ratio structures already present on the wafer, micro-bubbles appeared. To reduce their number, wafers were put 10 minutes in vacuum chamber with interruptions before the softbake step. On some wafers we have observed that the resist was uneven, especially on the extremities. This made the photolithography step more difficult as the mask would touch the resist surface. To reduce this phenomenon, we added a pre-soft bake step of 5 minutes at 60 °C.
The wafer is then diced into 8 mm x 8 mm chips, each containing 12 individual sensors.

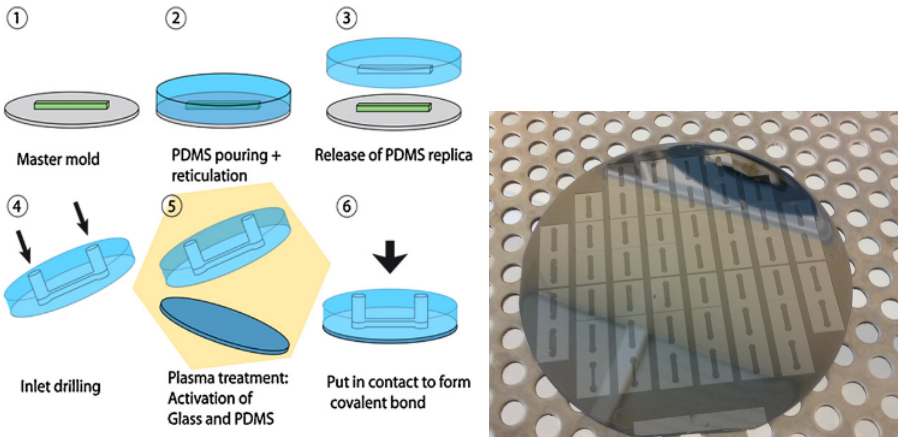


Figure 3.6: *"Fabrication procedure for a single layer microfluidic device."* (illustration from [74]) The same procedure was used to define our PDMS caps. On the right is a photograph of our mould of KMPR.

The same parameters are used to achieve a thick patterned photoresist which will be used as a mould (Figure 3.6) to define microfluidic caps. This time, the KMPR mould is covered with a thin hexamethyldisilazane (HMDS) layer which will prevent the PDMS from sticking onto it. Polydimethylsiloxane is a mineral-organic polymer of the siloxane family. Its preparation is done by mixing a PDMS monomer (liquid) with a cross-linking agent (10:1 in weight) until no bubbles are left.

Oxygen	Power	Raw time[a]	Effective exposition time
30 sccm	25 W	1 min	46 s

Table 3.3: Parameters for the oxygen plasma.

[a]The raw time includes the power adjustment.

The mould is then placed inside a Petri dish and covered with the liquid PDMS before incubating it at 60°C overnight. The microfluidic cap are then defined by cutting them individually using a cutter blade. An oxygen plasma (parameters in Table 3.3) is required before pressing the cap and the chip together to ensure the bonding (Figure 3.7). Microfluidic tubes are then plugged manually through the device. Despite this, the PDMS - KMPR bond was not strong enough to withstand the water pressure. A transparent pressure tool (visible in Figure 3.8) has also been used to ensure the tightness.
The PDMS cap put on top of KMPR walls forms a 1 mm-wide, 5 mm-long and 150 μm-thick microfluidic channel.



Figure 3.7: One quartz chip bonded with its PDMS cap.

3.3 Electrical tests

The capacitive sensor consists of two interdigitated comb-like electrodes. These electrodes are 150 μm long and their width, spacing, and thickness are variable.
No reference electrode is used because electrochemical reactions are almost inexistent [2].

"The tested liquid is considered as an imperfect dielectric of finite permittivity and conductivity; resulting in other terms in an R-C parallel dipole. The IDE device is thus represented by an electrical model of which the equivalent impedance is represented in the frequency domain." [98]

Initial test : First, we started with an impedance measurement at a certain range of frequency (10^3 to 10^6 Hz according to Couniot [2]) in dry environment. This allowed us to control the

	Air	H_2O (25°C)	Al_2O_3	SiO_2
ε_r:	1	80	9.3	3.9

Table 3.4: Relative permittivity for the materials used.

electrical validity of our sensors all along the fabrication by detecting short-circuits with a classic IV Sweep test or abnormal signals among other things.
Tests were carried out using the probe station **PM8 PS** [8] available in the WELCOME platform. Then, we ran a capacitive test for which we paid attention to impedance modulus and phase data with respect to signal frequency with an incoming AC voltage of amplitude $V_0 = 50$ mV [9].

Circuit model

The expected impedance should have a mostly capacitive behaviour which means the logarithm plot of its magnitude should meet the equation $log(Z) = -(log(\omega) + log(C))$. Knowing this, and b being the intercept of the regression $log(Z)$ line, an experimental capacity will be deduced in the following way: $C_{expe} = 10^{-b}$.

This global capacity results from a component combination. In chapter 2, we decscribed the circuit as "a system of linear capacitors and resistors", with the most important part being a series combination of C_{ins} and C_{DL} followed by a parallel association of R_{sol} and C_{sol}. All of them are in parallel with C_{ox} that represents the substrate oxyde layer. As no DC current flows through the solid-electrolyte interface (*non-faradaic* electrodes) R_{ct} and Z_w can be discarded.

Depending on conditions in which our sensor will be tested, it can sometimes be simplified even more.

Dry environments with no insulator :

When the environment is dry, C_{DL} does not make sense any more. Likewise, C_{ins} remains null as there is no insulation layer yet.
C_{sol} is now C_{air} and, as it is assumed that no current can flow through the air, R_{air} is considered as infinite.

The result is a simplified model which only involves C_{air} in parallel with C_{ox}. Expressions of capacitances can be simplified by the capacitance formula between two parallel plate conductors. Relative permittivity ε_r of the materials involved can be found in Table 3.4.

$$C_{air} \approx \frac{\varepsilon_0 \cdot hL \cdot (N_{fing} - 1)}{d} \tag{3.9}$$

$$C_{ox} \approx \frac{3.9\varepsilon_0 \cdot wL \cdot (N_{fing} - 1)}{2d} \tag{3.10}$$

with h being the height of electrodes, N_{fing} and L respectively number and the length of the fingers, w their width and d the distance between them.

[8] Low Signal probe station with Probeshield, thermal chuck (300 °C) for IV and CV measurements.
[9] Taken from *Couniot*'s thesis.

If we compare these two capacitances, as in Equation 3.11, for low aspect ratio electrodes, the dominating component appears to be C_{ox}.

$$\frac{C_{air}}{C_{ox}} = \frac{h}{3.9w} = \frac{10^{-6}}{7.8 \cdot 10^{-6}} \approx 0.13 \tag{3.11}$$

(h = 1 μm and w = 2 μm)

and the impedance has the following behaviour:

$$Z \approx \frac{1}{j\omega C_{ox}}$$

However, our electrodes also vary in height, width and gaps. Therefore we must pay a special attention to the ratio h/w. If $h \geq 3,9 \times w$ then C_{ox} is no longer dominant. Our sensors affected by this condition are these with a width of 4 μm and whose thickness is higher than 7.8 μm .

Dry environment with insulator :

In this configuration, C_{ins} has a value.

$$C_{ins} \approx \frac{9.3 \cdot \varepsilon_0 \cdot hL \cdot (N_{fing-1})}{d_{ins}} \cdot c_1$$

with d_{ins}, the insulator thickness.

Liquid environment with insulator :

The complete equivalent circuit in liquid medium is illustrated in Figure 4.12a.
A minor pre-test has been performed with DI water to control the microfluidic circuit permeability and connections. Details on improvements are available in appendices.

3.4 Measurements with Bacteria

3.4.1 Material

Liquid Culture Medium: Tryptic Soy Broth (TSB)
Solid Culture Medium: Tryptic Soy Agar (TSA)
Buffer: Phosphate Buffered Saline (PBS) (0.01 M)
Bacterial Strain: strain ATCC35984 from *S.epidermidis* species.

Due to a lack of time[10], all sensors couldn't be tested. To keep the maximum information, three different electrode thicknesses were chosen: 2.73 μm (wafer 6-7), 5.65 μm (wafer 4-8) and 11.2 μm (wafer 4-9). Only one type of sensors was measured, which is type 'C' with about 2 μm wide electrodes and a gap of 6 μm. This choice does not come from an optimisation but results from the fact that this type 'C' was the most available and exploitable among the wafers.

[10]More information are available in appendix A.

3.4.2 Bacteria handling

S.epidermidis ATCC 35984 was cultivated on agar plates and incubated at 37 °C overnight. Then, one single colony was suspended in 50 mL of Tryptic Soy Broth (TSB) and incubated overnight at 37 °C to obtain a stationary phase bacterial culture.
On the same day of the experiment, 40 mM of the bacteria suspension were put into a test tube and centrifuged. Then bacterial cells were re-suspended in pure PBS. This was repeated twice. The bacterial concentration was calculated the next day from surface plate counting and was usually around 5.8 $\cdot 10^8$ CFU/mL for a non diluted solution.

3.4.3 Surface plate counting

To evaluate the concentration of the prepared bacterial solution [11], we need to prepare 4 Petri dishes with solid medium, labelled from "-5" to "-8", and 9 Eppendorfs labelled from "0" to "-8". First, 1000 μL of the tested bacterial solution are transferred to the "0" Eppendorf while others are filled with 900 μL of PBS.
Then, 100 μL of "0" are transferred into "-1". The later is vortexed and 100 μL of it are transferred to "-2". These manipulations are repeated until "-8". This is done to obtain a ten-fold serial dilution.
Only the four last dilutions were spread onto Petri dishes and incubated overnight at $37°C$.

3.4.4 Polydopamine

The polydopamine was prepared with 40 mg of dopamine hydrochloride diluted in 10 mL of a Tris-Buffer at pH 9.2.
This buffer was obtained by the dilution of 50 mM Tris and 150 mM NaCl in miliQ water. The pH was adjusted with diluted HCl.

3.4.5 Measurements

Material:

To make the measurements, we used the probe station *PS5026 A* connected to an impedance analyser, the *LCR 4284A (Agilent, USA)* itself controlled by the software *LabView*.
Form the liquid flow we used a closed microfluidic system composed of small (100 ml) bottles, 1.5 mm wide pipes (internal diameter) and clamps from the laboratory MIAE. The pipes were connected to a peristaltic pump.

Preparation steps:

A pre-assembled and autoclaved system (illustrated in Figure 3.9) was connected to the PDMS-Chip cell using a small (1.58 mm outer diameter and 0.5 mm inner diameter) PEEK tubes (red in Figure 3.8) and connectors to ensure the sealing of the whole circuit.
First of all, sensors where individually measured in dry environment to identify at least three of them which were valid. An open sensor (no finger electrodes) of the same thickness was used to perform an appropriate calibration and reduce the background noise.

Then the whole system was filled with PBS. Once it has reached the sensor chip, PBS was flown during 5 min at 2 RPM [12] which correspond to 175 μL/min and 5 min at 1 RPM (125 μL/min) as a first rinsing at room temperature. A first measurement was made for each valid

[11] Expected around 10^8 CFU/mL.
[12] On the peristaltic pump.

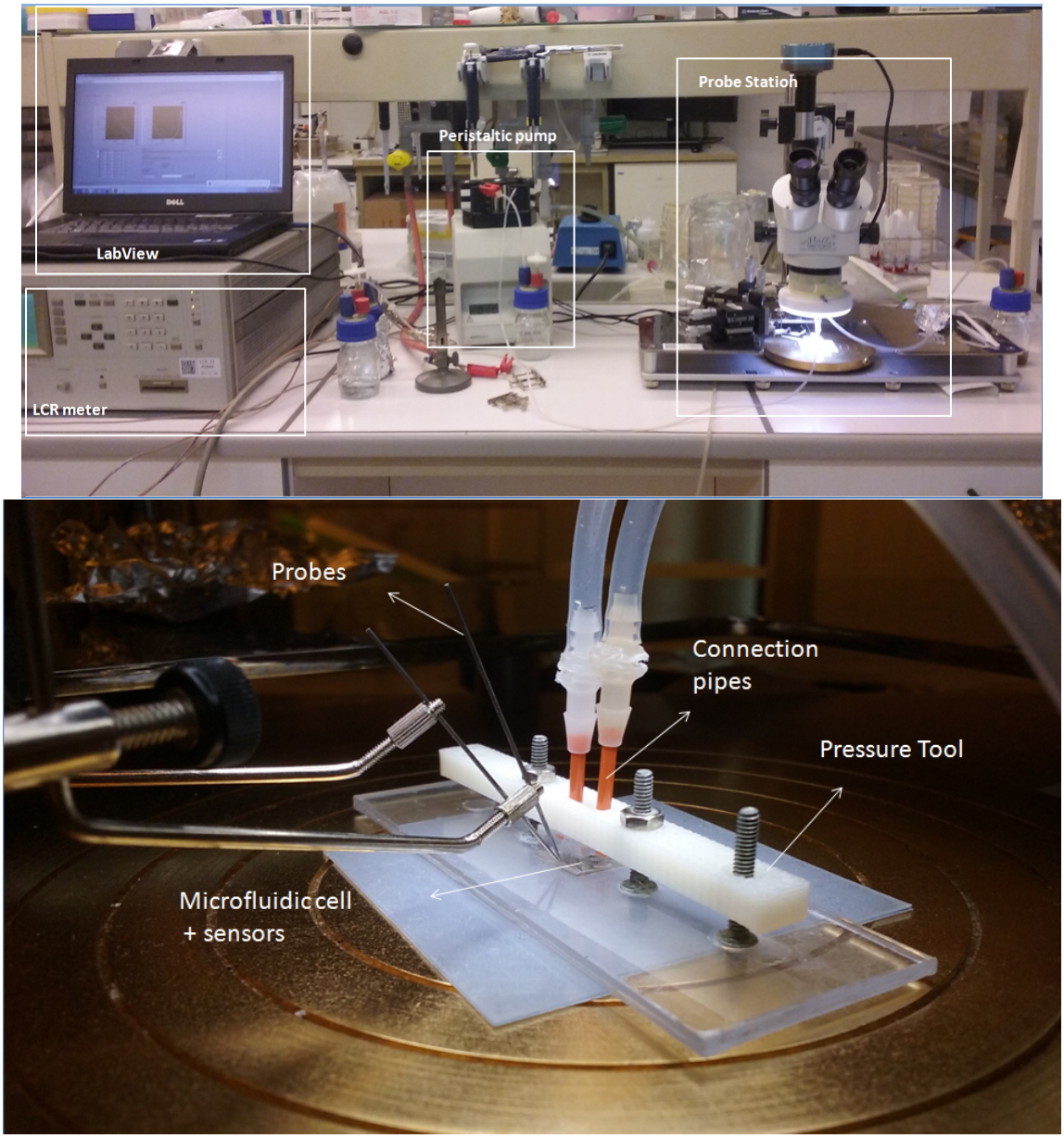


Figure 3.8: Measurement setup enabling electrical monitoring. The encapsulated sensor is positioned on the probe station and contacted through electrical probes to the LCR meter.

sensor.

The polydopamine solution was left 1 h in the dark to polymerize before being injected in the microfluidic channel. After about 6 minutes at 2 RPM to reach the sensor chip, polydopamine was left 30 minutes in dark environment without any flow or electric measurement to polymerize. Afterwards, the polydopamine was washed with PBS during 5 min at 2 RPM followed by 5 min at 1 RPM to get rid of the suspended dopamine clusters. A second electrical measurement was then made.

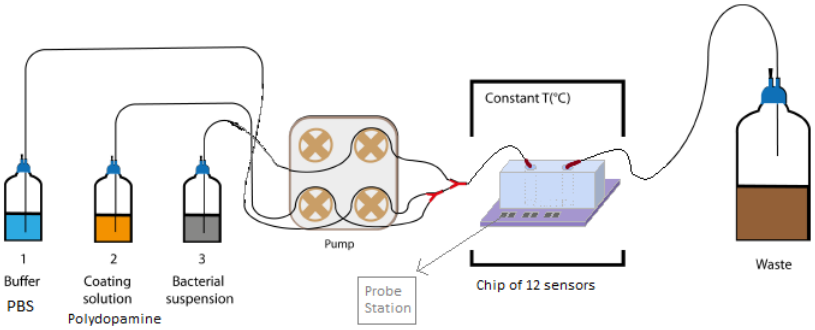


Figure 3.9: Scheme of the microfluidic setup, adapted from [99].

Bacteria entry:

Bacteria were introduced in the system at 2 RPM during 10 min followed by 5 min at 1 RPM to reach the sensor chip.
Then, speed was reduced to 0.1 RPM and measurements were performed on one sensor (identified as the best) during the 20 minutes of incubation.
Afterwards, all valid sensors were measured during 5 min then washed at high speed (3.2 mL/min).

Chapter 4

Experimental results and discussion

4.1 Fabrication

The first part of this master thesis consists in the manufacture of the desired sensors. As mentioned in Chapter 3, several types of sensors with various width and gap dimensions were build on each wafer. Therefore, it was not surprising that not all of them gave satisfying results. The aim was to maximise their quality as a function of their electrode width and gap.

The process described in Chapter 3 was applied to two different kinds of substrate: silicon and quartz.
We did not expect any difference between these two supports as they both were coated with the same adhesion layer (Ti-Cu-Ti) in the earliest steps. However, we experienced some difficulties around the electroplating that might be related to their different thermal properties. In the following sections, we will describe our results and how we coped with unforeseen problems. If necessary, the difference between silicon and quartz wafers will be highlighted.

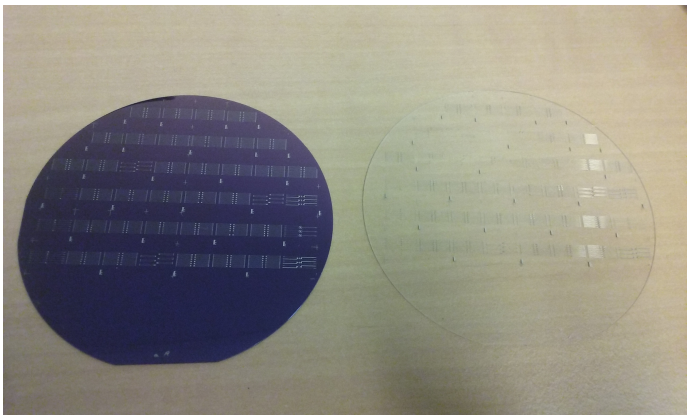


Figure 4.1: Silicon and glass wafers after electroplating and removal of resist, titanium and copper.

4.1.1 Photolithography

Both coated at 2000 rpm, AZ6632 leads to a thickness slightly thicker than 4 μm while AZ4562 reaches 10 μm in average.
After optimisation, we found the most adapted exposure time for each resist. With a voltage

Wafer name	**6-1**	**6-2**	**6-3**	**6-4**
Resist Type	AZ6632	AZ6632	AZ6632	AZ6632
Resist Thickness	3.7 μm	4.65 μm	4.7 μm	4.75 μm
Plating Time	8 min	15 min	18 min	36 min
Nickel thickness h	1.4 μm	2.3 μm	3 μm	5.1 μm
Wafer name	**4-1**	**4-2**	**4-3**	**4-4**
Resist Type	AZ4562	AZ4562	AZ4562	AZ4562
Resist Thickness	10.6 μm	10.1 μm	10.5 μm	10.3 μm
Plating Time	80 min	35 min	80 min	47 min
Nickel thickness h	9.15 μm	4.7 μm	9.32 μm	6.2 μm

Table 4.1: Summary of tests for the electrode fabrication on silicon substrate.

Wafer name	**6-5**	**6-6**	**6-7**
Resist Type	AZ6632	AZ6632	AZ6632
Resist Thickness	4.6 μm	4.53 μm	5.04 μm
Plating Time	16 min	8 min	16 min
Nickel thickness h	3.1 μm	1.57 μm	2.67 μm

Wafer name	**4-5**	**4-6**	**4-7**	**4-8**	**4-9**
Resist Type	AZ4562	AZ4562	AZ4632	AZ4562	AZ4632
Resist Thickness	10.8 μm	10 μm	9.67 μm	9.93 μm	11.8 μm
Plating Time	40 min	80 min	80 min	40 min	80 min
Nickel thickness h	5.66 μm	9.57 μm	9.79 μm	5.65 μm	11.2 μm

Table 4.2: Summary of tests for the electrode fabrication on quartz substrate.

set to 260 W, AZ4562 resist needs an exposure time of 48 seconds whereas the AZ6632 resist needs 12.5 seconds to expose the resist from surface to bottom. The calibration of the $K\&W$ light source indicated that an exposure of 4.3 second corresponded to an energy of 40 mJ/cm^2 and, therefore, 48 seconds approach 460 mJ/cm^2.
It is worth noting that, once developed, the resist is only present on all the surface that should not be later covered by nickel. Therefore, future spaces between electrodes are, at this step, narrow resist walls. It is a determining parameter. Indeed, the good resolution of these walls will later define the quality of our sensors.

It was observed that the critical dimension corresponds to the design **"A"** (in Table 4.3) with an electrode width of 2 μm and a 4 μm gap. While it developed well on a 3.7 μm thick AZ6632 resist [1], it was more variable on a 4.6 μm resist.
Design **"I"** (1 μm width) was never correctly defined and, with the AZ4562 resist ($\sim$ 10 μm), the spaces for future electrodes completely vanished.

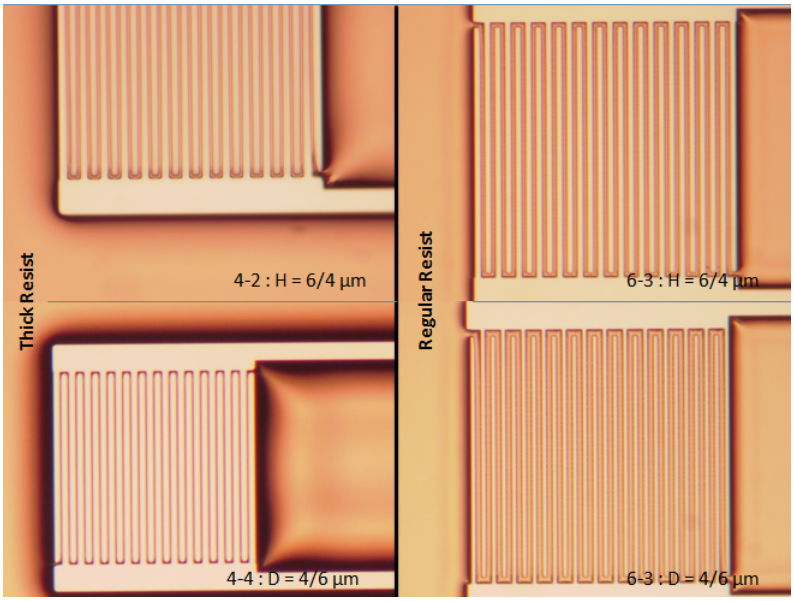


Figure 4.2: Photolithography rendering with 2 different types of resist: thick (AZ4562) and regular (AZ6632). Above is the design **H** and below is the design **D** with electrodes width of 6 μm and gaps of 4 μm and vice versa. Resist walls (darker on the picture), which define future gaps, clearly are thinner in the thick resist. These are optical microscope images with a 20$\times$ zoom.

Each wafer holds multiple sensors of various design but with one electrode thickness. In order to to distinguish them from each other, we named the wafers after the type of resist they were coated with. The first wafer coated with AZ**6**632 resist is labelled *"6-1"*, the second *"6-2"*, et cetera. For AZ**4**562 resist, it is *"4-1"*, *"4-2"*, ...
Depending on the results obtained with the first set of coated wafer, we tested various configurations which are detailed in Table 4.1. As for Quartz wafer, they are summarised in Table 4.2.

Thick photoresists complications:

At this stage, the most important problem is the lack of proportion homogeneity with resist AZ4562 (the thicker one).

[1] Obtained by a 3000 rpm coating.

Gap d (μm)	**2**	**4**	**6**	**8**
Width w (μm)				
1	/	I	/	/
2	K	A	C	L
4	J	B	D	E
6	/	H	G	F

Table 4.3: Summary of every electrode proportions tested. Each type name from 'A' to 'L' has a different combination of width and space between electrodes.

We faced a dilemma as it is almost impossible to correctly develop the resist throughout its depth and keep the exact same proportions as the ones of the mask. Indeed, we must make sure that no resist is left on areas to be plated with nickel. The compromise adopted leads to swollen-like electrode shapes because resist walls are over-exposed and thus, gaps later decrease.
In Figure 4.2, we can see that design **"D"** and **"H"** do not keep their proportions (respectively electrodes of $w = 4$ μm and gaps of $d = 6$ μm, and vice versa) in both resist type. **"D"** is the most obvious as we can see that resist walls are much smaller than they should be due to the higher exposition dose.

SEM pictures taken after electroplating confirms that electrodes are larger than expected, when thick resist is used for photolithography. Sensors with the smallest gaps (**"K"**, **"J"**) never gave good results so as those with the smallest electrode width (**"I"**) because the resist filled all the space. In Figure 4.3 is the example of the difference between sensors on wafer 6-6 (1.57 μm-thick) and wafer 4-8 (5.65 μm-thick). The latter experienced a systematic increase of the electrode width (up to 50 % of its targeted dimension) compared to the expected one (see the expected dimensions on Table 4.3).
In the end, dimensions of sensors of type **"B"** on wafer 6-6 are closer to that of type **"C"** than that of type **"B"** on wafer 4-8 .

Hardbake influence:

A further complication is the fact that hardbake (or postbake) step also contributes to the degradation of the electrode's resolution. Figure 4.4 shows the same resist pattern (design **"L"**, $w = 2$ μm and $d = 8$ μm) right before and after the harbake step. It has obviously even more repercussions on smaller features.

An attempt without hardbake was done but was not conclusive. This could be justified by this extract of *microChemicals*'datasheet [100]: *"If released to the electrolyte, the solvent may impact the metal deposition chemistry with a reduced deposition rate as a consequence. In this case, a longer softbake and/or elevated softbake temperatures are recommended. Thick resist films will have a comparable high solvent concentration especially near the substrate even after a prolonged softbake. In this case, a baking step after development at temperatures of approx. 10 °C below the resist softening point would be beneficial."*
The harbake is therefore retained but with a lower temperature of 110 °C and a duration of 30 second to avoid the "melting down".

4.1.2 Electroplating

For the first attempt, we tried a 15 minutes plating. Results were much better than planned: 2.3 μm instead of 1.6 μm expected (107.5582 nm/min x 15 min in Equation 3.7). This can be

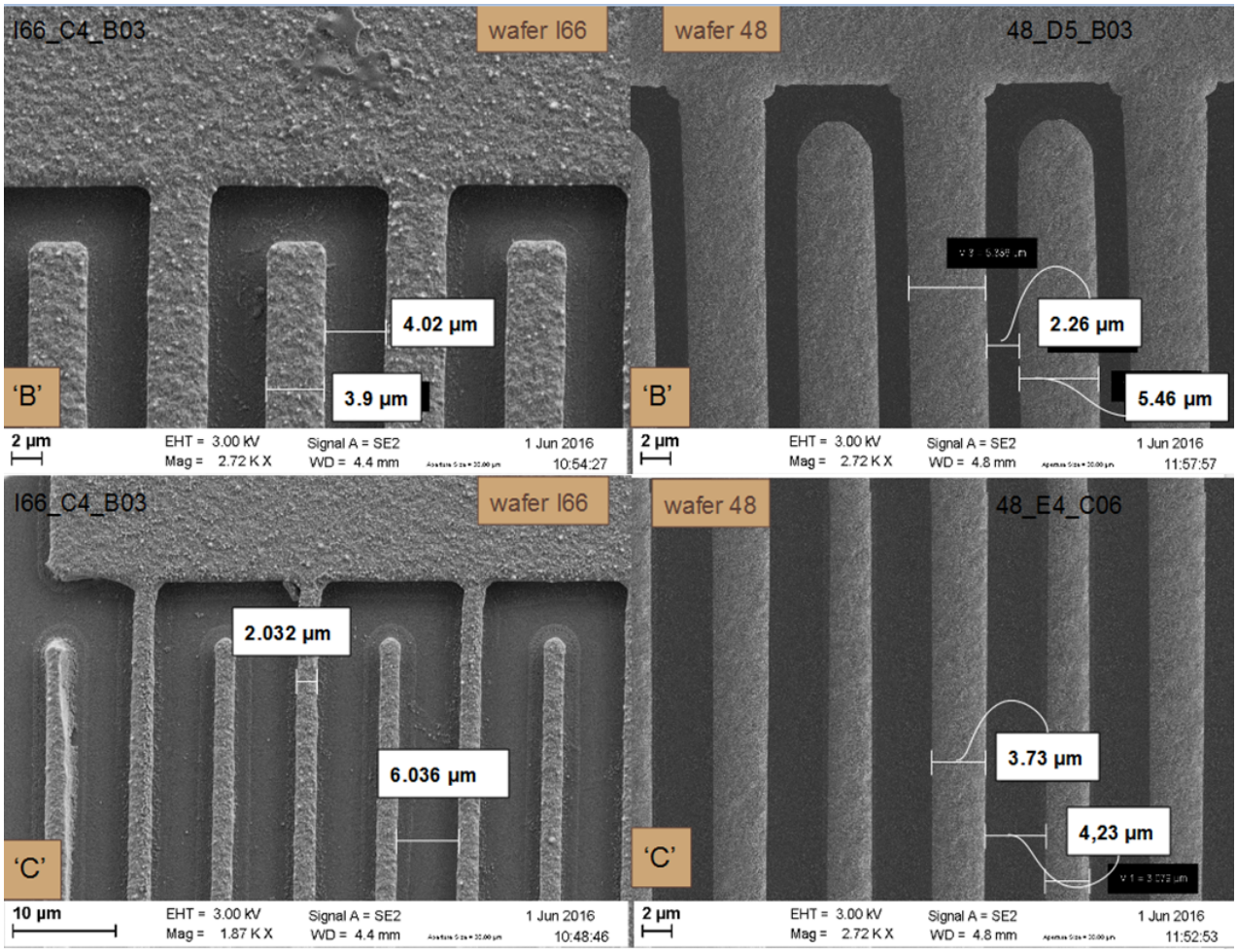


Figure 4.3: Pictures above are SEM images of sensors of type **"B"** and **"C"** of wafers 6-6 (1.57 μm-thick) and 4-8 (5.65 μm-thick). This highlights the difference of finale proportions whether we used resist AZ6632 or AZ4562. The expected proportions of sensor's type **"C"** and **"B"** on wafer 6-6 are very close from the expected ones (available on Table 4.3) whereas sensors' proportions of wafer 4-8 have experienced an increase of electrode width of ~ 1 μm.

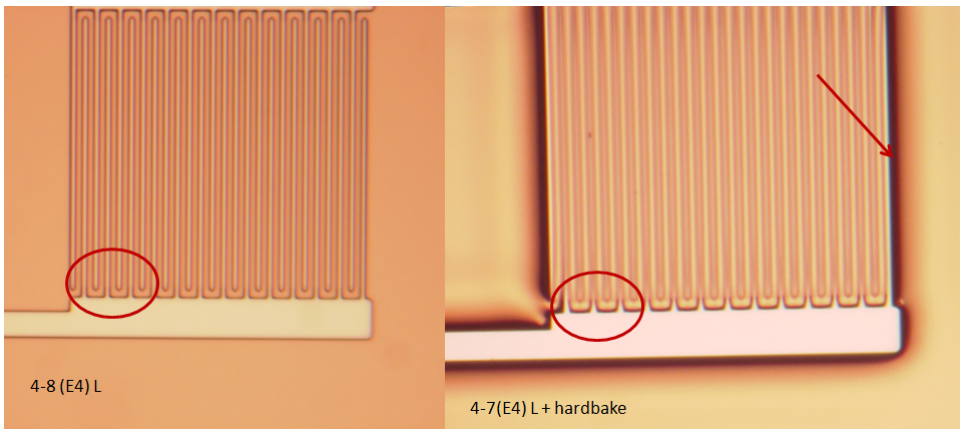


Figure 4.4: On these optical microscope (20× zoom) pictures, the same sensor design is presented before (left) and after the harbake step (right). The resist thickness is about 10 μm for both. After the hardbake, we can see that there is a pattern deterioration. Thin canals, which defines where electrodes will be, are shrinking.

explained by the fact that this rate was calculated for the complete surface but in reality, one line was never immersed in the plating solution during the process. Consequently, in formula $e = \frac{M \cdot \alpha}{nF\rho t} \cdot \frac{I}{S}$, S was smaller and the thickness e therefore more larger. If we correct the plated surface in the equation, results make perfect sense for an efficiency coefficient α of 0.75.
For first tests on silicon, we obtained a nickel thickness of 1.4 μm (wafer 6-1), 2.3 μm (wafer 6-2), 4.7 μm (wafer 4-2) and the highest was 9.15 μm (wafer 4-1) which are close enough to thicknesses initially targeted.
In Tables 4.1 and 4.2 you can notice that for one resulting thickness, electrodeposition times are not always identical. This is due to the lack of control on the actual quantity of plating solution covering the wafer. Indeed, from time to time, the evaporation, the tilting of the support, and even the differences of temperature caused variations.
All thicknesses (resist or nickel) were characterized with the surface profiler *Veeco Dektak 150* on the same spot, an alignment pattern at the center of the wafer. Indeed, the Dektak probe was too thick to scan between the electrodes.

Encountered defects:

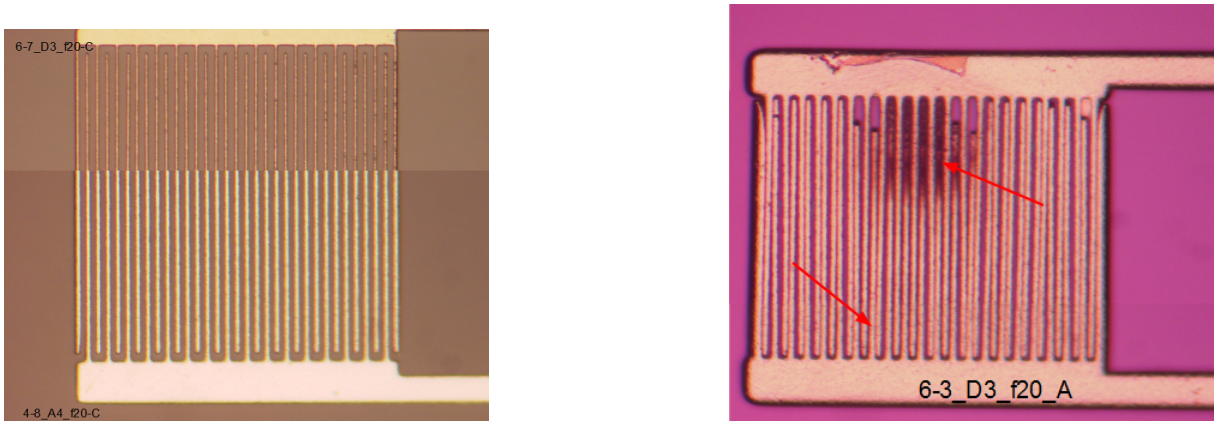
On silicon substrates, remaining **green spots** were frequently noticed (Figure 4.5a). We found two possible explanations. The first would be that these marks are **copper** which would have remained after copper etching. It made sense knowing that, for the first two wafers plated (6-2 and 4-2), *"Copper etch 49-1"* should have been used at 30 °C. But it was used at room temperature and copper etching was extremely slow and uneven. This might have led to remaining copper that would cause troubles if making contact between electrodes. When the copper etchant was used at an appropriate temperature, there were fewer marks but they did not completely vanished.
The second hypothesis is related to the use of ***TFT*** as titanium etchant. Indeed, unlike ***TFTN***, ***TFT*** has a non negligible etching rate regarding SiO_2. The titanium layer is really thin and might have been quickly completely etched, leaving the silicon oxide surface unprotected. A small **diminution of SiO_2 thickness** might be enough to produce a green colour.
Since those green marks were not found on quartz substrates, this explanation seems the most likely.



(a) (b)

Figure 4.5: Optical microscope images: a) Green spots all over the wafer (appears bluish here)are probably copper residues or a local diminution of the SiO_2 layer (20× zoom). b) Some black spots appear after nickel plating (10× zoom).

Black areas and **Collapsing electrodes** (Figure 4.6b) are two other commonly encountered imperfections.
The first one is linked to incomplete electrodes. The black effect come from a much rougher



(a) (b)

Figure 4.6: Problems encountered during the fabrication. a) These two sensors were made with the same mask dimensions. After electroplating, we can clearly see that the one obtained with a thicker resist (the bottom picture) has larger electrodes than expected. b) This picture shows two commonly encountered imperfections: incomplete electrodes and their collapsing against each other happening with thinner ones.

and insufficient nickel deposition. The fact that those black areas always appear on the same location on every sensors (upward in Figure 4.5b) let us think that this could be due to air bubbles trapped in between electrodes during the electroplating. To reduce this effect, we ensured that wafers were properly rinsed before electroplating and paid extra attention to the solution temperature. This successfully improves the results but they remain imperfect.
The electrode collapsing against each other clearly happened after the "layer removal" steps.
It was also noted that these electrodes were easily moved from their location, with a simple probe pressure, without finding any copper or titanium under-layers. This makes us think that there might have been too much under-etching to completely detach the thinnest electrodes. During the wafer drying, weakened electrodes would move and form contact with each others, making the whole sensor unusable.

4.1.3 Under-deposition of nickel

During the production of the quartz wafer series, a new issue has been highlighted. After the electroplating step, a thin greyish mark appeared sometimes in between electrodes. First, we thought it could be titanium residues but an extra immersion in titanium etchant did not change anything. Based on the fact that those marks were conductive, we deduced that it was in fact an under-deposition of nickel. Indeed, it is a well-known phenomenon, that happens in case of resist peeling.

In an application note from microChemicals [100], the importance of a proper adhesion between the resist and the wafer is detailed. Among other things, it described a thin titanium film as the best adhesion promoter. On the other hand, the etching of this titanium layer is also problematic. In case of too long etching, the resist film might experience an under-etching of the metallic adhesion layer underneath.
Given that our protective titanium film should be close to 10 nm, the required etching time is about four seconds which is extremely short. It might have been exceeded and this could be an explanation for the lifting of thin resist walls supposed to define the electrodes gaps.

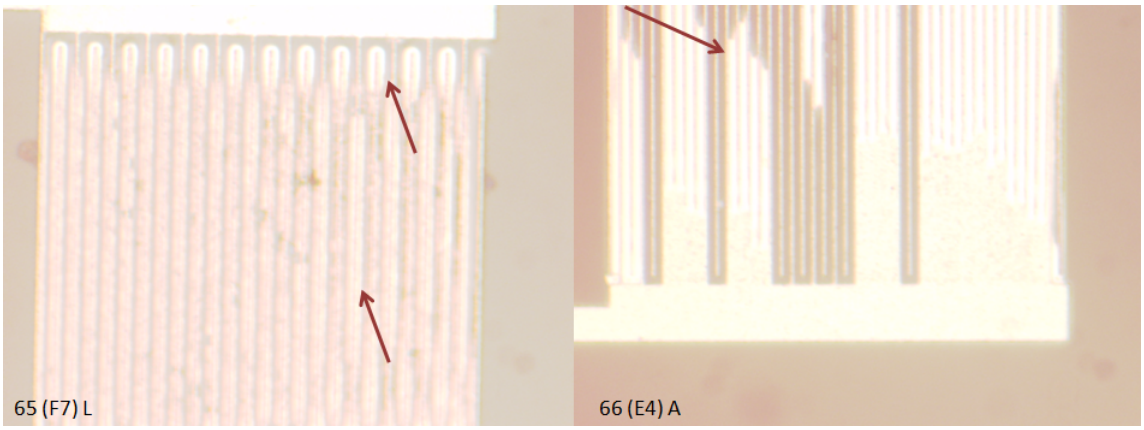


Figure 4.7: Optical microscope images of the nickel under-plating present on some quartz wafers. Both pictures were taken after the electroplating step and the removal of resist (about 5μm), Ti and Cu.

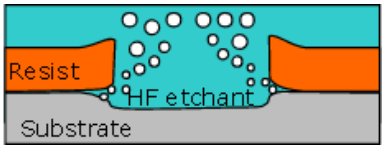


Figure 4.8: Schematic representation of the under-etching phenomenon during titanium removal (illustration from [101]).

Improving resist adhesion:

The resist peeling during electroplating can nevertheless be reduced by increasing the resist adhesion. This can be done in various ways [101]. For instance, the use of HDMS pre-treatment is recommended. An appropriate softbake will reduce the remaining solvent concentration and thus improve the resist adhesion to the substrate. *MicroChemicals application notes* also recommend a temperature of 100 °C on a contact hotplate for 1 min/μm and a slow cooling. The latter is different than the instructions provided by *AZ4500 serie data sheet* by *Clariant* which mentioned a softbake time of 50 second, independent from the resist thickness.

In the light of these information, the last sensors on quartz (wafers 6-7 , 4-7, 4-8, 4-9) were improved.

4.1.4 ALD

After a standard atomic layer deposition with parameters mentioned in the Chapter 3, we wanted to measure the deposited layer of alumina. Nevertheless, the ellipsometer requires information about the different existing layers to create a model. As we did not know the exact silicon oxide layer thickness therefore we used the targeted thickness: 300 nm. This gave us an approximation of 22.1 nm of alumina.

4.2 Electrical tests

The impedance of the manufactured sensors was measured using the probe station PM8PS for dry measurements and the PS5026 A connected to a LCR[2] for tests in liquid environment. The LCR is monitored by a software (LabView) which sends instructions and collects the results. In

[2]LCR 4284 AII

Wafer:	**6-7**	**4-8**	**4-9**
Discrepancy	3.8 %	0.5%	0.3%

Table 4.4: Maximum discrepancy between the theoretical value of a capacitive impedance and experimental measurements on sensors **"C"** in a dry environment for the three thicknesses of sensors that will be used in the bacterial experiments.

both cases, we analysed the impedance magnitude and phase over frequencies ranging from 1 kHz to 1 MHz. The normalised admittance $\| \frac{Y}{\omega} \|$ will be used to quantify the sensors sensitivity towards bacteria.
In order to determine frequencies which will be the most impacted by the presence of a bacteria, an equivalent circuit simulation was made and detailed in section 4.3.3.

4.2.1 Dry environment

In dry environment, sensors have a mostly capacitive response. This means we are expecting the phase of the impedance to be close to $-90°$ and its modulus, almost a straight line with -1 as a slope in a double logarithmic plot. On valid sensors, except for the noise presence on the phase signal, results were consistent with this hypothesis. In Figure 4.9, we can see three impedance measurements on sensors of type **"C"** ($w = 2$ μm and $d = 6$ μm) on the wafer 4-8 ($h = 5.65$ μm). We observed a discrepancy between the theoretical model and the experimental modulus of less than 0.5 %.

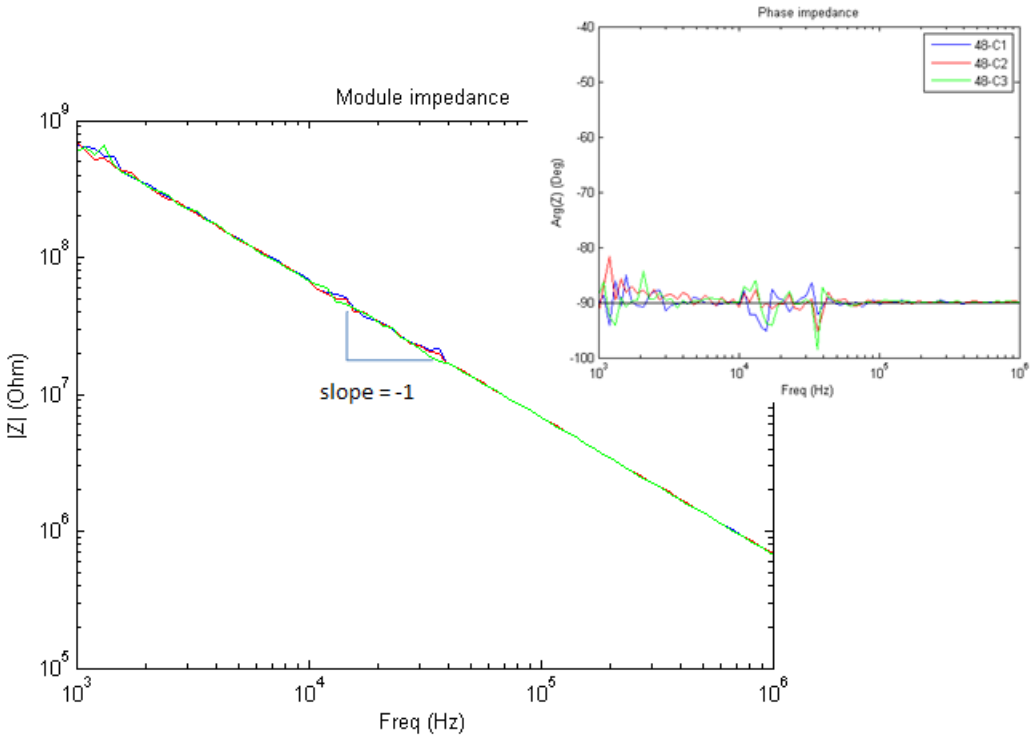


Figure 4.9: Impedance modulus and phase of sensors **"C"** on wafer 4-8 (5.65μm thick). The slope of the impedance modulus is $-1[\frac{log(Ohm)}{log(Hz)}]$ as expected for a mostly capacitive behaviour.

(Farad)	**6-4 'B'**	**6-4 'C'**	**6-4 'D'**	**6-4 'E'**
C_{ox}	$6.47{\cdot}10^{-14}$	$2.16{\cdot}10^{-14}$	$4.31{\cdot}10^{-14}$	$3.24{\cdot}10^{-14}$
C_{air}	$4.15{\cdot}10^{-14}$	$2.77{\cdot}10^{-14}$	$2.77{\cdot}10^{-14}$	$2.07{\cdot}10^{-14}$
C_{expe}	$1.02{\cdot}10^{-13}$	$1.14{\cdot}10^{-13}$	$1.35{\cdot}10^{-13}$	$1.28{\cdot}10^{-13}$
(Farad)	**6-4 'F'**	**6-4 'G'**	**6-4 'H'**	**6-4 'L'**
C_{ox}	$4.85{\cdot}10^{-14}$	$6.47{\cdot}10^{-14}$	$9.71{\cdot}10^{-14}$	$1.62{\cdot}10^{-14}$
C_{air}	$2.07{\cdot}10^{-14}$	$2.77{\cdot}10^{-14}$	$4.15{\cdot}10^{-14}$	$2.07{\cdot}10^{-14}$
C_{expe}	$8.79{\cdot}10^{-14}$	$7.98{\cdot}10^{-14}$	$8.69{\cdot}10^{-14}$	$1.86{\cdot}10^{-13}$

Table 4.5: C_{ox} and C_{air} are theoretical values and C_{expe} is the experimental capacitance measured for a dry medium and without insulator on wafer 6-4 ($h = 5$ μm).

Width/(Gap + Width)	**3/5**	**1/2**	**3/7**	**2/5**	**1/3**	**1/4**	**1/5**
	H	B	F	D	A	C	L
		G			E		I
		K			J		

Table 4.6: Ranking of various designs depending on their width over (width + gap) ratio.

We established earlier that the dominating component in this situation is the oxide capacitance:

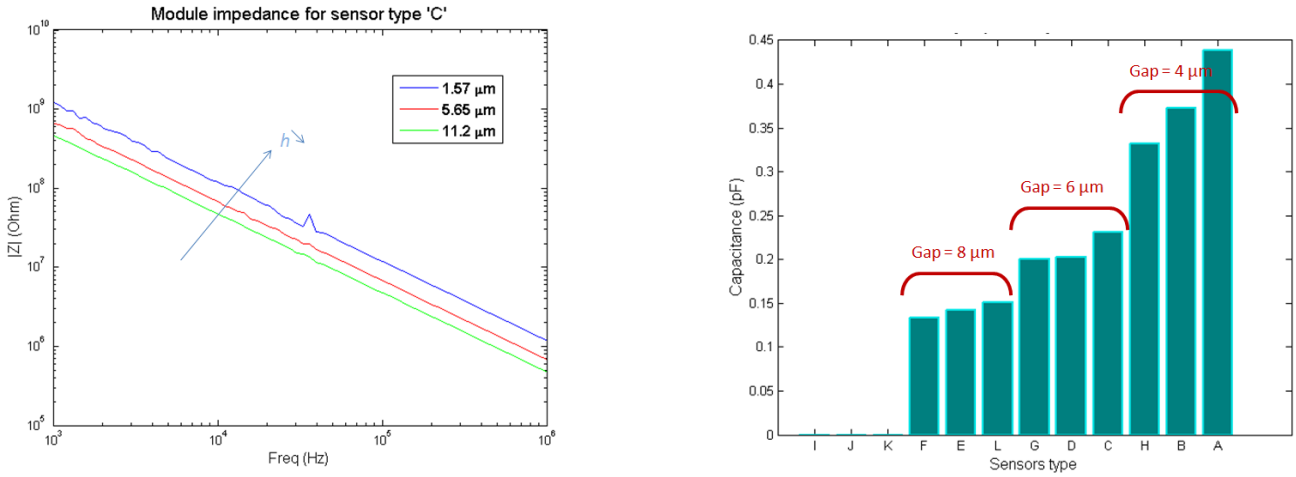
$$C_{ox} \approx \frac{3.9 \cdot \varepsilon_0 \cdot wL \cdot (N_{fing-1})}{2d}$$

with h being the thickness of electrodes, L the length of the fingers, w their width and d the distance between them.
By observing the experimental and the theoretical value of the global capacitance of different sensor's design (see example with wafer *6-4* in Table 4.5), we can see that the measured capacitance is always higher than the calculated one, C_{ox}. This means that, unlike what we thought, the parallel capacitance, C_{air}, is significant. The total capacity approximation is $C_T = C_{ox} + C_{air}$. The mean ratio $\frac{C_{expe}}{C_T}$ from wafer *6-4* is 1.48 with a variance of 0.53 [3]. Both C_{ox} and C_{air} feature d, the gap between electrodes, in their denominator. Therefore, a decreasing global capacitance with d increasing is not surprising. Sensors on quartz have capacitances mostly depending on d (Figure 4.10b), while sensors on silicon global capacitance can be ranked in the same order than their ratio $(\frac{w}{w+d})^{-1}$ (available on Table 4.6).
Therefore, the best sensor designs on quartz are type **"B"**($w = 4$ μm and $d = 4$ μm) and **"A"** ($w = 2$ μm and $d = 4$ μm) with respect to the highest global capacitance. Surprisingly, the highest capacitance on silicon is achieved by sensors of type **"H"** ($w = 6$ μm and $d = 4$ μm). These dimensions are nevertheless not suitable for an optimal sensor as larger electrodes increase the chances of bacteria depositing on top of them rather than between electrodes.

Alumina insulation layer:

All wafers were coated with alumina using the same parameters which gives approximately a 22 μm-thick layer. As illustrated in Figure 4.11, the capacitance component of this insulating layer, C_{ins}, is placed in series with the previous circuit. It will decrease the total capacitance. The

[3] Those values are obtained when 'L'-sensors are excluded.



(a) (b)

Figure 4.10: Influence of the sensor thickness: a) the graph shows for the same type of sensor (**"C"**, $w = 2$ μm and $d = 6$ μm), an increasing impedance modulus signal with a decreasing electrode thickness. This also means that capacitance is increasing with this parameter. b) The ranking of sensors' global capacitance on wafer 4-8 ($h = 5.65$ μm) shows that the larger the gap (d), the smaller the capacitance will be.

average shift calculated on a 2.73 μm thick sensor (wafer 6-7) is 0.0276 pF.

However, we did not find an explanation for the increase of C_{tot} for wafers 6-1 ($h = 1.4$ μm) and 6-6 ($h = 1.57$ μm) after their coating with insulator. The mean difference was respectively 0.0748 pF and 0.0417 pF and contradicted the logic of capacitance in series. Both were sensors with an electrode height inferior to 2 μm which might have an influence.

4.2.2 Liquid environment

When sensors are immersed in liquids, R_{sol}, the resistance component in parallel of C_{sol} is no longer infinite. Furthermore, the double layer capacitance C_{DL} must now be taken into account. In Figure 4.13, which compare measurements in air and in DI water, the overall impedance modulus decreases while the phase has an inverted bell-like shape and a much weaker noise.

PBS corrosion:

In parallel to the tests with bacteria, we ran an other experiment.
A chip of wafer 4-9 (11.2 μm thick), was exposed to PBS for the same duration as a test with bacteria cycle (about 4 hours). The aim of this test was to observe the impact of PBS on the insulator layer (alumina). However, liquid could evaporate and distort overall results. Details about it are given in appendix A.

4.3 Bacterial response

As mentioned in Chapter 3, only 3 thicknesses were tested under a flow of bacteria: 2.73 μm (wafer 6-7), 5.65 μm (4-8) and 11.2 μm (4-9).
for each manipulation, measurements under dry environment were first carried out to detect at least three valid sensors. An important thing to know before analysing the results is that, as mentioned in section 4.1.1, sensors coming from wafers 4-8 and 4-9 were made with thick resist

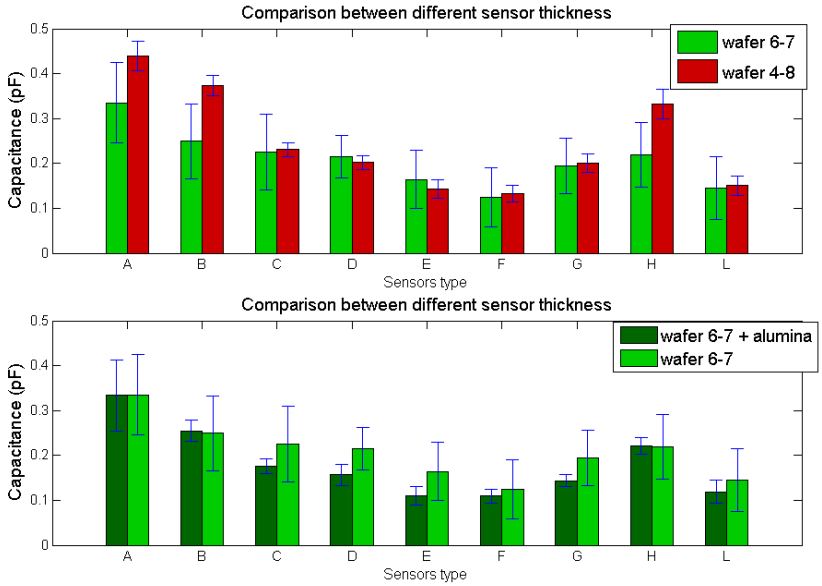
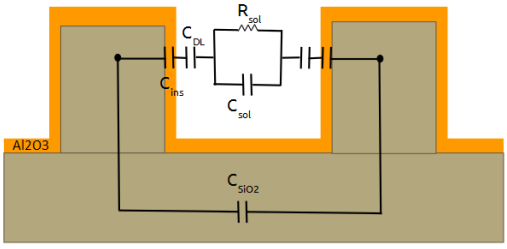
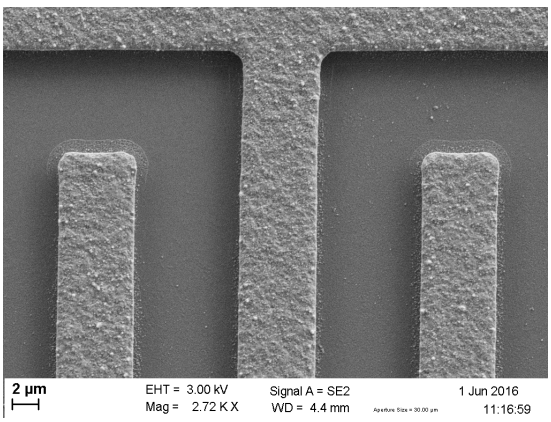


Figure 4.11: These plots gather the capacitances of each sensors type with two different thicknesses (2.73 μm and 5.65 μm respectively green and red). The graph below is the comparison between a sensor of thickness 1.57 μm with (dark green bar) and without a 22 μm Al_2O_3 layer (light green bar). Variances are smaller in wafer 4-8 than wafer 6-7. It also decrease with the insulator addition.



(a)



(b)

Figure 4.12: a) Equivalent impedance circuit based on finger electrodes in a solution. This solution has a resistance R_{sol} and a capacitance C_{sol}. C_{DL} is the ionic double layer capacitance. b) SEM top view of interdigitated electrodes of nickel covered by 22 nm of alumina on wafer 6-6 ($h = 1.57$ μm).

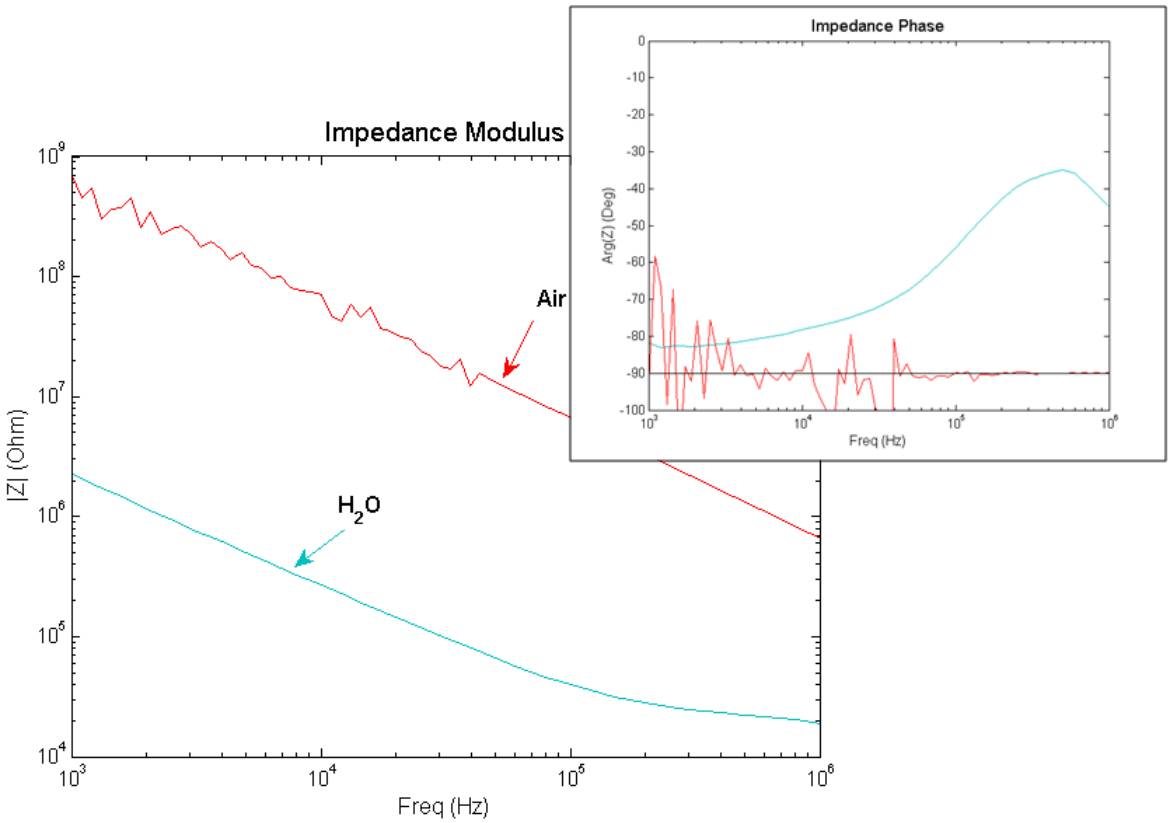


Figure 4.13: Impedance modulus and phase of sensor 'G' on wafer 4-5 (5.66μm thick) in dry environment (red curve) and under tap water (blue curve).

and therefore did not preserve the expected dimensions. Their electrodes width is thus closer to 4 μm than 2 μm and their spacing smaller than 6 μm. This is illustrated in Figure 4.3.

The analysis is done by observating the impedance modulus and phase on a frequency spectrum. For every thickness, we did several measurements with air, PBS, PBS + PolyDopamine and PolyDopamine + Bacterial solution. An example is given in Figure 4.14a and 4.14b for one sensor on the wafer 4-8.

Looking at the phase (Figure 4.14b), from 1 kHz to ~100 kHz the curve decrease to -90°. This divergence at the lower frequencies might be due to the measurement noise. Indeed, the phase in a dry medium, which should be constant, is also more noisy at lower frequencies. In liquid environment, a peak which tends to -70° appears at ~ 600 kHz.

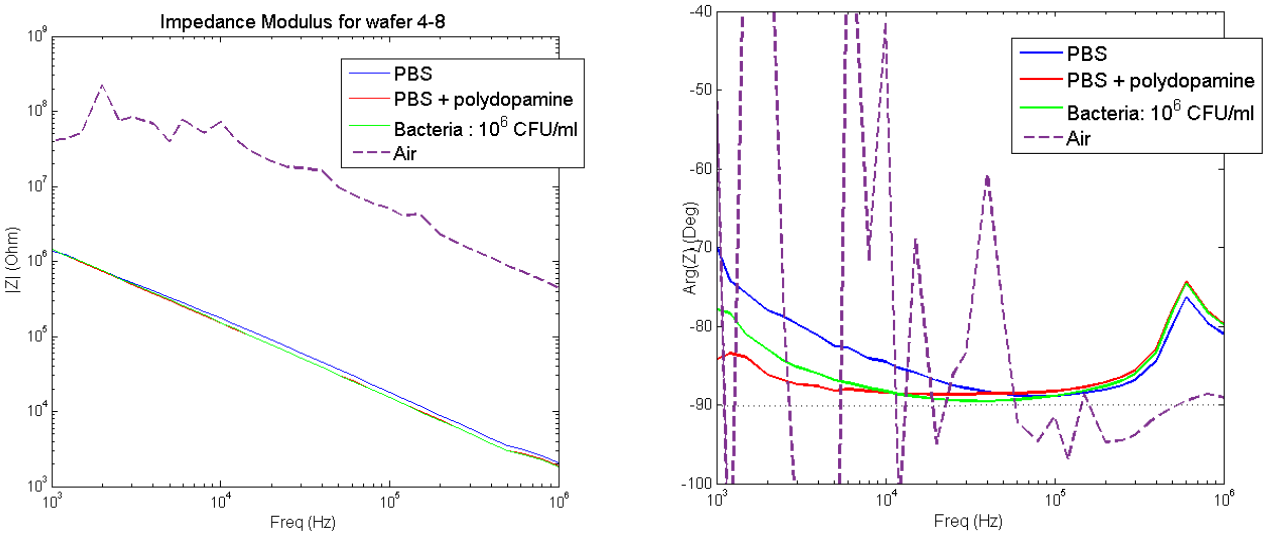
The quantification of the bacteria's impact can be done by analysing the sensitivity S defined as:

$$S = \| \frac{|Y_B| - |Y_D|}{Y_D} \| \tag{4.1}$$

with $|Y_B|$, the signal admittance with bacteria and dopamine and $|Y_D|$ the one with dopamine only.

4.3.1 Polydopamine layer

During the coating of electrodes with a polydopamine layer, the signal undergoes a first series of modifications. The phase is overall shifted toward higher values and global capacitance increases.



(a) (b)

Figure 4.14: Impedance modulus (*a)*) and phase (*b)*) for one sensor of type **"C"** under air, PBS, PBS + polydopamine and bacteria at 10^6 CFU/mL.

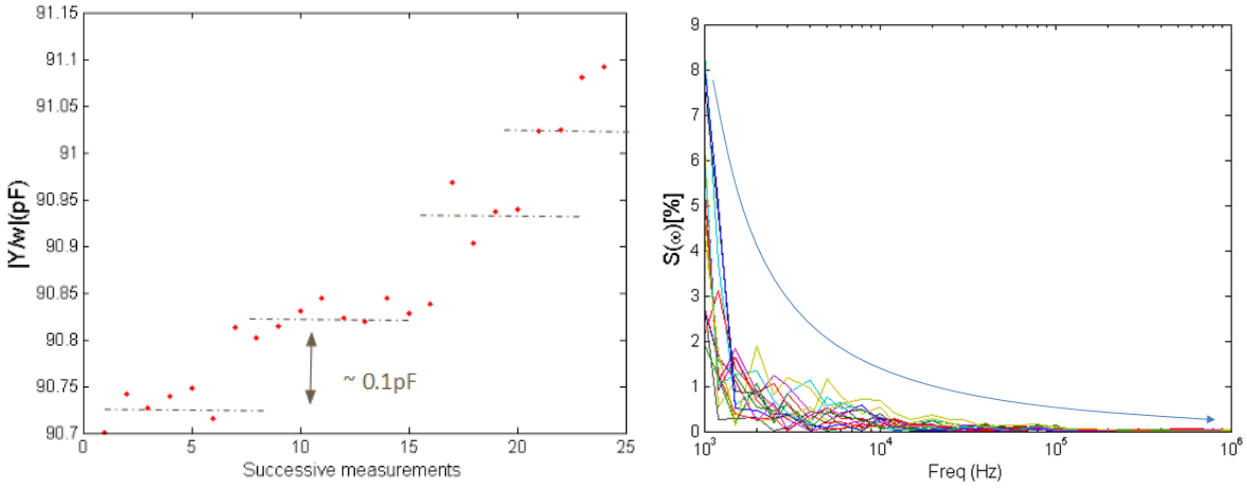
Wafer	**6-7**	**4-8**	**4-9**
Desired vs real	concentration	CFU/mL	
10^8	$6.6 \cdot 10^8$	$9.2 \cdot 10^8$	$6.6 \cdot 10^8$
10^6	$12 \cdot 10^6$	$11.9 \cdot 10^6$	$12 \cdot 10^6$
10^4	$10.8 \cdot 10^4$	$12.3 \cdot 10^4$	$12.3 \cdot 10^4$

Table 4.7: Real concentration of bacteria after plate counting.

The modulus shift varies widely and impacts especially frequencies under 3.162 $\cdot 10^4$ Hz.
The signals with polydopamine will then be used as "baseline signals" to detect bacteria's presence.

4.3.2 Bacterial incubation

Bacteria were injected in the system during twenty minutes at very low speed so that they could incubate and progressively bind to the sensor' surface. Over this time, $\| \frac{Y}{\omega} \|$ was increasing on average by 1.54 % over 20 minutes with a variance of 0.0428 % at the frequency of 10^5 Hz.
In [2][4], a real-time normalized admittance graph at 1 MHz is presented. For a *S.epidermidis* concentration of $7 \cdot 10^6$ CFU/mL, the growth rate during bacterial incubation was of 5 fF/min with AC-Electroosmosis.
In comparison, our $\| \frac{Y}{\omega} \|$ progression at 1 MHz and $\sim 10^7$ CFU/mL is 0.144 pF/20min for wafer 6-7 ($h = 2.73$ μm), 0.297 pF/20min for wafer 4-8 ($h = 5.65$ μm) and 0.104 pF/20min for wafer 4-9 ($h = 11.2$ μm). It gives respectively, 7.2 , 14.85 and 5.2 fF/min, a greater growth, without any bacterial attraction system.



(a) (b)

Figure 4.15: *a)* Progressive increase of $\| \frac{Y}{\omega} \|$ at 10^5 Hz with 0.1 pF increments and *b)* impedance modulus variations between successive measurements on wafer 4-8 ($h = 5.65$ μm) at a bacterial concentration of 10^8 CFU/mL. The noise decreases with higher frequencies to less than ~0.5%.

On some graph, especially in Figure 4.15a (W4-8[5] for a bacterial concentration of 10^8 CFU/mL), $\| \frac{Y}{\omega} \|$ seems to be increasing by increments of $\sim$ 0.1 pF . These increments could be the result of a progressive income of bacteria. N. Couniot evaluated, with inverted microscope images, the impact of a single bacterium on the total signal as being about $\sim$ 228 aF, whether it is bonded to the surface or not. If this value is still applicable in our experiments, the increments could either be the result of successive income of large (about 440 bacteria each time) clusters of bacteria, either be due to another phenomenon such as a spontaneous corrosion of alumina by PBS. The latter could not be confirmed.

Figure 4.15b represents the admittance variation between successive measurements on the same sensor (of wafer 4-8) at a bacterial concentration of 10^8 CFU/mL. The difference between two successive signals, supposed to be the same, is exponentially decreasing with respect to the frequency which confirms that the background noise is much more important at lower frequencies. Maximum variations observed between successive measurements at a frequency of 1 MHz are

[4] [2] p.117 Figure 3.9
[5] W4-8 stands for wafer 4-8.

Wafer:	**6-7**	**4-8**	**4-9**
Bacterial concentration			
10^8 CFU/mL	0.148%	0.0494%	0.354%
10^6 CFU/mL	0.0721%	0.0458%	0.0539%
10^4 CFU/mL	1.241%	0.0484%	0.074%

Table 4.8: Maximum variation between successive measurements on one sensor under the same bacterial concentration at 1 MHz.

gathered in Table 4.8. From here, we can suppose that a sensitivity under 0.2 % would not make sense as it would be too close to the background noise.

4.3.3 Sensitivity

In order to be able to compare experimental results and interpret them, we created a simplified model of the electrode - bacteria combination to have a look at the expected magnitude and phase of the resulting impedance signal. Physical values used in order to compute each component value are coming from [102] and are gathered in Table 4.9.

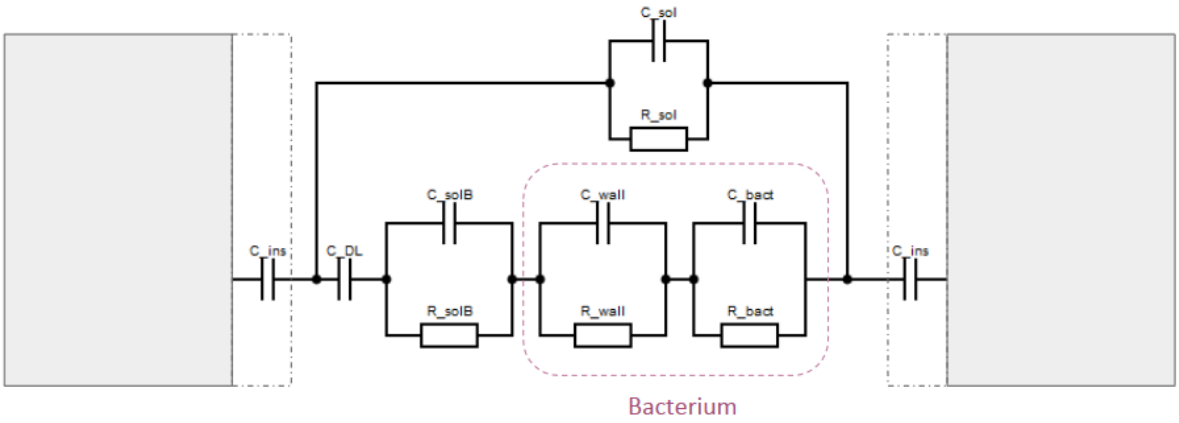


Figure 4.16: Equivalent circuits of a bacterium in PBS solution between two electrodes. The bacterium is placed against one electrode wall.

As illustrated in Figure 4.16 the equivalent circuit that we used is composed of C_{ins} (the capacitance of the insulator layer on each side) in series with a double layer capacitance, C_{DL}. We represent the solution behaviour by means of two set of parallel capacitance and resistance. One set was put in series with the bacteria (C_{solB} and R_{solB}) and the other in parallel (C_{sol} and R_{sol}). The latter will enable to take the solution all around the bacterium into account. The total circuit was a bit too simple without it and the impedance magnitude wouldn't fit. We considered the bacterium to be close to one electrode wall and to have therefore no solution between it and the electrode wall.
The bacterium itself is modelled by two consecutive parallel capacitance-resistance, one to represent the cell membrane (highly resistive) and the other the inside (highly conductive).

The total impedance of this circuit can be written as in Equation 4.2.

Symbols	Description	Values	Units
ε_0	Void permittivity	$8.85 \cdot 10^{-12}$	-
ε_{ox}	oxide relative permittivity	3.9	-
ε_{cyt}	cytoplasm permittivity	70	-
ε_{sol}	solution permittivity	80	-
ε_{wall}	cell wall permittivity	60	-
d_{ins}	insulator thickness	$22 \cdot 10^{-9}$	m
d_{cyt}	cytoplasm diameter	$1.2 \cdot 10^{-6}$	m
d_{bact}	bacteria diameter	$1.2 \cdot 10^{-6}$	m
d_{sol}	distance in solution	$d - d_{bact}$	m
t_{wall}	cell wall thickness	$20 \cdot 10^{-9}$	m
λ_D	Debye length	$24 \cdot 10^{-9}$	m
σ_{cyt}	cytoplasm conductivity	0.8	S/m
σ_{wall}	cell wall conductivity	$0.4 \cdot \sigma_{sol}$	S/m
σ_{sol}	solution conductivity	$1.8 \cdot 10^{-3}$	S/m

Table 4.9: Physical parameters (extracted from [102]) that are used for the equivalent electrical model with PBS as the solution and alumina as insulator.

$$Z_{Tot} = 2(j\omega C_{ins})^{-1} + [R_{sol}^{-1} + j\omega C_{sol} + [(j\omega C_{DL})^{-1} + (R_{solB}^{-1} + j\omega C_{solB})^{-1} + Z_{Bact}]^{-1}]^{-1} \quad (4.2)$$

$$Z_{Bact} = (R_{wall}^{-1} + j\omega C_{wall})^{-1} + (R_{Bact}^{-1} + j\omega C_{Bact})^{-1} \quad (4.3)$$

AT first, parameters values of Table 4.9 were used but the impedance magnitude was quite far from the experimental values. Therefore, we adapted this model by modifying some components so that experimental and simulation curves fitted at best. This adaptation can be seen in Figures 4.17 a) and b).

In Figure 4.19a, the blue curve represents the simulation of the sensitivity to one bacterium entry, calculated with parameters in Table 4.9 ($\sigma_{sol} = 1.8$ mS/m). As we can see, the impact of the bacterium components is the most significant in frequencies above 10^5 Hz with sensitivities above 73 %. Therefore, it seems logical to use manly sensitivity value corresponding with frequencies larger (or equal) than 10^5 Hz for the efficiency comparison. It can also be noted that this sensitivity seems to saturate at about 93 % which is very high.

Then we vary slightly (1%) each resistance and capacitance of the circuit to discuss their individual impact on the sensitivity. Table 4.10 gathers their maximum sensitivity percentage found between 1 kHz and 10 MHz. As we can see, the most important variations originate from C_{sol} and R_{sol}, components representing the solution all around the cell. However, our hypothesis is that this solution will not change during the experiment. Indeed, successive re-dilution of bacteria in PBS contributes to maintain the medium properties constant between successive flushing.
As for the bacterium related component, the most impact comes from R_{wall}, C_{wall} and R_{bact}. On Table 4.10, their respective maximum value frequency are 10^5, $8 \cdot 10^5$ and $3 \cdot 10^6$. Based on these information, we chose to select 10^5 Hz and 10^6 Hz as comparison points for the sensitivity of each sensors.

At the very end of the redaction, it was noticed that the impedance magnitude given by the model fitted much more when the σ_{sol} parameter was set to $1.8 \cdot 10^{-1}$ S/m instead of 1.8 mS/m, which is the value extracted from Numa Couniot's PhD thesis and articles. Exact conductivity

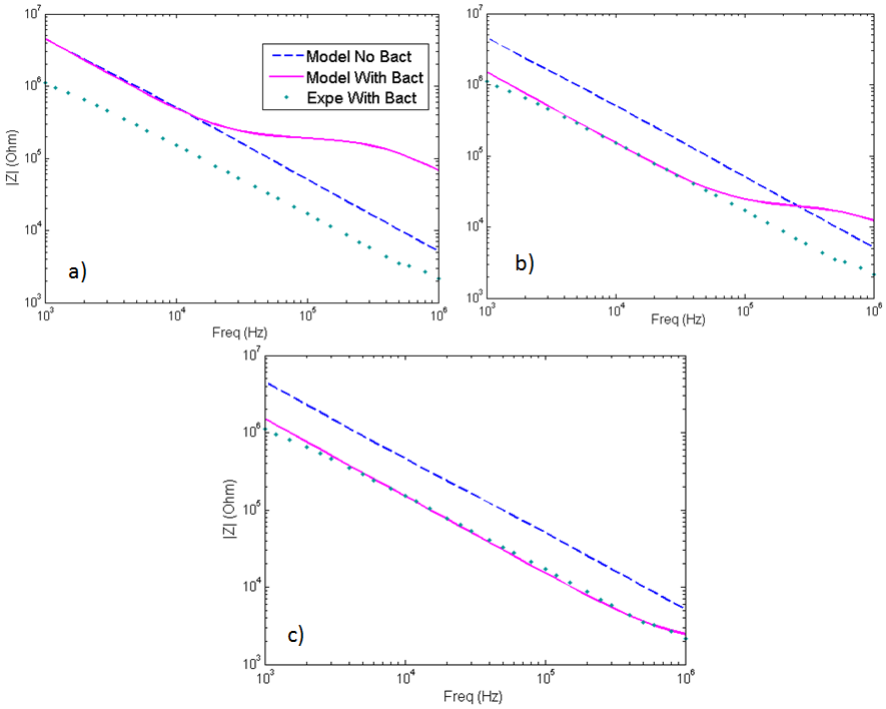


Figure 4.17: These graphs show the comparison of the impedance magnitude for the model without bacteria (in dark blue), the model with one bacteria (continuous line) and an experimental result on wafer 4-8 with 10^8 CFU/mL (dotted line). On **a)** is the results with values in Table 4.9, in **b)** the components in the model with bacteria were adjusted in the following way: $C_{ins} = 3$ times its previous value, $C_{sol} * 5$, $C_{solB} * 2$, R_{solB} and $R_{sol} * 0.1$. **c)** is the result of $\sigma_{sol} = 1.8 * 10^{-1}$ S/m and $C_{ins} * 3$.

Component + 1 %	Smax (%)	Freq max (Hz)
C_{solB}	$4.18 \cdot 10^{-6}$	10^7
C_{sol}	$9.352 \cdot 10^{-1}$	10^7
R_{solB}	$2.41 \cdot 10^{-3}$	$3 \cdot 10^6$
R_{sol}	$8.654 \cdot 10^{-1}$	10^5
C_{DL}	$2.24 \cdot 10^{-5}$	$1.5 \cdot 10^3$
C_{bact}	$2.18 \cdot 10^{-4}$	10^7
R_{bact}	$8.993 \cdot 10^{-3}$	$3 \cdot 10^6$
C_{wall}	$1.838 \cdot 10^{-2}$	$8 \cdot 10^5$
R_{wall}	$1.094 \cdot 10^{-2}$	10^5

Table 4.10: Sensitivity maxima responding to a 1% variation of components with respect to values in Table 4.9.

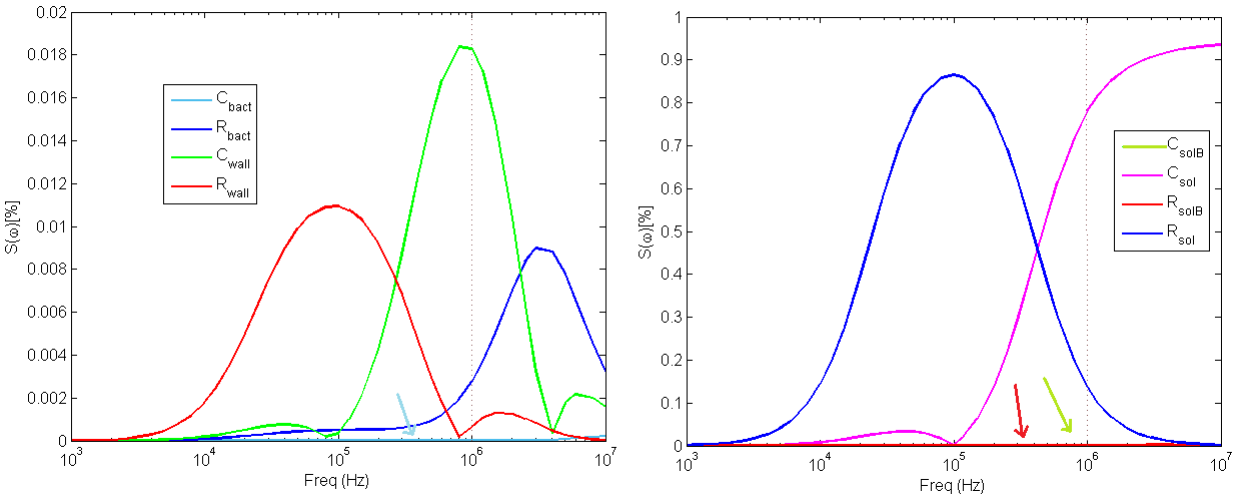
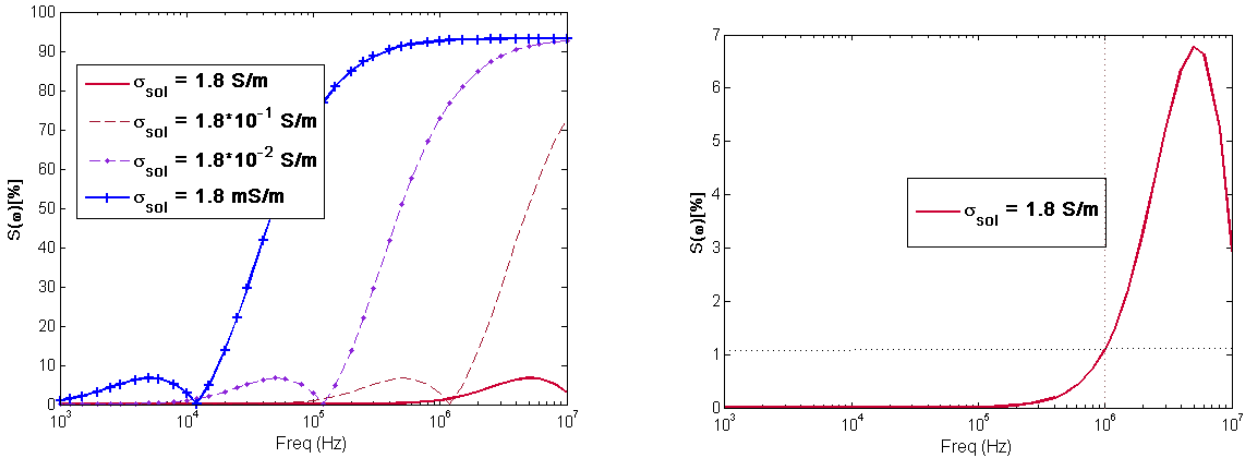


Figure 4.18: Sensitivity simulations for 1% variation of circuit's components with values in Table 4.9.



(a) (b)

Figure 4.19: *a)* Simulation of the sensitivity to the entry of one bacteria with an increasing σ_{sol}. *b)* Simulation of the sensitivity to the entry of one bacteria with $\sigma_{sol} = 1.8$ S/m.

values are difficult to find if not by direct measurements. However, we did manage to find a similar product and we were able to estimate that the actual conductivity was indeed closer to 1 S/m than to 1.8 mS/m. If so, this difference has a significant impact as the highly conductive PBS will have a screening effect on the bacteria's presence, which will reduce their detection. Therefore we re-simulated the sensitivity to the entry of one bacteria with an increasing σ_{sol}. As illustrated in Figure 4.19b, with a σ_{sol} of 1.8 S/m, the expected sensitivity at 1 MHz drops to approximately 1 %. To get a maximum response, we should have made the frequency rising up to 2.5 MHz but this frequency was out of the LCR limits.

In light of this, our choice of 100 kHz and 1 MHz as interest frequencies, in our opinion, stays a good one, even if the results would probably have been much more efficient if the solution had a lower conductivity.

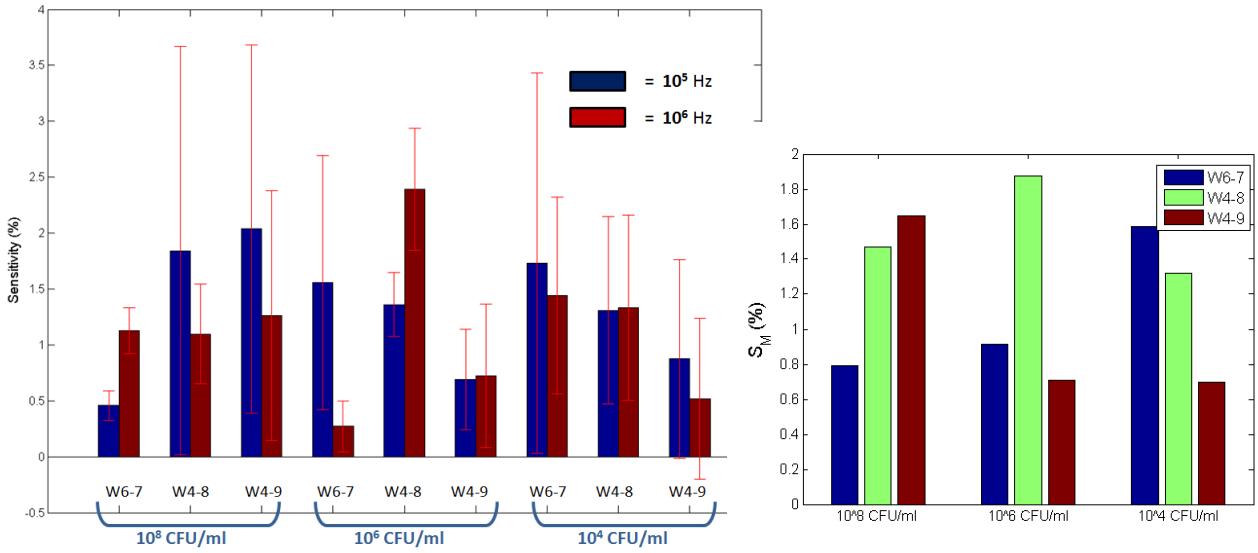
4.3.4 Influence of the thickness

To be able to compare the different sensitivities and potentially designate the best sensor, we need a metric.
Considering that the background noise is much more important at the lower frequencies (under $5 \cdot 10^4$ Hz) and that sensitivities at 10^5 and 10^6 Hz were the most relevant frequencies according to our simulations, S_M is therefore defined as an average between the sensitivities measured at 10^5 Hz and 10^6.
Figure 4.20a gathers results of sensitivity for the three different electrode thicknesses and three bacterial concentrations that were tested. It is worth noting that 10^8, 10^6 and 10^4 CFU/mL are the targeted concentrations. The real values after plate counting is available on Table 4.7.
The first difficulty is that most of the results have a large standard variation. The largest ones (up to $\pm$ 1.8 %) could be due to outliers. However, there were not enough sensors tested to dismiss some of them. It is important to mention that this variation reflects the fact that sensors supposed to be identical do not react exactly the same.
At 10^8 CFU/mL, the thickest sensor seems to be the most sensitive but this trend switches afterwards, at lower concentrations. On wafer 6-7 ($h = 2.73$ μm), the sensitivity even rises with lower bacterial concentration which is quite surprising and contributes to suggest that another phenomenon was involved. On Table 4.8, we can see that the wafer 6-7 is also that with the most variation under steady conditions. Under a concentration of 10^4 CFU/mL we note that there is a maximum variation of 1,24 % between successive measurements on the same sensor at a frequency of 1 MHz.
Wafer 4-8 ($h = 5.65$ μm), on the other hand, seems to be stable and have S_M of 1.47, 1.88 and 1.32 % respectively for concentrations of 10^8, 10^6 and 10^4 CFU/mL [6]. Its variations between successive measurements in the same environment (noise) is also the most steady, around 0.048 %.

Under the hypothesis that bacteria are the only source of variation in impedance signal, Figure 4.20b shows that there is still a detection at $\sim 10^5$ CFU/mL (real concentration) and that it rises to 1.586 % for a thickness of 2.73 μm and 0.696 % for a thickness of 11.2 μm.
The electrode thickness of 5.65 μm seems to give the best results with the lowest variance (0.794). It might be linked to the fact that it was also the sensor with the best definition.

In the absence of additional and methodical analyses of these sensors, it is difficult to draw a conclusion out of the graph trends. The high variability of results on a same wafer shows that even with the same production conditions, sensors still have a versatility way too high. The sensor itself has a significant impact compared to bacteria.

[6] Those are the targeted values. See the Table 4.7 for real bacterial concentration values.



(a) (b)

Figure 4.20: *a)* represents the sensitivity at 10^5 and 10^6 Hz for 10^8, 10^6 and 10^4 CFU/mL on sensors W6-7, W4-8 and W4-9 and *b)* is the metric S_M which is the average of the two frequencies.

However, with an appropriate case-by-case calibration, it could be improved.

The current results also lack of indication about the limit of detection. Indeed, the lowest concentration tested was $\sim 10^5$ CFU/mL and, at this level, there was still a noticeable detection. If we had identified the smallest concentration which generates a non-zero signal we would have a confirmation of the validity of our results.

4.4 Reconsiderations: variance factors encountered

All along this master thesis, plenty of factors could have influenced the final results. Starting with the fabrication itself which, despite the care taken in producing sensors, cannot be 100 percent reproducible.

- Measured heights, for resist as for nickel, were taken in the center of each wafer and might very likely vary with wafer radius. Additional control points could help to have a better idea of this variation.

- Resists *AZ6632* and *AZ4562* do not require the same exposition intensity. The second one, as a thick resist, needs a longer exposition to reach its whole height. This leads to much rougher and modified dimensions. It was observed that resist walls intended to define future gaps between electrodes are generally thinner than their pattern on the mask. Therefore, two sensors manufactured with the same mask will not necessarily keep the same dimension at the end of the process. To prevent this effect, chromium masks should have been designed in a way that anticipate the deviation.

- Imperfections can also be found in the measurement protocol itself. Between two sessions on the same sensor, noise levels were sometimes different without any obvious reasons. This

may be due to the internal settings that we could not control.

Among others, variance factors also include:

- Electroplating conditions
- ALD fluctuations
- Contact between the probe and the surface beneath insulator
- Actual bacterial concentration
- Environment conditions during the utilisation of bacteria
- Unknown additional species due to the lack of selectivity means
- Highly conductive PBS

All of this makes it difficult to generalize the results and objectively compare sensors with each others. However, our observations might still be enough to suggest a tendency yet to be confirmed. At the current stage of this study, the most promising sensor proportions were ~ 5 μm-thick electrodes, 2 μm-large and with a gap of 4 to 6 μm. A PBS with a conductivity of ~ 1 mS/m could increase the detection level. The next chapter, in addition to the conclusion, gathers some of our ideas that could be implemented to gain in certitude.

Chapter 5

Conclusion

Results

Detecting bacteria in extremely small concentration is a major challenge. Some of them, as *Staphilococcus aureus*, are considered as the main cause of infectious diseases related to the medical sector. Most virulent strains can be dangerous with less than 10 living cells.
To fight them, ever faster, smaller, more selective but above all more sensitive biosensors have been developed over the past years. Electrochemical sensors are part of them. In this master thesis, we placed emphasis on those based on impedance spectroscopy and more specifically on one kind of interditated electrodes sensor which was previously studied by *Numa Couniot* in its PhD thesis.

The main question was: "can we improve the sensitivity of this sensor by increasing its electrodes' height?".

The first step consists of the fabrication of such sensors. Modifying even only one parameter required a new process. Indeed, aluminium, which was selected for an eventual integration with CMOS technology, could no longer be used as the main component of the sensors. We selected nickel, which can, as copper, be electroplated onto silicon and glass substrate but has a better bio-compatibility. To avoid corrosion due to the PBS, electrodes were covered with alumina. As template for the electroplating, we chose resists AZ6632 and, to reach thicknesses greater than 3 μm, AZ4562.
Different electrode widths and spacings were created on the photolithography mask as we did not know what were the geometrical limitations. Each step has been adapted until the obtention of a satisfying result.

Thereafter, sensors were individually tested, and the impedance magnitude and phase were analysed. These tests were first conducted under a dry environment which gave us pieces of information about the impact of the width and gaps of electrodes on the measured global capacitance. Valid sensors had a predictable capacitive impedance and could be ranked according to their gaps.

The last part included tests under liquid environment with the inflow of *Staphylococcus Epidermidis* in PBS through a microfluidic system. This strain was selected for its proximity to the *Staphylococcus aureus* without its dangerousness. To increase the adhesion of bacteria to sensors' wall, we use polydopamine, known as a biological glue.

Experimental results showed that the normalised admittance increased all along the incubation period during which bacteria can be deposited on electrode walls.
We also calculated the sensitivity of each sensors as $S = ||\frac{|Y_B|-|Y_D|}{Y_D}||$, with Y_B and Y_D respectively

the signal admittance with and without bacteria. For a better comprehension of the results, simulations on a simplified equivalent circuit were conducted. The component-relative sensitivity was computed, which allowed us to identify the frequencies at which bacteria would have the most impact.
From the simulation and the background noise analyse, we defined a metric S_M which was the average of sensitivities calculated at 10^5 and 10^6 Hz.
We could not draw a clear conclusion from the comparison of S_M obtained on sensors with three different electrode thicknesses. Indeed, the thinnest sensors showed an increasing sensitivity, starting from 0.8 %, with respect to a decreasing bacteria concentration. The thickest sensor had the opposite behaviour (starting from 1.6 %) and the 5.65 μm-thick one showed sensitivity levels around 1.4 % for all concentrations. There is therefore no clear proof that a sensor with thicker electrodes will have a better sensitivity. However the tests with bacteria were conducted with highly conductive PBS ($\sim$1 S/m) unlike the work of reference. Simulation highlighted that by diluting slightly the PBS, we could increase the theoretical impact of the bacteria.
With the current results, we have no indication on the Limit of Detection. Indeed, at a $\sim 10^5$ CFU/mL concentration, there was still a noticeable detection. A null signal in response to an even lower concentration could have been a confirmation of the validity of our results.

Area for improvement

In the future, if those sensors performances were once again tested, few improvements ideas should be taken into account:

- **More experiment repetition:** Measurements with bacteria were done on a limited selection of sensors. We tried to keep the same proportions with thicknesses of 2.73, 5.65 and 11.8 μm but many more were initially fabricated. A lack of time prompted us to restrict our tests. However, increasing the number of thicknesses tested as well as the number of identical test on one type of sensor would bring more reliable results.
  In addition, running a test during several hours with only PBS in the same microfluidic system would determine if there is a spontaneous evolution of the impedance signal only due to the PBS.
  Finally, an experiment with an even more diluted bacterial solution ($10^2 - 10^3$ for example) could furnish a nearly zero sensitivity that would indicate the LoD as well as confirm the proper functioning of the sensors.

- **Diluted PBS:** As mentioned earlier, it is very likely that the PBS used in this work was not the same dilution than in Numa Couniot's thesis. However, sensitivity' simulations to individual components, as well as to a whole bacterium entry, in diluted PBS a theoretically more important sensitivity.
  The use of a diluted PBS (1:10 to 1:1000) could therefore increase the detection of bacteria.

- **Selectivity means:** For a matter of time, sensors were not tested with any selectivity means. It would be interesting to try the same protocol with lytic enzymes, lysostaphin for *staphylococci*, as a way to selectively suppress target bacteria.

- **Cleaner electrodes:** Despite all our efforts, we were not able to get sensors with exactly reproducible proportions in time. This could be improved by trying other resists of taking into account the deformation in the mask design.

- **Copper electrodes:** In this work, nickel was selected as the main material. However, copper can be electroplated as well and has very interesting conducting properties. The use of copper may give better results for the fabrication and its electrical performance could be tested as long as it is covered by a layer to protect it from the environment.

- **Deeper analysis of optimal proportions:** Initially, many different width-gap combinations were created, however, only one was tested with bacteria. It would be interesting to repeat the same experiment on various proportions to investigate the optimal one towards bacteria.

Bibliography

[1] Paul Schmid-Hempel and Steven A Frank. Pathogenesis, virulence, and infective dose. *PLoS Pathog*, 3(10):1372–1373, 2007.

[2] Numa Couniot. *Highly-sensitive CMOS capacitive biosensors towards detection of single bacterial cell in electrolyte solutions*. PhD thesis, UCL, 2015.

[3] Eric P Widmaier, Hershel Raff, and Kevin T Strang. *Physiologie humaine: les mécanismes du fonctionnement de l'organisme: Vander, Sherman, Luciano*. Chenelière éducation, 2013.

[4] Dmitri Ivnitski, Ihab Abdel-Hamid, Plamen Atanasov, and Ebtisam Wilkins. Biosensors for detection of pathogenic bacteria. *Biosensors and Bioelectronics*, 14(7):599–624, 1999.

[5] Shana O. Kelley. Disease detector. *Medicine*, 2015.

[6] Olivier Lazcka, F. Javier Del Campo, and F. Xavier Muñoz. Pathogen detection: A perspective of traditional methods and biosensors. *Biosensors and Bioelectronics*, 22(7):1205–1217, 2007.

[7] Louise Deschênes, Gregory De Crescenzo, and Mario Jolicoeur. *GCH2105 - Génie du Vivant*, 2015. Manuel de laboratoire.

[8] Directorate E. Working document on microbial contaminant limits for microbial pest control products. Technical Report SANCO/12116/2012 –rev. 0, EUROPEAN COMMISSION HEALTH and CONSUMER PROTECTION DIRECTORATE-GENERAL, September 2012.

[9] Oscar Fernando D'Urso, Palmiro Poltronieri, Santo Marsigliante, Carlo Storelli, Marta Hernández, and David Rodríguez-Lázaro. A filtration-based real-time {PCR} method for the quantitative detection of viable salmonella enterica and listeria monocytogenes in food samples. *Food Microbiology*, 26(3):311 – 316, 2009.

[10] Jonathan S. Daniels and Nader Pourmand. Label-free impedance biosensors: Opportunities and challenges. 19(12):1239–1257, 2007.

[11] Beibei Wang, Qi Wang, Zhaoxia Cai, and Meihu Ma. Simultaneous, rapid and sensitive detection of three food-borne pathogenic bacteria using multicolor quantum dot probes based on multiplex fluoroimmunoassay in food samples. *LWT - Food Science and Technology*, 61(2):368–376, may 2015.

[12] Staphylocoque : Fiche info institut pasteur. `http://www.pasteur.fr/fr/institut-pasteur/presse/fiches-info/staphylocoque`, October 2012. 2016-02-08.

[13] Culture and Sensitivity Testing. `http://www.bio.miami.edu/hare/culture.html`, 2015-12-31.

[14] Eo labs: Microbiological culture media. `http://www.eolabs.com/tryptone-soya-agar-irradiated.html`. 2016-05-20.

[15] Liju Yang and Rashid Bashir. Electrical/electrochemical impedance for rapid detection of foodborne pathogenic bacteria. *Biotechnology advances*, 26(2):135–150, 2008.

[16] Scott Sutton. Counting colonies. `http://www.microbiol.org/resources/monographswhite-papers/counting-colonies/`, January 2006. 2016-05-20.

[17] Ahmed E Yousef. Detection of bacterial pathogens in different matrices: Current practices and challenges. In *Principles of Bacterial Detection: Biosensors, Recognition Receptors and Microsystems*, pages 31–48. Springer, 2008.

[18] Xavier Muñoz-Berbel, Neus Godino, Olivier Laczka, and Eva Baldrich. Impedance-based biosensors for pathogen detection. In *Principles of bacterial detection: biosensors, recognition receptors and microsystems*, pages 341–376. Springer, 2008.

[19] Michel Gislain. Lgbio2010 - cours de bioinformatique, 2014.

[20] Philippe Baret and Pierre Bertin. Bir1322 - general genetics, 2007.

[21] Marie-Frédérique Lartigue. Matrix-assisted laser desorption ionization time-of-flight mass spectrometry for bacterial strain characterization. *Infection, genetics and evolution : journal of molecular epidemiology and evolutionary genetics in infectious diseases*, 13:230–5, 2013.

[22] Yi-Chung Chang, Chia-Ying Yang, Ruei-Lin Sun, Yi-Feng Cheng, Wei-Chen Kao, and Pan-Chyr Yang. Rapid single cell detection of staphylococcus aureus by aptamer-conjugated gold nanoparticles. *Scientific reports*, 3, 2013.

[23] Staffan Paulie, Peter Perlmann, and Hedvig Perlmann. Chapter 64 - enzyme-linked immunosorbent assay. In Julio E. Celis, editor, *Cell Biology (Third Edition)*, pages 533 – 538. Academic Press, Burlington, third edition edition, 2006.

[24] Etienne Carbonnelle, Cécile Mesquita, Emmanuelle Bille, Nesrine Day, Brunhilde Dauphin, Jean-Luc Beretti, Agnès Ferroni, Laurent Gutmann, and Xavier Nassif. MALDI-TOF mass spectrometry tools for bacterial identification in clinical microbiology laboratory. *Clinical biochemistry*, 44(1):104–9, jan 2011.

[25] Zongmin Du, Ruifu Yang, Zhaobiao Guo, Yajun Song, and Jin Wang. Identification of staphylococcus a ureus and determination of its methicillin resistance by matrix-assisted laser desorption/ionization time-of-flight mass spectrometry. *Analytical chemistry*, 74(21):5487–5491, 2002.

[26] Andreas Wieser, Lukas Schneider, Jette Jung, and Sören Schubert. Maldi-tof ms in microbiological diagnostics—identification of microorganisms and beyond (mini review). *Applied microbiology and biotechnology*, 93(3):965–974, 2012.

[27] J. Rose, M. Auffan, O. Proux, V. Niviere, and J.Y. Bottero. *Encyclopedia of Nanotechnology.* 2012.

[28] Tomoyuki Yasukawa, Yoshimi Yoshimoto, Takuya Goto, and Fumio Mizutani. Highly-sensitive electrochemical immunosensing method based on dual amplification systems. *Biosensors and Bioelectronics*, 37(1):19 – 23, 2012.

[29] Angela Leung, P. Mohana Shankar, and Raj Mutharasan. A review of fiber-optic biosensors. *Sensors and Actuators B: Chemical*, 125(2):688–703, aug 2007.

[30] S Sabban. *Development of an in vitro model system for studying the interaction of Equus caballus lgE with its high-affinity Fc receptor*. PhD thesis, PhD Thesis. University of Sheffield, Sheffield, 2011.

[31] "piézo-électricité" from encyclopaedia universalis. `http://www.universalis.fr/encyclopedie/piezo-electricite/`, 2016-02-24.

[32] Han Xia, Feng Wang, Qing Huang, Junfu Huang, Ming Chen, Jue Wang, Chunyan Yao, Qinghai Chen, Guoru Cai, and Weiling Fu. Detection of staphylococcus epidermidis by a quartz crystal microbalance nucleic acid biosensor array using au nanoparticle signal amplification. *Sensors*, 8(10):6453–6470, 2008.

[33] Eric Olsen, Arnold Vainrub, and Vitaly Vodyanoy. Acoustic wave (tsm) biosensors: weighing bacteria. In *Principles of bacterial detection: biosensors, recognition receptors and microsystems*, pages 255–298. Springer, 2008.

[34] Laurent Francis et al. *Thin film acoustic waveguides and resonators for gravimetric sensing applications in liquid*. PhD thesis, UCL., 2006.

[35] Kerstin Länge, Bastian E. Rapp, and Michael Rapp. Surface acoustic wave biosensors: A review. *Analytical and Bioanalytical Chemistry*, 391(5):1509–1519, 2008.

[36] Steven Saliterman. *Fundamentals of BioMEMS and medical microdevices*, volume 153. SPIE press, 2006.

[37] B L Weeks, J Camarero, A Noy, and A E Miller J J De. Development of a Microcantilever-Based Pathogen Detector. 2003.

[38] GY Chen, T Thundat, EA Wachter, and RJ Warmack. Adsorption-induced surface stress and its effects on resonance frequency of microcantilevers. *Journal of Applied Physics*, 77(8):3618–3622, 1995.

[39] Raj Mutharasan. Cantilever sensors for pathogen detection. In *Principles of bacterial detection: biosensors, recognition receptors and microsystems*, pages 459–479. Springer, 2008.

[40] Yves F. Durêne. Atomic Force Microscopy in Microbiology: New Structural and Functional Insights into the Microbial Cell Surface. 5, aug 2014.

[41] Dmitri Ivnitski, Ihab Abdel-Hamid, Plamen Atanasov, Ebtisam Wilkins, and Stephen Stricker. Application of electrochemical biosensors for detection of food pathogenic bacteria. *Electroanalysis*, 12(5):317–325, 2000.

[42] Ilaria Palchetti and Marco Mascini. Amperometric biosensors for pathogenic bacteria detection. In *Principles of bacterial detection: biosensors, recognition receptors and microsystems*, pages 299–312. Springer, 2008.

[43] Brian A Gregg and Adam Heller. Cross-linked redox gels containing glucose oxidase for amperometric biosensor applications. *Analytical Chemistry*, 62(3):258–263, 1990.

[44] Katsumi Takayama, Toshiyasu Kurosaki, and Tokuji Ikeda. Mediated electrocatalysis at a biocatalyst electrode based on a bacterium, gluconobacter industrius. *Journal of electroanalytical chemistry*, 356(1-2):295–301, 1993.

[45] Gustavo A Zelada Guillén, José Luis Sebastián-Avila, Pascal Blondeau, Jordi Riu, and F Xavier Rius. Label-free detection of staphylococcus aureus in skin using real-time potentiometric biosensors based on carbon nanotubes and aptamers. *Biosensors and bioelectronics*, 31(1):226–232, 2012.

[46] Myounggon Kim, Taekeon Jung, Youngjin Kim, Changgeun Lee, Kyungchul Woo, Jae Hun Seol, and Sung Yang. A microfluidic device for label-free detection of Escherichia coli in drinking water using positive dielectrophoretic focusing, capturing, and impedance measurement. *Biosensors and Bioelectronics*, 74:1011–1015, jul 2015.

[47] Seungkyung Park, Yi Zhang, Tza-Huei Wang, and Samuel Yang. Continuous dielectrophoretic bacterial separation and concentration from physiological media of high conductivity. *Lab Chip*, 11:2893–2900, 2011.

[48] Anodic stripping voltametry. `http://ion.chem.usu.edu/~sbialkow/Classes/565/ASV.html`, 2016-02-04.

[49] Allen D Taylor, Jon Ladd, Jiří Homola, and Shaoyi Jiang. Surface plasmon resonance (spr) sensors for the detection of bacterial pathogens. In *Principles of Bacterial Detection: Biosensors, Recognition Receptors and Microsystems*, pages 83–108. Springer, 2008.

[50] Nancy Tawil, Edward Sacher, Rosemonde Mandeville, and Michel Meunier. Surface plasmon resonance detection of e. coli and methicillin-resistant s. aureus using bacteriophages. *Biosensors and Bioelectronics*, 37(1):24–29, 2012.

[51] Sihem Bouguelia, Yoann Roupioz, Sami Slimani, Laure Mondani, Maria G. Casabona, Claire Durmort, Thierry Vernet, Roberto Calemczuk, and Thierry Livache. On-chip microbial culture for the specific detection of very low levels of bacteria. *Lab Chip*, 13:4024–4032, 2013.

[52] Wai-Sing Chan, Bone SF Tang, Maureen V Boost, Chit Chow, and Polly HM Leung. Detection of methicillin-resistant staphylococcus aureus using a gold nanoparticle-based colourimetric polymerase chain reaction assay. *Biosensors and Bioelectronics*, 53:105–111, 2014.

[53] Nuo Duan, Shijia Wu, Changqing Zhu, Xiaoyuan Ma, Zhouping Wang, Ye Yu, and Yuan Jiang. Dual-color upconversion fluorescence and aptamer-functionalized magnetic nanoparticles-based bioassay for the simultaneous detection of salmonella typhimurium and staphylococcus aureus. *Analytica Chimica Acta*, 723:1 – 6, 2012.

[54] Nicolas Moll, Emilie Pascal, Duy Haï Dinh, Jean-Paul Pillot, Bernard Bennetau, Dominique Rebiere, Daniel Moynet, Yan Mas, Djavad Mossalayi, Jacques Pistré, et al. A love wave immunosensor for whole e. coli bacteria detection using an innovative two-step immobilisation approach. *Biosensors and Bioelectronics*, 22(9):2145–2150, 2007.

[55] Yan Lian, Fengjiao He, Huan Wang, and Feifei Tong. A new aptamer/graphene interdigitated gold electrode piezoelectric sensor for rapid and specific detection of staphylococcus aureus. *Biosensors and Bioelectronics*, 65:314–319, 2015.

[56] Vanessa Escamilla-Gómez, Susana Campuzano, María Pedrero, and José M Pingarrón. Electrochemical immunosensor designs for the determination of staphylococcus aureus using 3, 3-dithiodipropionic acid di (n-succinimidyl ester)-modified gold electrodes. *Talanta*, 77(2):876–881, 2008.

[57] B Mirhabibollahi, Joy L Brooks, and RG Kroll. Development and performance of an enzyme-linked amperometric immunosensor for the detection of staphylococcus aureus in foods. *Journal of applied bacteriology*, 68(6):577–585, 1990.

[58] María Dolores Morales, Beatriz Serra, Ana Guzmán-Vázquez de Prada, Ángel Julio Reviejo, and José Manuel Pingarrón. An electrochemical method for simultaneous detection and identification of escherichia coli, staphylococcus aureus and salmonella choleraesuis using a glucose oxidase-peroxidase composite biosensor. *Analyst*, 132(6):572–578, 2007.

[59] Fei Tan, Polly HM Leung, Zong-bin Liu, Yu Zhang, Lidan Xiao, Weiwei Ye, Xin Zhang, Li Yi, and Mo Yang. A pdms microfluidic impedance immunosensor for e. coli o157: H7 and staphylococcus aureus detection via antibody-immobilized nanoporous membrane. *Sensors and Actuators B: Chemical*, 159(1):328–335, 2011.

[60] M. Braiek, K.B. Rokbani, A. Chrouda, B. Mrabet, A. Bakhrouf, A. Maaref, and N. Jaffrezic-Renault. An electrochemical immunosensor for detection of staphylococcus aureus bacteria based on immobilization of antibodies on self-assembled monolayers-functionalized gold electrode. *Biosensors*, 2(4):417–426, 2012.

[61] Damion K Corrigan, Holger Schulze, Grace Henihan, Ilenia Ciani, Gerard Giraud, Jonathan G Terry, Anthony J Walton, Ronald Pethig, Peter Ghazal, Jason Crain, et al. Impedimetric detection of single-stranded pcr products derived from methicillin resistant staphylococcus aureus (mrsa) isolates. *Biosensors and Bioelectronics*, 34(1):178–184, 2012.

[62] Jae Ho Yoon, Yong Duk Han, Pyung Cheon Lee, and Hyun C Yoon. Lysostaphin-mediated fragmentation of microbial peptidoglycans for label-free electrochemical impedance immunoanalysis of staphylococcus aureus. *BioChip Journal*, 7(4):344–352, 2013.

[63] Raquel A Villamizar, Alicia Maroto, F Xavier Rius, Isabel Inza, and Maria J Figueras. Fast detection of salmonella infantis with carbon nanotube field effect transistors. *Biosensors and Bioelectronics*, 24(2):279–283, 2008.

[64] Lysostaphin datasheet ProSpec. `http://www.prospecbio.com/Lysostaphin{\_}8{\_}181/`, 2016-01-27.

[65] Frank X Placencia, Lingkun Kong, and Leonard E Weisman. Treatment of methicillin-resistant staphylococcus aureus in neonatal mice: lysostaphin versus vancomycin. *Pediatric research*, 65(4):420–424, 2009.

[66] Junya Suehiro, Tetsuji Hatano, Masanori Shutou, and Masanori Hara. Improvement of electric pulse shape for electropermeabilization-assisted dielectrophoretic impedance measurement for high sensitive bacteria detection. *Sensors and Actuators B: Chemical*, 109(2):209–215, 2005.

[67] Sergi Brosel-Oliu, Naroa Uria, Natalia Abramova, and Andrey Bratov. Impedimetric sensors for bacteria detection. 2015.

[68] Giovanni Barbero, AL Alexe-Ionescu, and I Lelidis. Significance of small voltage in impedance spectroscopy measurements on electrolytic cells. *Journal of applied physics*, 98(11):113703, 2005.

[69] Karel Stulík, Christian Amatore, Karel Holub, Vladimír Marecek, and Wlodzimierz Kutner. Microelectrodes. definitions, characterization, and applications (technical report). *Pure and Applied Chemistry*, 72(8):1483–92, 2000.

[70] RW Erickson. Bode diagrams of transfer functions and impedances. *University of Colorado at Boulder ECEN*, 2260:13–18.

[71] Chuanmin Ruan, Liju Yang, and Yanbin Li. Immunobiosensor chips for detection of escherichia c oli o157: H7 using electrochemical impedance spectroscopy. *Analytical Chemistry*, 74(18):4814–4820, 2002.

[72] Rafael Gómez-Sjöberg, Dallas T Morisette, and Rashid Bashir. Impedance microbiology-on-a-chip: microfluidic bioprocessor for rapid detection of bacterial metabolism. *Microelectromechanical Systems, Journal of*, 14(4):829–838, 2005.

[73] F. Malloggi. Microfluidics: From basic principles to applications. *Lecture Notes in Physics*, 917:515–546, 2016. cited By 0.

[74] Guilhem Velve-Casquillas, Maël Le Berre, Matthieu Piel, and Phong T Tran. Microfluidic tools for cell biological research. *Nano today*, 5(1):28–47, 2010.

[75] S Zhang, G Wright, and Y Yang. Materials and techniques for electrochemical biosensor design and construction. *Biosensors & bioelectronics*, 15:273–282, 2000.

[76] RA Lawes. Manufacturing costs for microsystems/mems using high aspect ratio microfabrication techniques. *Microsystem technologies*, 13(1):85–95, 2007.

[77] Aránzazu del Campo and Christian Greiner. Su-8: a photoresist for high-aspect-ratio and 3d submicron lithography. *Journal of Micromechanics and Microengineering*, 17(6):R81, 2007.

[78] Mark G Allen et al. Metallic microstructures fabricated using photosensitive polyimide electroplating molds. *Microelectromechanical Systems, Journal of*, 2(2):87–94, 1993.

[79] Microchemicals : thick resist processing. `http://www.microchemicals.com/technical_information/thick_resist_processing.pdf`, November 2013. 2016-05-11.

[80] C H Lee and K Jiang. Fabrication of thick electroforming micro mould using a kmpr negative tone photoresist. *Journal of Micromechanics and Microengineering*, 18(5):055032, 2008.

[81] Holger Becker and Ulf Heim. Hot embossing as a method for the fabrication of polymer high aspect ratio structures. *Sensors and Actuators A: Physical*, 83(1):130–135, 2000.

[82] John D. Madden and Ian W. Hunter. Three-dimensional microfabrication by localized electrochemical deposition. *Journal of Microelectromechanical Systems*, 5(1):24–32, 1996.

[83] Microchemicals : Exposure of photoresist. `http://www.microchemicals.com/technical_information/exposure_photoresist.pdf`, November 2013. 2016-05-13.

[84] Dudley S Finch, Tammy Oreskovic, Krishna Ramadurai, Cari F Herrmann, Steven M George, and Roop L Mahajan. Biocompatibility of atomic layer-deposited alumina thin films. *Journal of Biomedical Materials Research Part A*, 87(1):100–106, 2008.

[85] The Editors of Encyclopaedia Britannica. Encyclopaedia Britannica: Aluminium. `http://www.britannica.com/science/alumina`, 2016-02-01.

[86] Markku Leskelä and Mikko Ritala. Atomic layer deposition (ald): from precursors to thin film structures. *Thin solid films*, 409(1):138–146, 2002.

[87] Jeffrey R Wank, Steven M George, and Alan W Weimer. Coating fine nickel particles with al2o3 utilizing an atomic layer deposition-fluidized bed reactor (ald–fbr). *Journal of the American Ceramic Society*, 87(4):762–765, 2004.

[88] HB Profijt, SE Potts, MCM Van de Sanden, and WMM Kessels. Plasma-assisted atomic layer deposition: Basics, opportunities, and challenges. *Journal of Vacuum Science & Technology A*, 29(5):050801, 2011.

[89] Wun Hsing Lee, Sen Cheh Tang, and Kung Cheng Chung. Effects of direct current and pulse-plating on the co-deposition of nickel and nanometer diamond powder. *Surface and Coatings Technology*, 120-121:607–611, 1999.

[90] Laurent Robert. *Etude des propriétés mécaniques du nickel utilisé dans la technologie LIGA. Réalisation d'un micropréhenseur*. PhD thesis, 1997.

[91] The nist reference on constants, units, and uncertainty: Faraday constant. `http://physics.nist.gov/cgi-bin/cuu/Value?f`, 2016-02-03.

[92] Mordechay Schlesinger and Milan Paunovic. Electrodeposition of Nickel. *Modern Electroplating: Fifth Edition*, pages 79–114, 2010.

[93] Prof. Robert White. Nickel sulfamate plating process:standard operating procedure, September 2012.

[94] Naoki Okamoto and Tohru Watanabe. The Adhesion of Electrodeposited Copper, Nickel and Silver Films on Copper, Nickel and Silver Substrates. *Nippon Kinzoku Gakkaishi/Journal of the Japan Institute of Metals*, 68(2):110–113, 2004.

[95] Sonja Sioncke, Annelies Delabie, Guy Brammertz, Thierry Conard, Alexis Franquet, Matty Caymax, Adam Urbanzcyk, Marc Heyns, Marc Meuris, JL Van Hemmen, et al. Thermal and plasma enhanced atomic layer deposition of al2o3 on gaas substrates. *Journal of The Electrochemical Society*, 156(4):H255–H262, 2009.

[96] Microchemicals : Photoresist removal. `http://www.microchemicals.com/technical_information/photoresist_removal.pdf`, November 2013. 2016-05-17.

[97] Transene, advanced materials for electronics :printed circuit copper etchants. `http://transene.com/cu-etchant/`, April 2016.

[98] Sylvain Druart et al. *Designing microsystems for liquid electrical properties and variable magnetic fields measurements*. PhD thesis, UCL, 2013.

[99] Catherine Nannan. Etude et modélisation de l'adhésion de Staphylococcus epidermidis à des biomatériaux. Master's thesis, UCL, 2013.

[100] Microchemicals : electroplating with photoresist mask. `http://www.microchemicals.com/technical_information/electroplating_photoresists.pdf`, January 2014. 2016-05-11.

[101] Microchemicals : Inferior resist adhesion. `http://www.microchemicals.com/technical_information/resist_adhesion.pdf`, Augustus 2005. 2016-05-11.

[102] Numa Couniot, Aryan Afzalian, N Van Overstraeten-Schlögel, LA Francis, and Denis Flandre. Capacitive biosensing of bacterial cells: analytical model and numerical simulations. *Sensors and Actuators B: Chemical*, 211:428–438, 2015.

Rue Archimède, 1 bte L6.11.01, 1348 Louvain-la-Neuve **www.uclouvain.be/epl**

